Towards a Corpuscular Model of Optical Phenomena

Fengping Jin

2011

To my parents and my wife

University of Groningen
Zernike Institute
for Advanced Materials

Zernike Institute PhD thesis series 2011-07
ISSN 1570-1530

The work described in this thesis was performed at the Department of Applied Physics of the Rijksuniversiteit Groningen, the Netherlands.

ISBN electronic version: 978-90-367-4739-4
ISBN printed version: 978-90-367-4740-0
Printed by Ipskamp Drukkers, the Netherlands

RIJKSUNIVERSITEIT GRONINGEN

Towards a Corpuscular Model of Optical Phenomena

Proefschrift

ter verkrijging van het doctoraat in de
Wiskunde en Natuurwetenschappen
aan de Rijksuniversiteit Groningen
op gezag van de
Rector Magnificus, dr. F. Zwarts,
in het openbaar te verdedigen op
vrijdag 25 februari 2011
om 16:15 uur

door

Fengping Jin

geboren op 2 april 1979
te Dongyang, Zhejiang, China

Promotor: Prof.dr. H.A. De Raedt

Beoordelingscommissie: Prof.dr. S. Miyashita
Prof.dr. K. Michielsen
Prof.dr. J.Th.M. De Hosson

Contents

Introduction

0.1 Overview

Physics aims to explore Nature. With the discovery of quantum theory, we seem to have the most powerful theory to interpret the physical phenomena. To date, there seems to be no evidence of experimental results that contradict quantum theory. Yet, there are serious conceptual problems with the theory itself, such as the quantum measurement paradox [1].

Indeed, the more we know, the more we do not know. Quantum theory (QT) gives us a deeper understanding of Nature. Meanwhile it shows more about Nature that we do not understand. For example, the single-electron double-slit experiment [2, 3] shows the interference pattern after collecting many of the detection events (clicks). Quantum theory explains the total interference pattern but it gives no clue of how the pattern is actually formed. It has become tradition in physics to declare that it is fundamentally impossible to give a description on the level of the events that occur on the quantum level. Concepts stemming from Quantum theory [1], such as "wave-particle duality", "nonlocality", "action at distance" and etc., that are supposed to only work within the framework of Quantum theory are abused. It is not wise to simply deny the things we do not know yet, or fasten our thoughts to the tradition. In this thesis, we demonstrate that it is possible to give event-based descriptions to quantum phenomena. We simulate several fundamental optics experiments by using the concept of a learning machine (LM). LMs are quite beyond quantum theory but reproduce the results of quantum theory when the simulation reaches the stationary regime. In our simulation, photons (messengers in our simulation) always keep their particle nature. The "wave" nature is somehow incorporated into the optical components, such as the beam splitter, wave plate, detector and so on.

Computer simulation is widely regarded as complementary to theory and experiment [4]. If computer simulation is indeed a third methodology, it should be not a surprise that quantum phenomena can be simulated on an event-by-event basis by a computer.

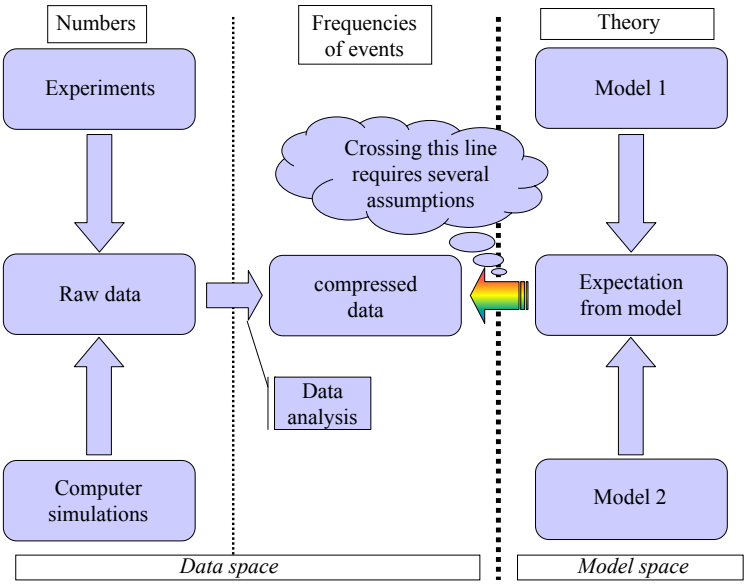

Figure 0.1: Logical relationship between data and theory. Left: Data space; Right: Model space. Crossing the line between data space and model space requires the assumption that there exist some processes that give rise the observed data. The real information about Nature all come from the Data space, from the experiments. The theory is supposed to explore the experimental data and is only complete within its own framework. If the theoretical model does not explain all the features that exist in data space, we have to revise the theory or build another model to complete the description, but never fasten our thoughts to the framework of the theory, to the extreme of leaving out features in data space. In a sense, simulation algorithms can produce the same kind data as the experimental data. So it is interesting to find algorithms that simulate physical phenomena about which the theory has nothing to say.

0.2 Fundamental problem

0.2.1 The hypothesis

In general, it is important to recognize that there are fundamental, conceptual differences between the set of experimental facts, their interpretation in terms of a mathematical model and a computer simulation of the facts. A graphical representation of the point of view is given in Fig. 0.1. On the left, we have processes that generate events. Each event is represented by one or more numbers, which we call raw data. Experience or a new idea provide inspiration to choose one or more methods to analyze the data. Typically, this analysis maps the raw data onto a few numbers, that is the raw data is being compressed. On the right hand side, we have several candidate mathematical models, "theories", that may "explain" the results of the data analysis.

But, how do we relate data to (quantum) theory? It is essential to recognize that before we can address this question, we have to make the assumption that there exists

some process that gives rise to the observed data. Otherwise, we cannot go beyond the description of merely giving the data as it is. Furthermore, a useful theoretical model should give a description of the data that is considerably more compact than the data itself.

Crossing the line that separates the model space from the data space requires making the fundamental hypothesis that the process that gives rise to the data can be described within the framework of (quantum) theory. Only then, we are in the position that we can use (quantum) theory to relate the mathematical model to the observed frequencies.

0.2.2 The paradoxes

Not realizing the existence of such hypothesis can cause some misunderstandings, and even paradoxes. In a sense, the experimental data are always at the first level and the theoretical model is at the second level, trying to interpret the data based on the hypothesis. But if someone would think in the opposite way, many problems may appear. Since quantum theory is so successful in giving the description of the phenomena, many would think that quantum theory takes charge of the world. Many concepts, such as "wave-particle duality", "nonlocality" and so on, that come from quantum theory, are extended beyond the theory itself. As things go further, many even doubt the "reality" that represents the world we are living. The concepts do change the thought of human beings, but never change the "reality".

The quantum measurement paradox [1] is one of the famous paradoxes, which is intimately related to the concept of "wave-particle duality". According to this concept, photons exhibit both wave and particle behavior depending upon the circumstances of the experiment. But when we examine the experiment, this duality never appears. Each time we observe one detection event. As the events accumulate, the interference pattern shows up. Quantum theory only tells us the probability for an event to occur. Reconciling the mathematical formalism that does not describe individual events with the experimental fact that each observation yields a definite outcome is referred to as the quantum measurement paradox and is the most fundamental problem in the foundation of quantum theory.

Why does this happen? The answer may be simple if we examine the Fig. 0.1 carefully. All the concepts comes from the model space. When we connect the concepts to the data space, the hypothesis has to been investigated firstly and seriously. A similar situation happens in the case of the Bell's theorem. All these fundamental problems come from overlooking a hypothesis and stressing the power of the theory.

It is important to realize that the paradoxes result from ignoring the hypothesis. Without carefully investigating the hypothesis that there exists some process that can give rise to the observed data, attempts to apply the concepts and the formalism of QT to a description of the experimental results in terms of individual events create the paradoxes [1]. Logically speaking, there are two possibilities:

1. We accept the postulate that it is fundamentally impossible to give a logically consistent description of the experimental results in terms of individual events, that is we accept that there is no explanation that goes beyond the quantum theoretical description in terms of averages over many events.

2. We search for an explanation of the experimental facts that goes beyond a description in terms of averages.

In this thesis, we demonstrate that the second option is a viable one. Thus, we adopt the point of view that although QT correctly predicts averages of many detection events, it has nothing to say about individual events [1]. From Fig. 0.1, we demand that the simulation produces data which are of the same kind as the experimental data and agree with theory.

0.3 Irrelevance of Bell's theorem

It is not uncommon to find in the recent literature, statements that it is impossible to simulate quantum phenomena by classical processes. Such statements are thought to be a direct consequence of Bell's theorem [5] but are in conflict with other work that has pointed out the irrelevance of Bell's theorem [6–28]. A survey of the literature suggests that, roughly speaking, physicists can be classified as those who believe in the reasonableness of Bell's arguments, those who advance logical and mathematical arguments to show that a violation of Bell's (and related) inequalities does not support the far-reaching conclusions of the former group of physicists and those who do not care about Bell's theorem at all. The author of this thesis belongs to the second group.

Although discussions of philosophical or metaphysical aspects of Bell's theorem may continue forever, as explained in a review article [29], from the viewpoint of simulating quantum phenomena on a digital computer, Bell's no-go theorem is of no relevance whatsoever.

This conclusion is supported by several explicit examples that prove that it is possible to construct algorithms that satisfy Einstein's criteria for locality and causality, yet reproduce *exactly* the two-particle correlations of a quantum system in the singlet state, without invoking any concept of quantum theory [29–34]. It is therefore an established fact that purely classical processes can produce the correlations that are characteristic for a quantum system in an entangled state, thereby disposing of the mysticism that is created by Bell's no-go theorem.

The key point is to realize that QT or the probabilistic models proposed by Bell cannot, on a fundamental level, address the (non)existence of algorithms, that is of well-defined processes, that give rise to the distributions of the events, described by these theories/models.

0.4 Computational approach: Event-by-event simulation

The philosophy behind our simulation approach is very simple: If we can construct an algorithm that

1. does not rely on the solution of a wave equation,
2. satisfies the elementary criteria of locality and causality as formulated by Einstein,
3. produces data of the same type as the data collected in the laboratory experiment,
4. by analyzing the simulated data according to the procedure used to analyze the experimental data leads to the same conclusion, namely that certain averages of the raw data agree with the quantum theoretical description of the whole experiment,
5. contains algorithms that simulate the various components (beam splitter, etc.) of the experiment and can, with no change, be re-used to simulate other experiments,

then we may conclude that we have built a simulation model for the laboratory experiment.

Loosely speaking, if the experimenter would be unable to distinguish between data recorded in a genuine experiment and data provided by the simulation algorithm, then the experiment has been "de-mystified" in the sense that we have found a process that offers a description of the observed phenomena on the level of individual events and without invoking (concepts of) quantum theory.

Our event-by-event simulation strictly follows the above philosophy.

We build a network consisting of processing units. The processing units are mimicking the functions of optical components like a beam splitter, wave plate, detector, etc.. Photons are regarded as messengers, carrying a message that represents its time-of-flight (phase) and polarization, while traveling through the network. As all the parts in the simulation algorithm are quite general and consistent, we can build a (computer) experiment by combining the processing units. Our event-by-event simulation model describes a particle-like, classical, local and causal dynamical system, satisfies Einstein's criterion of local causality, and reproduces the results of QT, without first solving a wave equation.

A key feature of the processing units is that they can learn. These so-called learning machines (LM) use an adaptive algorithm to learn from the data of the incoming messages without counting the numbers of messengers. The LM is essential to our

event-by-event simulation and is the same for all components used in the simulation network.

0.5 Structure of the thesis

The structure of the thesis is as follows:

Chapter 1: We describe the fundamental experiment, the double-slit experiment with single photons. As the individual photons build up the interference pattern one-by-one and there is no direct communication between photons, the interference pattern can only be due to the internal operation of the detector [35]. We present a model for the detector which accounts for the memory and the threshold behavior of the detectors. The behavior of model also satisfies the constitutive equations in Maxwell's theory.

Chapter 2: Directly using the model of detector described in Chapter 1 and the models of optical components such as beam splitter invented earlier which simulate the Mach-Zehnder interferometer successfully, we build an computational experiment which is one-to-one copy of a real Hanbury Brown-Twiss experiment in Ref. [36]. The simulation results agree with the experimental data and wave theory.

Chapter 3: We present a computer simulation model of a quantum eraser experiment [37]. The model has all the parts that correspond to the real optical components, such as beam splitters, polarized beam splitter, half-wave plate and quarter-wave plate. The simulation results agree with the experimental data and wave theory.

Chapter 4: We describe an Einstein-Podolosky-Rosen-Bohm experiment with photons polarized and, by analyzing the real experimental data [38, 39], stress that the time window W is essential to get a quantum correlation. Then we present an event-based simulation of EPRB experiment [40] that satisfies Einstein's criteria of local causality, generates the same kind of data as in experiment, and is capable of reproducing exactly the single- and two-particle averages of quantum correlation of singlet state.

The four chapters can be read in any order: They are self-contained.

0.6 Disclaimer

To avoid misunderstandings, we emphasize that the work presented in this thesis is not concerned with the interpretation or an extension of quantum theory. The fact that there exist simulation algorithms that reproduce the results of quantum theory has no direct implications to the foundations of quantum theory: The algorithm describes the process of generating events on a level of detail about which quantum theory has nothing to say (quantum measurement paradox). The average properties of the data may be in perfect agreement with quantum theory but the algorithms that generate such data are outside of the scope of what quantum theory can describe. This may

sound a little strange but it is not if one recognizes that probability theory does not contain nor provides an algorithm to generate the values of the random variables either, which in a sense, is at the heart of the quantum measurement paradox.

Chapter 1

Double-slit Experiment with Single Photons

This chapter was previously published as
F.Jin, S. Yuan, H. De Raedt, K. Michielsen, and S. Miyashita, J. Phys. Soc. Jpn. **79**, 074401 (2010).

1.1 Introduction

In 1802, Young performed a double-slit experiment with light in order to resolve the question whether light was composed of particles, confirming Newton's particle picture of light, or rather consisted of waves [41]. His experiment showed that the light emerging from the slits produces a fringe pattern on the screen that is characteristic for interference, discrediting Newton's corpuscular theory of light [41]. Hence, from the point of view of classical physics, the particle and wave character of light did not seem to be compatible. Moreover, the interpretation in terms of particles or waves of the observations in experiments with light became even more complicated after conduction of the Michelson-Morley experiment [42] which provided evidence that light waves do not need a medium (the ether) to propagate through, in contrast to water

and sound waves which require media. However, explanation of the photoelectric effect by Einstein in terms of photons [43] is perhaps the most direct and convincing evidence of the corpuscular nature of light. Einstein's explanation of the photoelectric effect was the start of understanding the quantum nature of light and influenced the development of the concept of wave-particle duality in quantum theory.

In 1924, de Broglie introduced the idea that also matter, not just light, can exhibit wave-like properties [44]. This idea has been confirmed in various double-slit experiments with massive objects such as electrons [2, 3, 45, 46], neutrons [47, 48], atoms [49, 50] and molecules such as C_{60} and C_{70} [51, 52], all showing interference. In some of the double-slit experiments [2, 3, 53] the interference pattern is built up by recording individual clicks of the detectors. Identifying the registration of a detector click, the "event", with the arrival of a particle and assuming that the time between successive clicks is sufficiently long such that these particles do not interact, it becomes a challenge to explain how the detection of individual objects that do not interact with each other can give rise to the interference patterns that are being observed. According to Feynman, the observation that the interference patterns are built up event-by-event is "impossible, absolutely impossible to explain in any classical way and has in it the heart of quantum mechanics" [54].

Although wave-particle duality is a central concept of quantum theory, in practice quantum theory only works with wave functions to describe the total system under study. In order to describe the single occurrences observed in various experiments the process of wave function collapse has been introduced. However, the precise mechanism of a wave function collapse is not known.

Recently, various experiments have been performed that measure individual events generated by microscopic objects. Hence, it is of interest to study how the particle and wave picture of these experiments are contradicting each other. It is often said that wave properties like interference cannot be realized by non-interacting particles which satisfy Einstein's criterion of local causality. In earlier work we have presented an event-based corpuscular simulation model which demonstrates that such particles can indeed produce interference patterns and applied it to a variety of single-photon experiments like beam splitter and Mach-Zehnder interferometer experiments, Wheeler's delayed choice experiments and many others [29–32, 34, 55–61]. What these experiments have in common is that the interference can be described as two-path interference, that is the observed interference pattern is the result of having only two possible paths for the particles travelling between source and detector. In order to simulate such experiments it is sufficient to use adaptive models for the optical apparatuses and to use detectors that simply count the number of detection events [29–32, 34, 55–61]. In this chapter we extend the simulation model towards simulating multipath interference patterns as observed in single-photon two-beam interference and two-slit experiments, for example. Detectors that are simply counting the detection events cannot be used for this purpose. Therefore we introduce a new simulation model for the single-photon detector that takes into account the memory

and threshold behavior of such a detector. The model is a natural extension of the earlier work mentioned and is fully compatible, that is interchanging in our earlier work the simple counting detector model with this more complex detector does not change the conclusions. In this sense, the present detector model adds a new, fully compatible, component to the collection of event-by-event simulation algorithms.

Note that the event-based simulation model is not a corpuscular model in the classical-physics sense. In our model, particles are objects that carry information. As a particle encounters a material device, it exchanges information with this device. In our model, this information exchange is the cause of the appearance of an interference pattern. In other words, in our approach we construct a mechanism which produces wave-like phenomena by local variables only. To this end, we introduce independent objects which carry information. These objects we call "particles". Each particle interacts with the material of the device only and the effect of many of such interactions is to build up a situation which causes the appearance of a first-order interference pattern.

To head off possible misunderstandings, the present chapter is not concerned with an interpretation or an extension of quantum theory nor does it affect the validity and applicability of quantum theory. Furthermore, the event-based detector models that we introduce in this chapter should not be regarded as realistic models for say, a photomultiplier or a photographic plate and the chemical process that renders the image. Our aim is to show that, in the spirit of Occam's razor, these very simple event-based models can produce interference patterns without making reference to the solution of a wave equation.

Although waves can be the physical cause of interference, the key point of our work is that it is wrong to think that waves are the **only** possible physical cause of interference: In our approach, the clicks produced by non-interacting / non-communicating detectors, caused by non-interacting / non-communicating particles that arrive at single detectors one-by-one, build up a pattern that is identical to the one that is obtained by solving a wave equation. However, our event-based simulation approach does not require knowledge of the wave amplitudes obtained by first solving the wave mechanical problem or requires the solution of the Schrödinger equation. Interference patterns appear as a result of an event-by-event simulation of classical, locally causal, adaptive dynamical systems.

The chapter is structured as follows. In Section 1.2, we introduce the interference experiments that we simulate. In Section 1.3, we review the main features of the photon detection process. Section 1.4 specifies the new detector models and the simulation algorithm in full detail. A Mathematica implementation of this algorithm for the case of the double-slit experiment can be downloaded from the Wolfram Demonstration Project web site [62]. In Section 1.5, we compare the event-by-event simulation results with the numerical results obtained from wave theory for the two-beam interference experiments discussed in Section 1.2, showing that our event-based, particle-like approach reproduces the results of quantum theory without making use of concepts thereof. In Section 1.6, we propose a realizable experiment to test our event-based

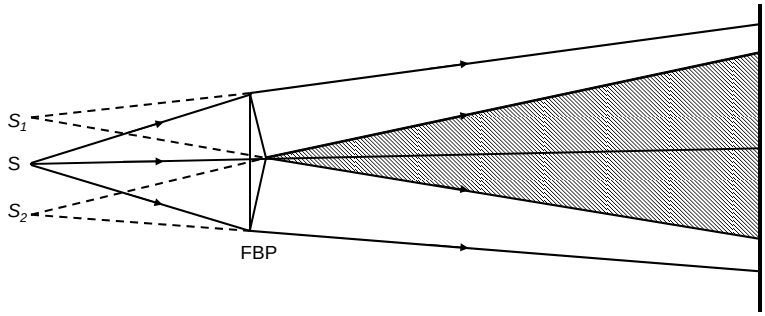

Figure 1.1: Schematic diagram of an interference experiment with a Fresnel biprism (FBP) [63]. S, S_1, S_2 denote the point source and its two virtual images, respectively. The grey area is the region in which an interference pattern can be observed.

models for interference. Our conclusions are given in Section 1.7.

1.2 Two-beam interference

In this chapter, we focus on interference experiments with single-photons, leaving the case of massive particles for further research. As a prototype problem, we consider two-beam interference experiments with a Fresnel biprism [63]. A schematic diagram of such an experiment is shown in Figure 1.1. A pencil of light, emitted by the source S, is divided by refraction into two pencils [63]. Interference can be obtained in the region where both pencils overlap, denoted by the grey area in Fig. 1.1. As a Fresnel biprism consists of two equal prisms with small refraction angle and as the angular aperture of the pencils is small, we may neglect aberrations [63]. The system consisting of the source S and the Fresnel biprism can then be replaced by a system with two virtual sources S_1 and S_2 [63], see Fig. 1.1. Alternatively, following Young [63] we can let the light impinge on a screen with two apertures and regard these apertures as the two virtual sources S_1 and S_2, see Figs. 1.2 and 1.3. Results of a single-photon interference experiment with a Fresnel biprism and a time-resolved interference experiment for the system schematically depicted in Fig. 1.3 are reported in Refs. [53] and [64], respectively.

For all these simplified systems, a straightforward application of Maxwell's theory yields the intensity at the detection screen. We consider a few representative cases for which closed-form expressions can be obtained:

- The sources S_1 and S_2 are lines of length a, separated by a center-to-center distance d, see Fig. 1.2. These sources emit light according to a uniform current distribution, that is

$$J(x,y) = \delta(x)\left[\Theta(a/2-|y-d/2|)+\Theta(a/2-|y+d/2|)\right], \tag{1.1}$$

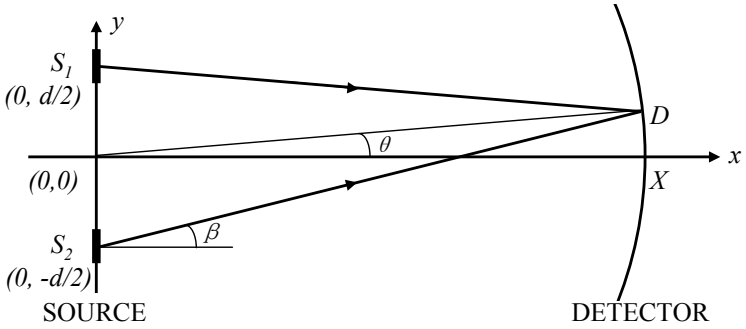

Figure 1.2: Schematic diagram of a simplified double-slit experiment with two sources S_1 and S_2 of width a, separated by a center-to-center distance d, emitting light according to a uniform current distribution (see Eq. (1.1)) and with a uniform angular distribution, β denoting the angle. The light is recorded by detectors D positioned on a semi-circle with radius X. The angular position of a detector is denoted by θ.

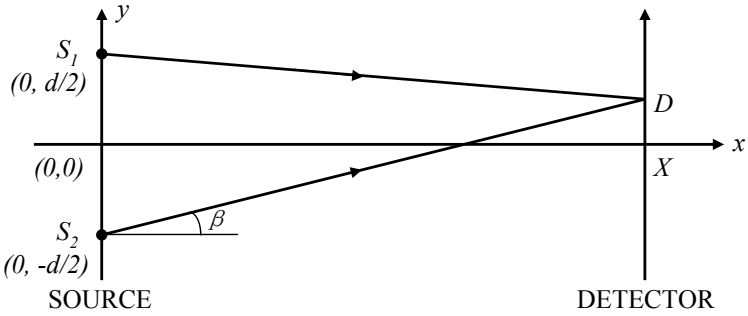

Figure 1.3: Schematic diagram of a two-beam interference experiment with two line sources S_1 and S_2 having a spatial Gaussian profile (see Eq. (1.3)), emitting light according to a uniform angular distribution, β denoting the angle. The sources are separated by a center-to-center distance d. The light is detected by detectors D positioned at (X, y).

where $\Theta(.)$ denotes the unit step function. In the Fraunhofer regime, the light intensity at the detector on a circular screen is given by [63]

$$I(\theta) = A \left(\frac{\sin \frac{qa \sin\theta}{2}}{\frac{qa \sin\theta}{2}} \right)^2 \cos^2 \frac{qd \sin\theta}{2}, \tag{1.2}$$

where A is a constant, q is the wave number, and θ denotes the angular position of the detector D on the circular screen, see Fig. 1.2.

- The sources S_1 and S_2 form a line source with a current distribution given by

$$J(x, y) = \delta(x) \sum_{s=\pm 1} e^{-(y - sd/2)^2 / 2\sigma^2}, \tag{1.3}$$

where σ is the variance and d denotes the distance between the centers of the two sources, see Fig. 1.3. The intensity of the overlapping pencils at the detector reads

$$I(y) = B\left(\cosh\frac{byd}{\sigma^2} + \cos\frac{(1-b)qyd}{X}\right)e^{-b(y^2+d^2/4)/\sigma^2}, \tag{1.4}$$

where B is a constant, $b = q^2\sigma^4/(X^2+q^2\sigma^4)$, and (X, y) are the coordinates of the detector D (see Fig. 1.3). Closed-form expression Eq. (1.4) was obtained by assuming that $d \ll X$ and $\sigma \ll X$.

- The two sources S_1 and S_2 are circles with a radius a and their centers are separated by a distance d. The current distribution is given by

$$J(x,y,z) = \delta(x)\left[\Theta(a^2/4-(y-d/2)^2-z^2) + \Theta(a^2/4-(y+d/2)^2-z^2)\right]. \tag{1.5}$$

In the Fraunhofer regime, the light intensity at a detector placed on a sphere is given by [63]

$$I(\theta) = C\left(\frac{2J_1(qa\sin\theta)}{qa\sin\theta}\right)^2\cos^2\frac{qd\sin\theta}{2}, \tag{1.6}$$

where C is a constant, θ denotes the zenith of the detector D on the spherical detection screen and $J_1(.)$ is the Bessel function of the first kind of order one.

From Eqs. (1.2), (1.4) and (1.6), it directly follows that the intensity distribution on the detection screen, displays fringes that are characteristic for interference.

1.3 Event-by-event simulation and detector model

Imagine that individual particles build up the interference pattern one by one and exclude the possibility that there is direct communication between the particles (even if one particle has arrived at the detector while another particle is at the source or at a detector). If we then simply look at Fig. 1.2 or 1.3, we arrive at the logically unescapable conclusion that the interference pattern can only be due to the internal operation of the detector: There is nothing else that can cause the interference pattern to appear.

Obviously a simple, passive detector model that only counts the number of particles fails to reproduce the interference patterns of two-beam interference experiments in which there are sources and detectors only, as in Figs. 1.2 and 1.3. Before we introduce new event-based models for the detector, it is expedient to review the conventional theory of the photon detection process.

In its simplest form, a light detector consists of a material that can be ionized by light. The electric charges that result from the ionization process are then amplified, chemically in the case of a photographic plate or electronically in the case of photo diodes

or photomultipliers. In the wave-mechanical picture, the interaction between the incident electric field $\mathbf{E}$ and the material takes the form $\mathbf{P}\cdot\mathbf{E}$, where $\mathbf{P}$ is the polarization vector of the material [63]. Treating this interaction in first-order perturbation theory, the detection probability reads $P_{detection}(t) = \int_0^t \int_0^t \langle\langle \mathbf{E}^T(t')\cdot\mathbf{K}(t'-t'')\cdot\mathbf{E}(t'')\rangle\rangle dt' dt''$ where $\mathbf{K}(t'-t'')$ is a memory kernel that is characteristic for the material only and $\langle\langle . \rangle\rangle$ denotes the average with respect to the initial state of the electric field [65]. Both the constitutive equation [63] $\mathbf{P}(\omega) = \chi(\omega)\mathbf{E}(\omega)$ as well as the expression for $P_{detection}(t)$ show that the detection process involves some kind of memory. Furthermore, very sensitive photon detectors such as photomultipliers and avalanche diodes are trigger devices, meaning that the recorded signal depends on an intrinsic threshold. Conceptually, the chemical process that renders the image encoded in the photographic material plays a similar role.

From these general considerations, it is clear that a minimal model for the detector should be able to account for the memory and the threshold behavior of the detectors. An event-based model for the detector cannot be "derived" from quantum theory, simply because quantum theory has nothing to say about individual events [1]. Therefore, from the perspective of quantum theory, any model for the detector that operates on the level of single events must necessarily appear as "ad hoc". In contrast, from the viewpoint of a contextual description, the introduction of such a model is a necessity [1].

1.4 Simulation model

In our simulation model, every essential component of the laboratory experiment such as the source, the Fresnel biprism, and detector array has a counterpart in the algorithm. The data is analyzed by counting detection events, just as in the laboratory experiment [53]. The simulation model is solely based on experimental facts.

The simulation can be viewed as a message-processing and message-passing process routing messengers through a network of units that processes messages. The processing units play the role of the components of the laboratory experiment and the network represents the complete experimental set-up. We now specify the operation of the basic components of the simulation model in full detail. Other components that are specific to a particular interference experiment are described together with the presentation of the simulation results.

1.4.1 Messenger

In our simulation approach, we view each photon as a messenger carrying a message. Each messenger has its own internal clock, the hand of which rotates with frequency f. As the messenger travels from one position in space to another, the clock encodes the time-of-flight t modulo the period $1/f$. The message, the position of the clock's hand,

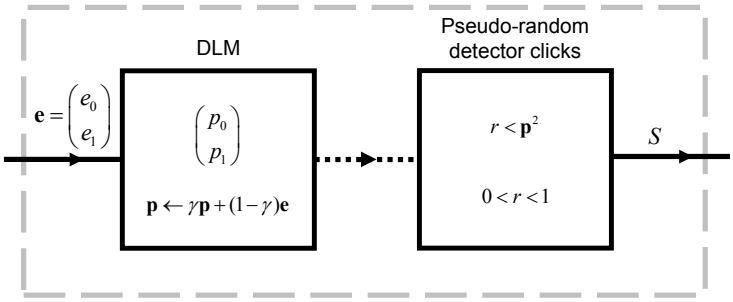

Figure 1.4: Diagram of the event-based detector model defined by Eqs. (1.7) and (1.8). The dashed line indicates the data flow within the processing unit.

is most conveniently represented by a two-dimensional unit vector $\mathbf{e}_k = (e_{0,k}, e_{1,k}) = (\cos\phi_k, \sin\phi_k)$, where the subscript $k > 0$ labels the successive messages, $\phi_k = 2\pi f t_k$, and t_k is the time-of-flight of the k-th messenger. The messenger travels with a speed c/n where c denotes the speed of light in vacuum and n is the refractive index of the medium in which the messenger moves.

1.4.2 Source

In a simulation model in which the photons are viewed as messengers, the single-photon source is trivially realized by creating a messenger and waiting until its message has been processed by the detector before creating the next messenger. This ensures that there can be no direct information exchange between the messengers, even if one particle has arrived at the detector while another particle is at the source or at a detector, implying that our simulation model (trivially) satisfies Einstein's criterion of local causality.

For the double-slit, two-beam interference, and circular slits simulations, messengers leave the source at positions generated randomly according to the current distributions Eqs. (1.1), (1.3), and (1.5), respectively. The distribution of the angle β is chosen to be uniform. When messenger k is created, its internal clock time t_k is set to zero.

1.4.3 Detector

A single photon detector, such as a photographic plate, consists of many identical detection units each having a predefined spatial window in which they can detect photons. Because these small detection units are photon detectors themselves we also name them detectors in what follows. Here we construct a processing unit that acts as a detector for individual messages. A schematic diagram of the unit is shown in Fig. 1.4. The first stage consists of a deterministic learning machine (DLM) that

receives on its input channel the kth message represented by the two-dimensional vector $\mathbf{e}_k = (\cos\phi_k, \sin\phi_k)$. In its simplest form the DLM contains a single two-dimensional internal vector with Euclidean norm less or equal than one. We write $\mathbf{p}_k = (p_{0,k}, p_{1,k})$ to denote the value of this vector after the kth message has been received. Upon receipt of the kth message the internal vector is updated according to the rule

$$\mathbf{p}_k = \gamma \mathbf{p}_{k-1} + (1-\gamma)\mathbf{e}_k, \tag{1.7}$$

where $0 < \gamma < 1$ and $k > 0$. Update rule Eq. (1.7) clearly indicates that the first stage learns from the incoming messages in a deterministic way and therefore it is given the name deterministic learning machine. Obviously, if $\gamma \neq 0$, a machine that operates according to the update rule Eq. (1.7) has memory.

The second stage of the detector (see Fig. 1.4) uses the information stored in the internal vector to decide whether or not to generate a click (threshold behavior). As a highly simplified model for the bistable character of the real photodetector or photographic plate, we let the machine generate a binary output signal S_k using the intrinsic threshold function

$$S_k = \Theta(\mathbf{p}_k^2 - r_k), \tag{1.8}$$

where $\Theta(.)$ is the unit step function and $0 \leq r_k < 1$ is a uniform pseudo-random number. Note that in contrast to experiment, in a simulation, we could register both the $S_k = 0$ and $S_k = 1$ events such that the number of input messages equals the sum of the $S_k = 0$ and $S_k = 1$ detection events. Since in experiment it cannot be known whether a photon has gone undetected, we discard the information about the $S_k = 0$ detection events in our future analysis.

The total detector count is defined as

$$N = \sum_{j=1}^{k} S_j, \tag{1.9}$$

where k is the number of messages received. Thus, N counts the number of one's generated by the machine. As noted before a detector screen is just a collection of identical detectors and is modeled as such. Each detector has a predefined spatial window within which it accepts messages.

In Appendix A we prove that as $\gamma \to 1^-$, the internal vector $\mathbf{p}_k$ converges to the average of the messages $\mathbf{e}_1, \ldots, \mathbf{e}_k$. In general, the parameter γ controls the precision with which the machine defined by Eq. (1.7) learns the average of the sequence of messages $\mathbf{e}_1, \mathbf{e}_2, \ldots$ and also controls the pace at which new messages affect the internal state of the DLM (memory effect) [55]. In Appendix B we show how to modify the update rule Eq. (1.7) such that the transient regime of the detector becomes shorter. The transient behavior of the simplest and the slightly more complicated detector models may be accessible to real experiments, as explained in Section 1.6. In appendix B, we also give an alternative for Eq. (1.8) that does not make use of pseudo-random numbers.

Before we proceed we make a few notes on the memory and threshold behavior of our detector simulation models. Although the word memory may give the impression that the detector keeps track of all the photons that pass, all the event-based detector models introduced in this chapter have barely enough memory to store the equivalent of one message. Thus, these models derive their power, not from storing a lot of data, but from the way they process successive messages. Most importantly, the DLMs do not need to keep track of the number k of messages that they receive, a number that we cannot assume to be known because in real experiments we can only count the clicks of the detector, not the photons that were not detected. As shown in Appendix C, the role of the local memory of the detector is similar to that of the dielectric function in Maxwell's theory. Our detector models do not incorporate a memory fade-out as a function of time. Although this could be an essential feature in time frames in which the detectors do not receive photons, we do not consider it to be of importance for our present study.

We also want to emphasize that the presence of a threshold does not cause our detector model to operate with less than 100% efficiency. In general, the detection efficiency is defined as the overall probability of registering a count if a photon arrives at the detector [66] Using this definition, our event-based detector model simulates an ideal single-photon detector that has 100% detection efficiency. This can easily be demonstrated by performing the simulation of an experiment (which is very different from a double-slit experiment) that measures the detection efficiency [66]. In such an experiment a point source emitting single photons (messengers) is placed far away from a single detector. As all photons that reach the detector have the same time-of-flight (to very good approximation), all the messengers that arrive at this detector will carry the same message. As a result, the internal vector rapidly converges to one, so that the detector clicks every time a photon arrives. Thus, the detection efficiency, as defined for real detectors, of our detector model is very close to 100%. Although the detection efficiency of the detector model itself is very close to 100%, the ratio of detected to emitted photons is much less than one. Note however that, in general, as is well known, a photon detector + electronics is an open system (powered by external electrical sources etc.), hence photon-energy conservation within the detector-photon system is not an issue.

1.4.4 Discussion

In our approach, interference appears as a result of processing individual events, but definitely not because we have introduced "wave-like" ingredients in a sneaky manner. In our corpuscular model, each particle carries its own clock, that is, it carries its own local oscillator. This oscillator only serves to mimic the frequency of the individual particle (photon). A the particle hits the detector, the detector "observes" the state of the oscillator that is attached to this particular particle and determines its time-of-flight. Note that the idea of introducing the time-of-flight does not mean that

we obtain interference by summing wave functions $a_k e^{-i\omega t_k}$ where t_k denotes the time-of-flight of the kth particle.

There is no communication/interaction between the detectors that make up the detection screen, hence there is no wave equation (i.e. no partial differential equation) that enforces a relation between the internal variables of these detectors. Likewise, the oscillator that is carried by a particle never interacts with an oscillator of another particle, hence the motion of these two oscillators is also not governed by a wave equation. Naively, one might imagine the oscillators tracing out a wavy pattern in space as they travel from the source to the detector screen. However, in our model there is no relation between the times at which the particles leave the source, hence it is impossible to characterize all these traces by a field that depends on one set of space-time coordinates, as required for a wave theory.

1.5 Simulation results

First, we demonstrate that our event-by-event simulation model reproduces the wave mechanical results Eq. (1.2) of the double-slit experiment. Second, we simulate a two-beam interference experiment and show that the simulation data agree with Eq. (1.4). Third, we validate the simulation approach by reproducing the interference patterns for two circular sources, see Eq. (1.6). Finally, we present the results for the simulation of the single-photon interference experiment with a Fresnel biprism [53], see Fig. 1.1. The results presented in this section have all been obtained using the detector model described in Section 1.4. Simulation data produced by the detector models described in Appendix B are given in Section 1.6.

1.5.1 Double-slit experiment

As a first example, we consider the two-slit experiment with sources that are slits of width $a = \lambda$ ($\lambda = 670$ nm in all our simulations), separated by a center-to-center distance $d = 5\lambda$, see Fig. 1.2. In Fig. 1.5(a), we present the simulation results for a source-detector distance $X = 0.05$ mm. When a messenger (photon) travels from the source at $(0, y)$ to the circular detector screen with radius X, it updates its own time-of-flight, or equivalently its angle ϕ. This time-of-flight is calculated according to geometrical optics [63]. More specifically, a messenger leaving the source at $(0, y)$ under an angle β (see Fig. 1.2) will hit the detector screen at a position determined by the angle θ given by

$$\sin\theta = z\cos^2\beta + \sin\beta\sqrt{1 - z^2\cos^2\beta}, \tag{1.10}$$

where $z = y/X$ and $|z| < 1$. The distance traveled is then given by

$$s = X\sqrt{1 - 2z\sin\beta + z^2}, \tag{1.11}$$

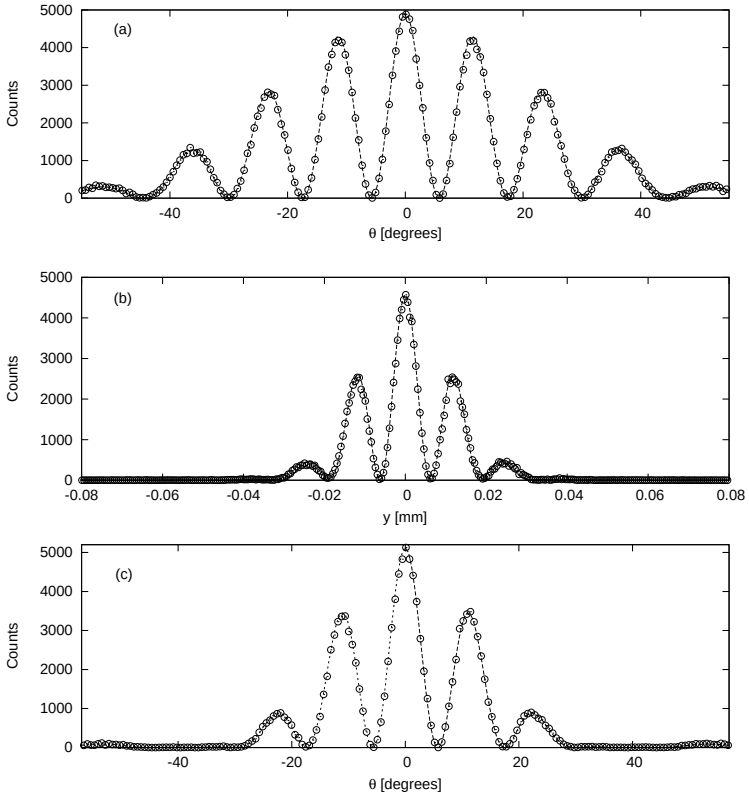

Figure 1.5: Detector counts as a function of the angular (spatial) detector position θ (y) as obtained from event-by-event simulations of the interference experiment shown in Fig. 1.2 (Fig. 1.3). The circles denote the event-based simulation results produced by the detector model defined in Section 1.4. The dashed lines are the results of wave theory (see Eqs. (1.2), (1.4) and (1.6)). (a) The sources are slits of width $a = \lambda$ ($\lambda = 670$ nm in all our simulations), separated by a distance $d = 5\lambda$ and the source-detector distance $X = 0.05$ mm, see Fig. 1.2. The sources emit particles according to the current distribution Eq. (1.1). An interactive program for the double-slit simulation can be downloaded from the Wolfram Demonstration Project web site [62]; (b) The sources S_1 and S_2, separated by a distance $d = 8\lambda$, emit particles according to a Gaussian current distribution Eq. (1.3) with variance $\sigma = \lambda$ and mean $d/2$ and $-d/2$, respectively (see Fig. 1.3). The source-detector distance $X = 0.1$ mm; (c) The two circular sources S_1 and S_2 of radius $a = \lambda$ with centers separated by a distance $d = 5\lambda$ emit particles according to the current distribution Eq. (1.5). The distance between the center of the two-source system and the spherical detection screen is $X = 0.1$ mm.

and hence the message is determined by the angle $\phi = 2\pi f s/c$ where c is the speed of light. As the messenger hits a detector, the detector updates its internal vector and decides whether to output a zero or a one.

This process is repeated many times. The initial y-coordinate of the messenger is chosen randomly from a uniform distribution on the interval $[-d/2 - a/2, -d/2 + a/2] \cup [+d/2 - a/2, +d/2 + a/2]$. The angle β is a uniform pseudo-random number between $-\pi/2$ and $\pi/2$.

The markers in Fig. 1.5(a) show the event-by-event simulation results produced by the detector model described in Section 1.4 with $\gamma = 0.999$. We used a set of thousand detectors positioned equidistantly in the interval $[-57^o, 57^o]$, each of them receiving on average by six thousand photons.The number of clicks generated by the detectors, that is the number of so-called detected photons, is approximately 16.10^5. Hence, the ratio of detected to emitted photons is of the order 0.25, a fairly large number compared to those achieved in laboratory experiments with single-photons (see Section 1.5.4). The result of wave theory, as given by the closed-form expression Eq. (1.2), is represented by the dashed line. Without using any knowledge about the solution of a wave equation, the event-based simulation (markers) reproduces the results of wave theory.

According to our mathematical analysis of the performance of the machines (see Appendix A), accurate results (relative to the predictions of quantum theory) are to be expected for γ close to one only. Taking for instance $\gamma = 0.99$ does not change the qualitative features although it changes the number of counts by small amounts (data not shown).

An interactive Mathematica program of the event-based double-slit simulation which allows the user to change the model parameters and to verify that the simulation reproduces the results of wave theory may be downloaded from the Wolfram Demonstration Project web site [62].

1.5.2 Two-beam interference experiment

As a second example we consider the two-beam interference experiment depicted in Fig. 1.3. We assume that the messengers leave either source S_1 or S_2 from a position y that is distributed according to a Gaussian distribution with variance σ and mean $+d/2$ or $-d/2$, respectively. Also in this case, the time-of-flight is calculated according to geometrical optics [63]. A messenger leaving the source at $(0, y)$ under an angle β (see Fig. 1.3) will hit the detector screen at a position (X, y')

$$y' = X \tan\beta + y, \tag{1.12}$$

the distance traveled is given by $s = X \sec\beta$ and the message is determined by the angle $\phi = 2\pi f s/c$ where c is the speed of light.

The simulation results for a source-detector distance $X = 0.1$ mm, for $\gamma = 0.999$ are shown in Fig. 1.5(b). The dashed line is the result of wave theory, see closed form expression Eq. (1.4). Also in this case, the agreement between wave theory and the event-by-event simulation is extremely good.

1.5.3 Double-slit experiment with circular sources

As a third example, we consider the double-slit experiment with circular sources, a straightforward extension of the two-dimensional double-slit system to three dimen-

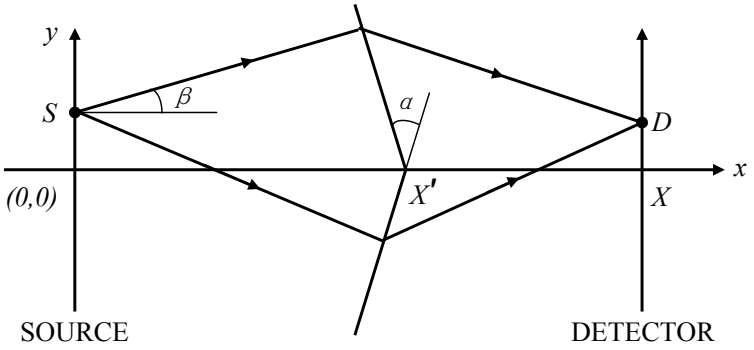

Figure 1.6: Schematic diagram of the simulation setup of a single-photon experiment with a Fresnel biprism. The apex of the Fresnel biprism with summit angle α is positioned at $(X', 0)$. In the simulation, a line source emits particles from positions drawn from the current distribution Eq. (1.13) with random angles β chosen uniformly from the interval $[-\alpha/2, \alpha/2]$. The detectors D positioned at (X, y) count the photons.

sions. As shown in Fig. 1.5(c), there is excellent agreement between the event-by-event simulation and the analytical expression Eq. (1.6).

1.5.4 Experiment with a Fresnel biprism

Finally, we consider the single-photon experiment with a Fresnel biprism [53]. Figure 1.6 shows the schematic representation of the single-photon interference experiment that we simulate. For simplicity, we assume that the source S is located in the Fresnel biprism. Then, the results do not depend on the dimensions of the Fresnel biprism. Simulations with a Fresnel biprism of finite size yield results that differ quantitatively only (results not shown).

Messengers are created at positions drawn randomly from the distribution

$$J(x, y) = \delta(x) e^{-y^2/2\sigma^2}, \tag{1.13}$$

As in all other cases, the time-of-flight of the messenger is calculated according to the rules of geometric optics [63]. A messenger starting at $(0, y)$ with angle β (see Fig. 1.6) leaves the Fresnel biprism at

$$\begin{aligned} x_\pm &= \frac{X' \mp y \tan\alpha/2}{1 \pm \tan\beta \tan\alpha/2}, \\ y_\pm &= \frac{y' + X' \tan\beta}{1 \pm \tan\beta \tan\alpha/2}, \end{aligned} \tag{1.14}$$

where the sign has to be chosen such that $x_\pm \leq X'$ and $\pm y_\pm \geq 0$, that is such that the path of the messenger crosses the Fresnel biprism boundary. Using the fact

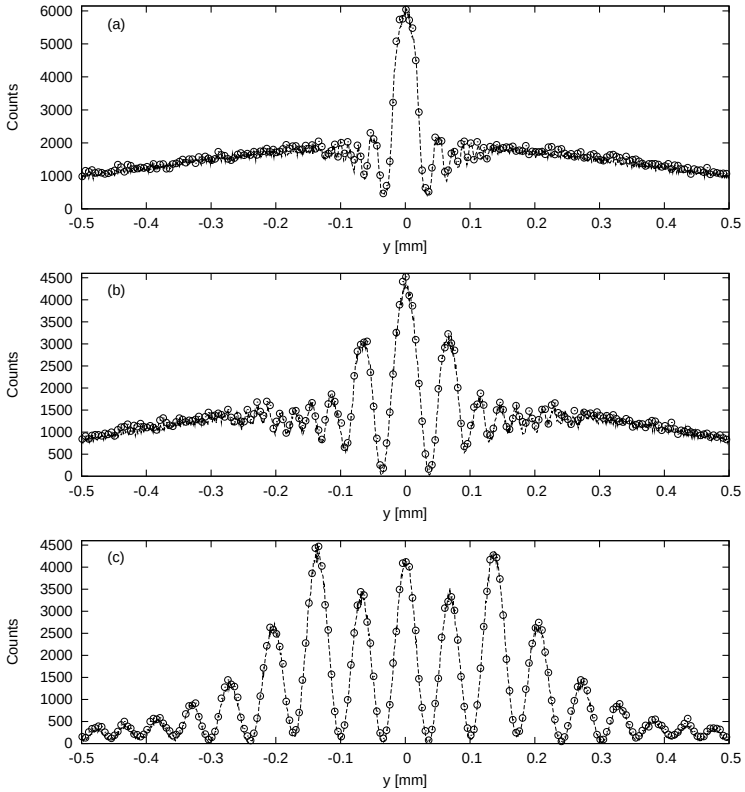

Figure 1.7: Detector counts as a function of the detector position y of the detector array positioned at X for a single photon interference experiment with a Fresnel biprism (see Fig. 1.6). The Fresnel biprism has an index of refraction $n = 1.5631$ and a summit angle $\alpha = 1^\circ$. Its apex is positioned at $(X', 0)$ with $X' = 45$ mm. The source emits particles according to a Gaussian current distribution with variance $\sigma = 0.531$ mm and wavelength $\lambda = 670$ nm [53]. The circles denote the event-based simulation results. The dashed lines denote the numerical results as obtained from wave theory. (a) $X - X' = 7$ mm; (b) $X - X' = 15$ mm; (c) $X - X' = 55$ mm. Thousand detectors where used to record the individual events.

that the tangential component of the velocity is continuous across the Fresnel biprism boundary [63], we have

$$\beta'_{\pm} = \frac{\pm\alpha}{2} + \arcsin\left[n \sin(\beta \mp \frac{\alpha}{2})\right], \tag{1.15}$$

and we find that the messenger hits the screen at $D = (X, (X - x_{\pm}) \tan\beta'_{\pm} + y_{\pm})$ and that the total time traveled is given by

$$t = n\frac{x_{\pm}}{c} \sec\beta + \frac{X - x_{\pm}}{c} \sec\beta'_{\pm}. \tag{1.16}$$

In the simulation, the angle of incidence β of the photons is selected randomly from the interval $[-\alpha/2, \alpha/2]$, where α denotes the summit angle of the Fresnel biprism. A

collection of representative simulation results for $\gamma = 0.999$ is presented in Fig. 1.7. The dashed lines are the numerical results obtained from wave theory by Monte Carlo sampling. Again, we find that there is excellent quantitative agreement between the event-by-event simulation data and wave theory. Furthermore, the simulation data presented in Fig. 1.7 is qualitatively very similar to the results reported in Ref. [53] (compare with Fig. 4(d) and Fig. 5(a)(b) of Ref. [53]). Figure 4(c) and (4d) of Ref. [53] are made of approximately 20000 photocounts on the CCD camera, while the number of photodetections on the avalanche photodiodes in absence of the CCD camera would be 40.10^6 during the exposure time of 2000 s. Hence the ratio of detected to emitted photons is of the order of 0.0005. This ratio is much smaller than what we observe in our idealized simulation experiment. Namely, each of the thousand detectors making up the detection area is hit on average by sixty thousand photons and the number of clicks generated by the detectors is approximately 16.10^5. Hence, the ratio of detected to emitted photons is of the order of 0.026, much larger than the 0.0005 observed in experiment [53].

1.6 Experimental tests: A proposal

The simulation models that we propose in this chapter make specific predictions that may be tested by carefully designed, time-resolved single-photon interference experiments. However, not all experiments one can think off are as easy to realize. One of the simplest proposals to test the simulation models would be to consider a large number (M) of identical and independent two-beam (or double-slit) interference experiments in which only one photon is detected at each of the M detection screens. According to quantum theory, summing up the single spots of the M detection screens gives the same interference pattern as if one would conduct one two-beam interference experiment with M photons being detected on the same detection screen (all under the assumption that every time a photon is emitted and that all emitted photons are detected). For this experiment, the simulation models that we have introduced do not yield an interference pattern, as is clear from their description. Thus, at least in principle, this experiment should be able to refute the corpuscular model. Note that in the absence of any experimental evidence and bearing in mind that quantum theory has nothing to say about individual events [1], it is only a hypothesis that the experiment with finite M will yield results that agree with quantum theory. Whether this hypothesis is actually true remains to be demonstrated by an experiment. Unfortunately, in practice, this experiment may be difficult to realize, the central question being how large M should be before one observes a pattern that resembles the one predicted by wave theory. A rough estimate, based on experiments with electrons [67] suggests that $M > 50000$, a number which makes this proposal very hard to realize in practice. Therefore, we propose another experiment that may be realizable with present-day technology.

As explained earlier, if our simulation models operate in the stationary-state regime,

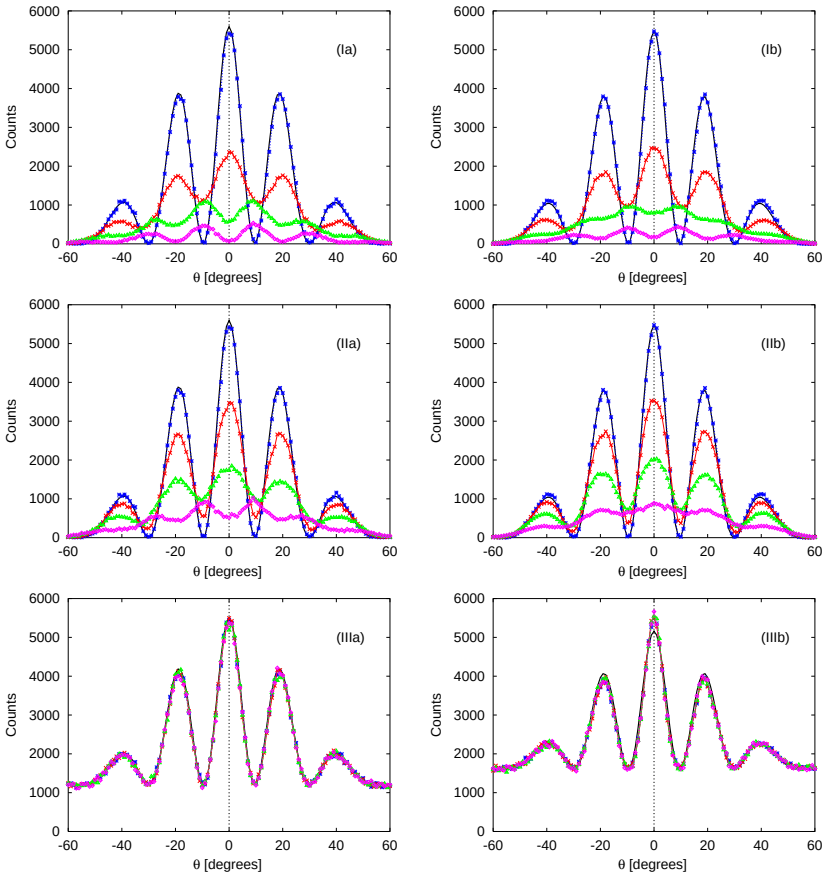

Figure 1.8: (color online) Detector counts as a function of the angular detector position θ for the interference experiment shown in Fig. 1.2 which employs only one single-photon detector that is swept over the half circle with a fixed angular velocity. The results are obtained from event-by-event simulations with six different detector models. The line sources have a width $a = \lambda$ are separated by a center-to-center distance $d = 3\lambda$, and $X = 0.05$ mm (see Fig. 1.2). The labels in the figures indicate the detector model (algorithms) used. Roman numbers refer to the DLM update rule. The letters a and b refer to the pseudo-random and deterministic generation of clicks, respectively. Ia: Eqs. (1.7) and (1.8); Ib: Eqs. (1.7) and (1.24); IIa: Eqs. (1.22) and (1.8); IIb: Eqs. (1.22) and (1.24); IIIa: Eqs. (1.23) and (1.8); IIIb: Eqs. (1.23) and (1.24). Stars: $N_{sweeps} = 1$; Crosses: $N_{sweeps} = 25$; Triangles: $N_{sweeps} = 50$; Diamonds: $N_{sweeps} = 100$; Solid lines: Wave theory, see Eq. (1.2). Other lines are guide to the eye only.

they reproduce the wave theoretical results. Therefore, to falsify our event-based models the single-photon experiment should be designed such that it is sensitive to the transient behavior of the whole setup. In other words, the experiment should operate on a time scale that is sufficiently short to prevent the DLM in our detector models to reach the stationary state. For a fair comparison between experiment and our simulation models, it is essential that the experimenter does not discard data

that is recorded during the "calibration" or "warm-up" stage because this data may contain valuable information about the transient behavior of the experimental setup.

In this section, we use our simulation approach to make predictions of laboratory experiments that may be realizable. Consider again the double-slit experiment depicted in Fig. 1.2 but instead of having many detectors at different angles θ, we use only one detector placed on a goniometer. The idea is to keep the total exposure time constant while the detector is swept back-and-forth over (part of) the half-circle (see Fig. 1.2). In our simulation models, the recorded interference pattern will then depend on the angular velocity of the detector. For velocities that are sufficiently small to allow the DLM to reach the stationary state, the interference pattern obtained agrees with the one predicted by wave theory. On the other hand, if the detector position changes rapidly, the DLM may not receive enough events to accurately reproduce the wave mechanical result. Therefore, if we keep the total exposure time constant and perform a set of experiments for several choices of the sweep velocity, our simulation models predict that the interference patterns will change and that these changes reflect the internal dynamics of the detector model used.

The procedure that we propose is the following. First, we fix the angle $\delta\theta$ by which the detector position will be moved. For simplicity, we assume that the aperture of the detector is equal to $\delta\theta$. Then, we fix the total number of events N_{total} which, on average, will arrive within each arc of angle $\delta\theta$. Finally, we select the number of times N_{sweeps} that the detector will be swept back-and-forth over the half circle.

In the simulation, the internal variables of the detector models are initialized once. The simulation results presented in this section have been obtained using $\delta\theta = 1^\circ$, $N_{total} = 10^6$, $N_{sweeps} = 1, 25, 50, 100$, $\gamma = 0.999$, and for the modified detector models introduced in Appendix B, $\kappa = 0.9$, $w_0 = 0.9$ and $\nu = 0.99$. In all figures, the theoretical result Eq. (1.2) is rescaled to fit to the maximum of the simulation data at the smallest sweep velocity and, in the case of IIIa and IIIb, also shifted to account for the non-zero bias.

As explained in Appendix B, the simple detector model introduced in Section 1.4 with the DLM defined by Eq. (1.7) may require a significant amount (order of thousands) of input events to reach the stationary state. Hence, if we move the detector before the DLM reaches its stationary state, this detector model may not produce results that agree with wave theory. This expectation is confirmed by the results shown in Figs. 1.8(Ia) and (Ib). If the detector moves slowly ($N_{sweeps} = 1$), the event-based simulation data are in concert with wave theory, as is clear from the comparison of the stars and the solid lines in Figs. 1.8(Ia) and (Ib). From Figs. 1.8(Ia) and (Ib) it is also clear that increasing the number of sweeps to $N_{sweep} = 25$ (recall that the total amount of events corresponding to the total exposure time in the experiment is fixed) leads to a reduction of the visibility of the fringes. If we increase the number of sweeps to $N_{sweep} = 50$, the detector model fails qualitatively.

Thus, an experiment that uses a moving detector might be able to rule out event-based models Ia and Ib as candidate descriptions of the single-photon interferences.

However, this does not yet imply that our approach as such should be abandoned: It may be that the detector model is too simple. Therefore, it is of interest to explore to what extent the results depend on the particular algorithms used.

It is not difficult to modify the DLM defined by Eq. (1.7) such that the convergence to the stationary state is much faster or that the response to changes in the input data is faster. In Appendix B, we give the details of two of such variants.

DLM II is constructed such that its stationary state behavior is the same as that of the simple DLM (Eq. (1.7)), hence the detector model using this DLM reproduces the results of wave theory if we employ an array of detectors or move the single detector very slowly. From Figs. 1.8(IIa) and (IIb), we may conclude that this model is an improvement over the simple model in that it still shows interference fringes at a sweeping rate of $N_{sweep} = 50$. For $N_{sweeps} = 100$, the detector receives approximately $N_{total}/(180N_{sweeps}/\delta\theta) \approx 55$ events before it moves to the next position. With this small amount of input events, DLM II does not reach the stationary state (see also Fig. 1.9).

DLM III is a little different than DLM II: It is sensitive to differences between the internal state and the input message. As Figs. 1.8(IIIa) and (IIIb) show, these detector models produce output signals that are insensitive to the speed at which the detector moves but this comes at the price of a nonzero bias which is, within statistical fluctuations, independent of the detector position or velocity. Subtracting this bias, all the data fit the theoretical curve very well.

Summarizing: For experiments that use detectors that have fixed positions, our event-based models for the detector yield results that cannot be distinguished from those of wave theory. However, our simulation models for single-photon two-beam interference show features that may be tested experimentally by measuring the intensity as a function of the speed of a moving detector. We have proposed and analyzed a realizable, time-resolved experiment that directly probes the dynamics of our detector models and predicted the outcome of such future experiments.

1.7 Conclusion

We have demonstrated that it is possible to give a corpuscular description for single-photon interference experiments with a double-slit, two beams, and with a Fresnel biprism. Our event-by-event simulation model

- does not require any knowledge about the solution of a wave equation,
- reproduces the results from wave theory,
- satisfies Einstein's criterion of local causality,
- provides a simple, logically consistent, particle-based description of interference.

We do not exclude that there are other event-by-event algorithms that reproduce the interference patterns of wave theory. For instance, in the case of the single-electron experiment with the biprism [67], it may suffice to have an adaptive machine handle the electron-biprism interaction without having adaptive machines modeling the detectors. We leave this topic for future research.

We hope that our simulation results will stimulate the design of new time-resolved single-photon experiments to test our corpuscular model for interference. In Section 1.6, we proposed such an experiment and also predicted the outcome if our simulation model captures the essence of the event-based processes. Note however that the models we have employed are not unique, as shown explicitly in Section 1.4. This leaves some freedom to adapt the simulation models to the actual experiments that will be performed.

Finally, it may be of interest to mention that our approach opens a route for incorporating interference phenomena into ray-tracing software. In our simulation method, each messenger simply follows one of the rays through the medium, updating the message (corresponding to the phase information) as it travels along. Therefore, for applications where the solution of the Maxwell equations is prohibitive, the combination of our technique and ray tracing may be a viable alternative.

1.8 Appendix A

We demonstrate that as $\gamma \to 1^-$ the internal vector $\mathbf{p}_k$ in Eq. (1.7) converges to the average of the messages $\mathbf{e}_1, \mathbf{e}_2, \ldots$.

Let $\|\mathbf{x}\|$ denote the Euclidean norm of the vector $\mathbf{x}$. Then, as $0 < \gamma < 1$, $\|\mathbf{e}_k\| = 1$ for all $k > 0$, and $\|\mathbf{p}_0\| = 1$ it follows immediately from Eq. (1.25) that $\|\mathbf{p}_k\| \leq 1$ for all $k > 0$, hence $\lim_{k\to\infty} \mathbf{p}_k$ exists. To determine $\mathbf{p} = \lim_{k\to\infty} \mathbf{p}_k$, we have to make assumptions about the properties of the sequence $\{\mathbf{e}_1, \mathbf{e}_2, \ldots\}$. For instance, if the sequence $\{\mathbf{e}_1, \mathbf{e}_2, \ldots\}$ is generated by a stochastic process with mean $\langle \mathbf{e}_{j+1} \rangle = \mathbf{e}$ for $j = 0, \ldots, k-1$, then it is easy to show that $\mathbf{p} = \mathbf{e}$. Thus, in this case, the machine defined by the rule Eq. (1.7) learns the average $\mathbf{e}$ by updating its internal vector for each message it receives.

In practice, only finite sequences $\{\mathbf{e}_1, \mathbf{e}_2, \ldots, \mathbf{e}_K\}$ are available. In this case, we can estimate the limiting value by assuming that the sequence repeats itself, an assumption that is common in Fourier analysis and signal processing in general [68]. From

Eq. (1.25), we have

$$\begin{aligned}\mathbf{p}_{nK} &= \gamma^K \mathbf{p}_{(n-1)K} + (1-\gamma)\sum_{j=(n-1)K}^{nK-1} \gamma^{nK-j-1}\mathbf{e}_{j+1} \\ &= \gamma^K \mathbf{p}_{(n-1)K} + (1-\gamma)\sum_{j=0}^{K-1} \gamma^{K-j-1}\mathbf{e}_{j+1+(n-1)K} \\ &= \gamma^K \mathbf{p}_{(n-1)K} + (1-\gamma)\mathbf{f}_K, \end{aligned} \tag{1.17}$$

where

$$\mathbf{f}_K = \sum_{j=0}^{K-1} \gamma^{K-j-1}\mathbf{e}_{j+1}, \tag{1.18}$$

and $n > 0$. From Eq. (1.17) we find

$$\mathbf{p}_{nK} = \gamma^{nK}\mathbf{p}_0 + (1-\gamma)\frac{1-\gamma^{nK}}{1-\gamma^K}\mathbf{f}_K, \tag{1.19}$$

and hence

$$\lim_{n\to\infty} \mathbf{p}_{nK} = \frac{1-\gamma}{1-\gamma^K}\sum_{j=0}^{K-1} \gamma^{K-j-1}\mathbf{e}_{j+1}, \tag{1.20}$$

such that

$$\lim_{\gamma\to 1^-}\lim_{n\to\infty} \mathbf{p}_{nK} = \frac{1}{K}\sum_{j=0}^{K-1} \mathbf{e}_{j+1}. \tag{1.21}$$

From Eq. (1.21), we conclude that as $\gamma \to 1^-$ the internal vector $\mathbf{p}_k$ converges to the average of the messages $\mathbf{e}_1, \ldots, \mathbf{e}_K$. In general, the parameter γ controls the precision with which the machine defined by Eq. (1.7) learns the average of a sequence of messages and also controls the pace at which new messages affect the internal state of the learning machine [55].

1.9 Appendix B

Without performing any simulation, we can already see from Eq. (1.7) that the simple machine may not perform very well in some cases. Suppose that $\mathbf{p}_0 = 0$ and that $\mathbf{e}_k = \mathbf{e}$ for all k. Then, from Eq. (1.7) it follows that $\mathbf{p}_k = (1-\gamma^k)\mathbf{e}$ such that $\|\mathbf{p}_k - \mathbf{e}\| = \gamma^k$. Although the latter equation shows that the convergence of $\mathbf{p}_k$ to the input vector $\mathbf{e}$ is exponentially fast, for γ very close to one, in practice, it may take quite a number of events to reach the stationary state.

In this Appendix, we describe two modifications of the algorithm Eq. (1.7) of the first stage (DLM) and one alternative for the algorithm Eq. (1.8) of the second stage. The modifications of the first stage reduce the amount of events required for the detector

model to reach the stationary regime. The alternative for the second stage eliminates the need for a pseudo-random number generator.

It is not difficult to modify the machine such that its asymptotic behavior remains the same while improving, significantly, the speed with which it learns from the input $\mathbf{e}_k$. A simple, but by no means unique, modification is to add one memory element to store one variable, denoted by w_k, which keeps track of the differences between $\mathbf{p}_k$ and $\mathbf{p}_{k-1}$. For $k > 0$, these variables are updated according to the rule

$$\begin{aligned} \mu_{k-1} &= \gamma(1 - w_{k-1}), \\ \mathbf{p}_k &= \mu_{k-1}\mathbf{p}_{k-1} + (1 - \mu_{k-1})\mathbf{e}_k, \\ w_k &= \kappa w_{k-1} + (1 - \kappa)\frac{\|\mathbf{p}_k - \mathbf{p}_{k-1}\|}{2}, \end{aligned} \tag{1.22}$$

where $0 < \kappa < 1$ is another control parameter and $0 \leq w_0 \leq 1$. Although the variable μ_k is redundant, we wrote Eq. (1.22) such that it is obvious that it is an extension of Eq. (1.7). In essence, instead of keeping γ fixed in the rule to update $\mathbf{p}_k$ (see Eq. (1.7)), in Eq. (1.22), the value of μ_k in the rule to update $\mathbf{p}_k$ is made variable. This flexibility is then exploited through the first and last rule in Eq. (1.22). The last rule defines a machine that learns the distance between $\mathbf{p}_k$ and $\mathbf{p}_{k-1}$, the learning speed being controlled by κ. The basic idea is that if this distance is large (say close to but less than 2), the last rule will drive w_k to one such that μ_k is small and the change of $\mathbf{p}_k$ may be large. In the opposite situation, the last rule will force w_k to zero and $\mathbf{p}_k$ will change by small amounts (assuming γ is close to but less than one). As $\mu_k \leq \gamma$, the asymptotic behavior of the machine defined by the rule Eq. (1.22) is easily shown to be the same as that of the simple version in which we keep $\mu_k = \gamma$. Thus, although equations that govern the dynamics of the machine Eq. (1.22) are nonlinear (in the $\mathbf{p}$'s), asymptotically the dynamics is governed by the linear equation Eq. (1.7).

It is not easy to study the transient behavior of the classical, dynamical systems defined by Eqs. (1.7) and (1.22) by analytical methods but it is almost trivial to simulate these models on a computer. In Fig. 1.9, we show some representative simulation results to illustrate that the slightly more complicated machine Eq. (1.22) performs significantly better than the simple machine Eq. (1.7) with respect to the number of events it takes for the machine to reach the stationary state. Roughly speaking, after about 60 events, machine Eq. (1.22) has learned enough to reproduce the correct averages. As expected on theoretical grounds, both machines converge to the same stationary state.

A minor modification of algorithm Eq. (1.22) yields the DLM defined by

$$\begin{aligned} \mu_{k-1} &= \gamma(1 - w_{k-1}), \\ \mathbf{p}_k &= \mu_{k-1}\mathbf{p}_{k-1} + (1 - \mu_{k-1})\mathbf{e}_k, \\ w_k &= \kappa w_{k-1} + (1 - \kappa)\frac{\|\mathbf{p}_k - \mathbf{e}_k\|}{2}. \end{aligned} \tag{1.23}$$

Note that the only change is in the third rule where we replaced $\mathbf{p}_{k-1}$ by $\mathbf{e}_k$. This replacement causes the machine to respond very fast to changes in the sequence of

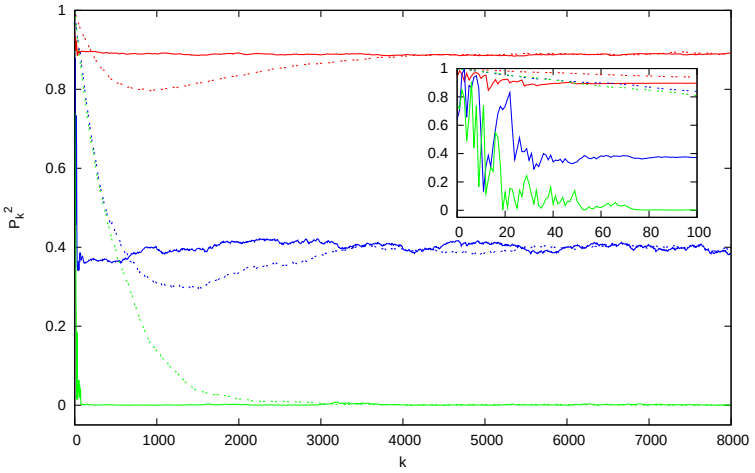

Figure 1.9: (color online) The square of the length of the internal vector $\mathbf{p}_k^2$ as a function of the number of received events k for three different input messages $\mathbf{e}_k = (r_k^{1/2}, (1-r_k)^{1/2})$ (top lines), $\mathbf{e}_k = (\cos \pi r_k, \sin \pi r_k)$ (middle lines), and $\mathbf{e}_k = (\cos 2\pi r_k, \sin 2\pi r_k)$ (bottom lines) where the $0 \leq r_k < 1$ are uniform pseudo-random numbers. Dashed lines: Model Eq. (1.7). Solid lines: Model Eq. (1.22) with $\kappa = 0.9$. The inset shows the short-time response of models Eq. (1.7) and Eq. (1.22) in more detail. In all cases $\mathbf{p}_0 = (1, 0)$, $w_0 = 0.9$ and $\gamma = 0.999$.

input messages $\{\mathbf{e}_k\}$ but, at the same time, also leads to a reduction of the average value of μ_{k-1} which in turn, will cause the detector model to produce a nonzero signal, independent of the input messages (see Figs. 1.8(IIIa) and (IIIb)).

As an alternative to the pseudo-random "click generator" Eq. (1.8), we may generate the clicks by means of a very simple DLM [56] containing a single internal variable $0 \leq z_k \leq 1$ that is updated according to

$$\begin{aligned} S_k &= \begin{cases} 0 & \text{if } |\mathbf{p}_k^2 - \nu z_{k-1}| < |\mathbf{p}_k^2 - \nu z_{k-1} - 1 + \nu| \\ 1 & \text{otherwise} \end{cases}, \\ z_k &= \nu z_{k-1} + (1-\nu) S_k. \end{aligned} \tag{1.24}$$

Here, the parameter $0 < \nu < 1$ plays the same role as γ in Eq. (1.7). The non negative number $\mathbf{p}_k^2$ is the input message for the DLM. The dynamics of the system defined by Eq. (1.24) is very different from that of Eq. (1.7) [56]. Elsewhere, we have shown that for a fixed input message $\mathbf{p}^2$, the machine defined by Eq. (1.24) generates a binary sequence (the S_k's) such that in the long run the ratio of the number of ones relative to the total number of events is equal to the time average of $\mathbf{p}_k^2$ [56]. Thus, the machine defined by Eq. (1.24) produces clicks with a rate that is determined by $\mathbf{p}_k^2$.

1.10 Appendix C: Relation between simulation model and wave mechanics

The simulation results presented in Section 1.5 demonstrate that the event-based model is capable of reproducing the results of wave theory without making recourse to the solution of the wave equation or even a single concept of wave theory. As there seems to be a general consensus that such models are not supposed to exist, it is of interest to show that for the problems that we deal with in this chapter, the event-based model contains the description that derives from Maxwell's equations.

Our demonstration consists of two steps. First we relate the variables of the event-based model to those of classical electrodynamics. Second, in analogy with the derivation of the diffusion equation from the discrete random walk model, we show how our event-based model leads to the Debye model for the interaction between material and electric field. Other models such as the Drude or Lorentz model can be derived in a similar manner but to keep the presentation concise, these derivations are relegated to a future paper.

As is evident from Table 1.1, the messenger can be viewed as the event-based equivalent of a classical, linearly polarized electromagnetic wave with frequency f: The message $\mathbf{e}_k$ corresponds to a plane wave with wave vector $\mathbf{q}$ ($q = 2\pi f/c$). The time-of-flight t_k corresponds to the phase of the electric field. Adding another clock to the messenger suffices to model the second electric field component orthogonal to the first one, and hence the fully polarized plane wave [60]. For the systems studied in the present chapter including this extra feature, namely the equivalent of the polarization of the wave, is not necessary and therefore we confine the discussion to messages that are represented by two-dimensional unit vectors.

The internal vector $\mathbf{p}_k$ plays the role of the polarization vector $\mathbf{P}(t)$ of the detector material. Indeed, comparing the formal solution of Eq. (1.7)

$$\mathbf{p}_k = \gamma^k \mathbf{p}_0 + (1-\gamma)\sum_{j=0}^{k-1} \gamma^j \mathbf{e}_{k-j}, \tag{1.25}$$

with the constitutive equation

$$\mathbf{P}(t) = \int_0^t \chi(u)\mathbf{E}(t-u)du, \tag{1.26}$$

in Maxwell's theory [63], it is clear that both equations have the same mathematical structure: The left hand sides are convolutions of the incoming (applied) message (field) with memory kernel γ^j ($\chi(u)$) (in applications, we may assume that the initial value $\mathbf{p}_0 = 0$). Thus, the DLM is a simple model for the interaction of the individual photons with the material of the detector. The time-of-flight, corresponding to the phase of the electric field, is used to update the internal vector which corresponds to the polarization vector of the material.

Table 1.1: Correspondence between Maxwell's theory and the particle-based, event-by-event simulation model. For simplicity of presentation, we consider the case of a linearly polarized wave only.

	Classical electrodynamics	Event-based simulation model
Description	wave	particle
Properties	oscillator frequency f direction $\mathbf{q}$ propagation time t phase velocity c	oscillator frequency f direction $\mathbf{q}$ time-of-flight t_k velocity c
Message	$\mathbf{E} = \mathbf{E_0}\cos(\omega t - \mathbf{q}\cdot\mathbf{r} + \varphi)$	$\mathbf{e}_k = (\cos 2\pi f t_k, \sin 2\pi f t_k)$
Material	Polarization $\mathbf{P}(t)$	Internal vector $\mathbf{p}_k$
Interaction with material	$\mathbf{P}(t) = \int_0^t \chi(u)\mathbf{E}(t-u)du$	$\mathbf{p}_k = \gamma\mathbf{p}_{k-1} + (1-\gamma)\mathbf{e}_k$

Next, we show that this analogy can be carried much further by mimicking the derivation that relates the discrete random walk on a line to the one-dimensional diffusion equation [69]. The essential steps for both the random walk and our event-based detector model are summarized in Table 1.2. Both models describe a process that proceeds in discrete time steps τ. The random walk model is formulated on a lattice with mesh size δ. In the case of the random walk, we let the time step τ and mesh size δ go to zero. In the event-based model we let the time step τ, that is the time between the arrival of successive messages, approach zero and let γ approach one. For both models, we demand that the resulting continuum equations make sense. This enforces relations between τ and δ^2 and between τ and γ, as shown in Table 1.2. Then, the former relation yields an explicit expression of the diffusion coefficient $D = \delta^2/2\tau$ in terms of the length and time scale of the discrete random walk model. Likewise, the latter leads to the Debye model for a dispersive medium [70] and gives an explicit expression for the relaxation time $1/\Gamma = \tau\gamma/(1-\gamma)$ in terms of the parameters of the event-based model.

As Table 1.2 shows, under certain conditions, the discrete models can be approximated by continuum equations that describe the coarse-grained (in space-time for the random walkers and in time for the event-based model) behavior but the discrete models provide a description with details that can never be extracted from the corresponding continuum equations. Of course, the ultimate justification of the event-based model is that, as shown in Section 1.5, it can reproduce the results of wave theory. Appendix D gives a further justification of our approach from a computational point of view.

Table 1.2: Analogy between the derivation of the diffusion equation from the random walk model and the derivation of one of the constitutive equations in Maxwell's theory from the discrete model Eq. (1.7) proposed in this chapter. The assumptions that the limiting values $D = \lim_{\delta\to 0}\lim_{\tau\to 0}\delta^2/2\tau$ and $\Gamma = \lim_{\gamma\to 1-}\lim_{\tau\to 0}(1-\gamma)/\tau\gamma$ are nonzero and finite are essential to obtain a well-defined continuum approximation of the discrete update rules.

	Random walk	Detector model
Update rule	$p_{l,k} = \frac{1}{2}(p_{l+1,k-1} + p_{l-1,k-1})$	$\mathbf{p}_k = \gamma\mathbf{p}_{k-1} + (1-\gamma)\mathbf{e}_k$
Length scale: δ Time scale: τ	$p_{l,k} = p(l\delta, k\tau) = p(x,t)$	$\mathbf{p}_k = \mathbf{p}(k\tau) = \mathbf{p}(t)$ $\mathbf{e}_k = \mathbf{e}(k\tau) = \mathbf{e}(t)$
Small τ	$p_{l,k-1} = p(x,t) - \tau\frac{\partial p(x,t)}{\partial t} + \mathcal{O}(\tau^2)$	$\mathbf{p}_{k-1} = \mathbf{p}(t) - \tau\frac{\partial \mathbf{p}(t)}{\partial t} + \mathcal{O}(\tau^2)$
Small δ	$p_{l\pm 1,k} = p(x,t) \pm \delta\frac{\partial p(x,t)}{\partial x} + \frac{\delta^2}{2}\frac{\partial^2 p(x,t)}{\partial x^2} + \mathcal{O}(\delta^3)$	
Small δ and τ	$\frac{\partial p(x,t)}{\partial t} \approx \frac{\delta^2}{2\tau}\frac{\partial^2 p(x,t)}{\partial x^2}$	$\frac{\partial \mathbf{p}(t)}{\partial t} \approx -\frac{1-\gamma}{\tau\gamma}\mathbf{p}(t) + \frac{1-\gamma}{\tau\gamma}\mathbf{e}(t)$
$\lim_{\delta\to 0}\lim_{\tau\to 0}$	$\frac{\delta^2}{2\tau} \to D, \;\; 0 < D < \infty$	
$\lim_{\gamma\to 1-}\lim_{\tau\to 0}$		$\frac{1-\gamma}{\tau\gamma} \to \Gamma, \;\; 0 < \Gamma < \infty$
Differential equation	$\frac{\partial p(x,t)}{\partial t} = D\frac{\partial^2 p(x,t)}{\partial x^2}$	$\frac{\partial \mathbf{p}(t)}{\partial t} = -\Gamma\mathbf{p}(t) + \Gamma\mathbf{e}(t)$
Fourier space		$\mathbf{p}(\omega) = \Gamma(i\omega + \Gamma)^{-1}\mathbf{e}(\omega)$
		$\mathbf{P}(\omega) = \chi(\omega)\mathbf{E}(\omega)$
	$\Downarrow$	$\Downarrow$
	diffusion equation	constitutive equation

Appendix D: Computational point of view

There is a general consensus that unless we first solve the wave equation and use this solution as the probability distribution for generating events, there are very fundamental, apparently unsurmountable, problems to derive from a wave mechanical description a process that produces the events that are observed in experiment [1]. The arguments used are rather abstract and general [1] and to understand the subtilities that are involved it may help to address this issue from a computational point of view.

For phenomena that cannot (yet) be described by a deductive theory, it is common practice to use probabilistic models. Although Kolmogorov's probability theory provides a rigorous framework to formulate such models, there are ample examples that illustrate how easy it is to make plausible assumptions that create all kinds of paradoxes, also for every-day problems [65, 69, 71, 72]. Subtle mistakes such as dropping (some of the essential) conditions, like in the discussion of the double-slit

experiment [73, 74], mixing up the meaning of physical and statistical independence or changing one probability space for another during the course of an argument, can give rise to all kinds of paradoxes [12, 18, 65, 73, 75, 76]. For instance, Feynman used the double-slit experiment as an example to argue that "far more fundamental was the discovery that in nature the laws of combining probabilities were not those of the classical probability theory of Laplace" [77], but this statement has been shown to result from an erroneous application of probability theory [65, 73, 74].

By construction, if we use a digital computer to produce numbers as we do in this chapter, we stay in the domain of elementary arithmetic and we do not have to worry about the subtleties of Kolmogorov's probability theory.

Instead of discussing the apparently unsurmountable problem in its full generality, which we could, it is more instructive to examine in detail the simple, concrete example of the double-slit model depicted in Fig. 1.2. According to Maxwell's theory, in the Fraunhofer regime the light intensity at the detector on a circular screen is given by [63]

$$\frac{I(\theta)}{I(0)} = \left| \int_{-\infty}^{+\infty} e^{iqy' \sin\theta} \rho(y') dy' \right|^2, \tag{1.27}$$

$$= \left(\frac{\sin \frac{qa \sin\theta}{2}}{\frac{qa \sin\theta}{2}} \right)^2 \cos^2 \frac{qd \sin\theta}{2}, \tag{1.28}$$

where $\rho(y') = [\Theta(a - |y' - d/2|) + \Theta(a - |y' + d/2|)]/2a$ is the normalized density distribution for the coordinate y'.

First, starting from the explicit expression Eq. (1.28) for the density $I(\theta)/I(0)$, it is trivial to construct an algorithm that generates events according to this density. Indeed, let us define

$$S_j(\theta) = \Theta(I(\theta) - r_j I(0)), \tag{1.29}$$

where $0 \leq r_j < 1$ denotes a uniform pseudo-random number. Then, the number of clicks of the detector at angular position θ is given by

$$N_k(\theta) = \frac{1}{k} \sum_{j=1}^{k} S_j(\theta), \tag{1.30}$$

and for sufficiently large k, we have $N_k(\theta) \to I(\theta)/I(0)$ with probability one. This completes the construction of the event-based algorithm based on the knowledge of $I(\theta)/I(0)$. Obviously, this algorithm is built on the knowledge of the explicit solution $I(\theta)$ of the wave problem. The events generated by this algorithm build up the interference pattern one-by-one and can be identified with the clicks of the detectors. This is as far as the quantum theoretical description goes in making contact to the experimental observations: It provides a prescription to calculate the probability density to observe a click on a detector. It is quite common to postulate that there does not exist a description that goes beyond the specification of the probability,

excluding that no further advance in a deeper understanding of the process that produces the events can be made.

Disregarding this postulate, we may wonder what happens if we take one step back and assume that we only know about expression Eq. (1.27) in terms of the wave amplitudes $\exp(iqy' \sin\theta)$ and density $\rho(y')$. Then, the obvious thing to do is to compute the integral in Eq. (1.27) numerically. Without loss of generality, we may write

$$A(\theta) \quad = \quad \frac{1}{N(\mathcal{S})} \sum_{y' \in \mathcal{S}} e^{iqy' \sin\theta}, \tag{1.31}$$

where the summation is over all y' of the set $\mathcal{S}$ accounting for the density $\rho(y')$ and $N(\mathcal{S})$ is the normalization factor. By definition of the integral, if the number of elements of the set $\mathcal{S}$ goes to infinity, we have $|A(\theta)|^2 \to I(\theta)/I(0)$.

Although the numerical calculation of the amplitude $A(\theta)$ is straightforward, there obviously is no relation between the points y' of the set $\mathcal{S}$ and the number of clicks of the detector at θ. In fact, the essence of quantum theory is that there is only a relation between $|A(\theta)|^2$ and the number of clicks but to know $A(\theta)$ requires that we first generate (a lot of) pseudo-events y'. Obviously, these pseudo-events y' cannot have an interpretation in terms of observed clicks.

The conclusion therefore is that the description in terms of individual waves (Eq. (1.27)) does not contain the ingredients, not even conceptual, to define a process that generates the clicks of the detectors that we observe. Therefore, from a computational perspective, it is futile to try inventing an event-based, particle-like process based on the wave mechanical expression for the intensity in terms of sums over amplitudes.

One may take the position that it is fundamentally impossible to go beyond an event-level description based on the knowledge of $I(\theta)/I(0)$ but by postulating this to be true, one simply postulates that it is impossible to make any advance in a deeper understanding of event-based phenomena. As we have shown by this and many earlier papers, there is no rational argument that supports this postulate other than that it is what we have been taught in physics courses.

Having shown that our event-by-event simulation model reproduces the results of wave theory without resorting to a description in terms of waves, we now explain why, from a computational point of view, we consider this to be an accomplishment and why our approach works.

The crux of our approach is that we do not start from expression Eq. (1.27) but construct a discrete event process that converges to Eq. (1.27) while generating events that directly correspond to the observed events. During the initial phase, this process may generate events that are accidental but once the process has reached its stationary state, the events appear with frequencies that corresponds to those predicted by wave theory.

To understand the idea behind our approach, it may be helpful to draw an analogy with the well-known Metropolis Monte Carlo (MMC) method for solving statistical

mechanical problems [4, 78]. The MMC method generates states S, events in our terminology, with a probability density [4, 78]

$$p(S) = \frac{e^{-E(S)/k_B T}}{\sum_S e^{-E(S)/k_B T}}, \tag{1.32}$$

where $E(S)$ denotes the energy of the state S, k_B is Boltzmann's constant and T is the temperature. At first sight, sampling from Eq. (1.32) is impossible because in all but a few nontrivial cases for which the partition function $\sum_S e^{-E(S)/k_B T}$ is known, we do not know the denominator. The MMC method solves this problem by constructing a Markov chain that generates a sequence of events S such that asymptotically these events are distributed according to the (unknown) probability density Eq. (1.32) [4, 78].

The analogy with our approach is the following. Although very different in all details, our event-based method uses a deterministic process (implemented as a DLM, see Eq. (1.7)) of which the sampling distribution converges to the unknown probability distribution $I(\theta)/I(0)$. The one-to-one correspondence between the objects in the corpuscular, event-based description and those in Maxwell's theory (see Section 1.10) ensures that in the long run, the event-based detector model generates clicks with frequencies that correspond to those of the unknown probability distribution $I(\theta)/I(0)$.

Chapter 2

Hanbury Brown-Twiss Experiment with Coherent Light

This chapter was previously published as
F.Jin, H. De Raedt, and K. Michielsen, Commun. Comput. Phys. **7**, 813 (2010).

2.1 Introduction

Computer simulation is widely regarded as complementary to theory and experiment [4]. Usually, the fundamental theories of physics provide the framework to formulate a mathematical model of the observed phenomenon, often in terms of differential equations. Solving these equations analytically is a task that is often prohibitive but usually it is possible to study the model by computer simulation. Experience has shown that computer simulation is a very powerful approach to study a wide variety of physical phenomena. However, recent advances in nanotechnology are paving the way to prepare, manipulate, couple and measure single microscopic systems and the interpretation of the results of such experiments requires a theory that allows us

to construct processes that describe the individual events that are being observed. Such a theory does not yet exist. Indeed, although quantum theory (QT) provides a recipe to compute the frequencies for observing events, it does not describe individual events, such as the arrival of a single electron at a particular position on the detection screen [1, 54, 65, 67]. Thus, we face the situation that we cannot rely on an established physical theory to build a simulation model for the individual processes that we observe in real experiments. Of course, we could simply use pseudo-random numbers to generate events according to the probability distribution that is obtained by solving the Schrödinger equation. However, that is not what the statement "QT does not describe individual events" means. What it means is that QT tells us nothing about the underlying processes that give rise to the frequencies of events observed after many of these events have been recorded. Therefore, in order to gain a deeper understanding in the processes that cause the observed event-based phenomena, it is necessary to model these processes on the level of individual events without using QT. The challenge therefore is to find algorithms that simulate, event-by-event, the experimental observations that, for instance, interference patterns appear only after a large number of individual events have been recorded by the detector [67, 79], without first solving the Schrödinger equation.

In this chapter, we leave the conventional line-of-thought, postulating that it is fundamentally impossible to give a logically consistent description of the experimental results in terms of causal processes of individual events. In other words, we reject the dogma that there is no explanation that goes beyond the quantum theoretical description in terms of averages over many events and search for an explanation of the experimental facts in terms of elementary, particle-like processes. It is not uncommon to find in the recent literature, statements that it is impossible to simulate quantum phenomena by classical processes. Such statements are thought to be a direct consequence of Bell's theorem [5] but are in conflict with other work that has pointed out the irrelevance of Bell's theorem [6–28, 80]. This conclusion is supported by several explicit examples that prove that it is possible to construct algorithms that satisfy Einstein's criterion for locality and causality, yet reproduce *exactly* the two-particle correlations of a quantum system in the singlet state, without invoking any concept of QT [29–34]. It is therefore an established fact that purely classical processes can produce the correlations that are characteristic for a quantum system in an entangled state, proving that from the viewpoint of simulating quantum phenomena on a digital computer, Bell's no-go theorem is of no relevance whatsoever.

The present chapter builds on earlier work [29–34, 55–61, 81] that demonstrates that quantum phenomena can be simulated on the level of individual events without first solving a wave equation or invoking concepts of QT, wave theory or probability theory. Specifically, we have demonstrated that it is possible to construct event-by-event processes, that reproduce the results of QT for single-photon beam-splitter and Mach-Zehnder interferometer experiments [79], Einstein-Podolsky-Rosen-Bohm experiments with photons [38, 82, 83], Wheeler's delayed-choice experiment with single

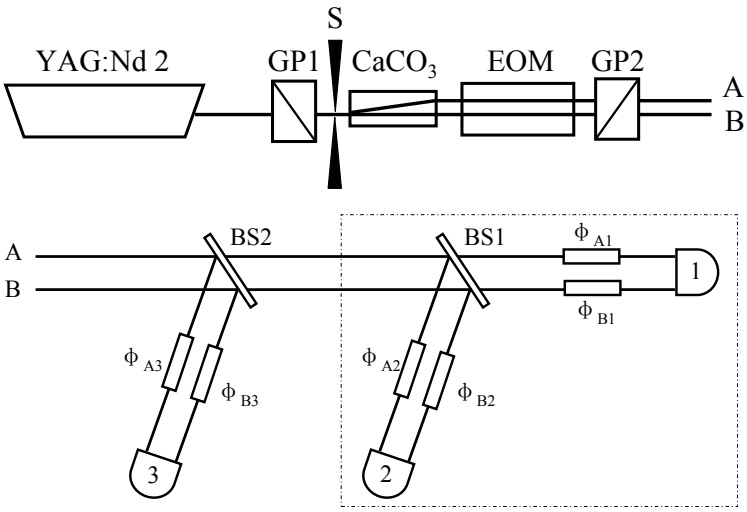

Figure 2.1: Schematic picture of a HBT experiment [36]. Top: Source. Coherent light, generated by a YAG laser, is sent through the Gan prism GP1,a single slit S, a beam splitter (a $CaCO_3$ crystal), an electro-optic modulator (EOM) and another Gan prism GP2 to produce two beams A and B as if they would have emerged from a double slit separated by 1.3 mm [36]. The EOM is switched rapidly to destroy the first-order coherence between beams A and B. Bottom: The interferometer consists of two beam splitters $BS1$ and $BS2$ and phase shifters ϕ_{An} and ϕ_{Bn} $(n = 1, 2, 3)$. Light intensity is measured by the three detectors D_1, D_2 and D_3.

photons [84], quantum eraser experiments with photons [37], double-slit and two-beam single-photon interference, quantum cryptography protocols, and universal quantum computation [57, 58]. According to the theory of quantum computation, the latter proves that at least in principle, we can construct particle-like, event-by-event processes that can simulate any quantum system [85]. Some interactive demonstration programs can be downloaded from `http://www.compphys.net` and Ref. [62].

In our earlier work, we studied first-order interference only. In this chapter, we extend the range of applications of the event-based simulation approach by demonstrating that the event-based algorithms, used in our previous work, can be re-used, without modification, to build a particle-only simulation model for another fundamental physics experiment, the Hanbury Brown-Twiss (HBT) experiment [86]. The HBT effect refers to a variety of correlation and anti-correlation effects in the intensities received by two or more detectors from a beam of particles [87–89], examples being second and third order interference. According to common lore, when a HBT experiment is performed using single-particle detectors, the HBT effect is attributed to the wave-particle duality of the beam. In this chapter, we present a particle-only model of the HBT effect, demonstrating that it is possible to construct causal, particle-like processes that describe the experimental facts without invoking concepts of QT.

As a concrete realization, we consider a recent HBT experiment [36], a schematic

picture of which is shown in Fig. 2.1. A radiation source, a frequency doubled Q-switched Nd:YAG laser with wavelength $532nm$, is used. The coherent light from this source is split by a beam splitter. The electro-optical modulator (EOM) erases the first-order interference of the light [36]. The two beams that emerge are labeled A and B, see Fig. 2.1(top). Then, the two beams are sent to three detectors through two beam splitters (BS), see Fig. 2.1(bottom). After measuring the coincidences between the signals of the three detectors by means of a triple coincidence circuit (TCC), the third-order intensity interference pattern is observed [36].

The purpose of this chapter is to demonstrate that one can construct a simulation model of this experiment that

- is a one-to-one copy of the experimental setup such that each device in the real experiment has a counterpart in the simulation algorithm
- is event-based and satisfies elementary physical (Einstein's) requirements of local causality
- reproduces the results of wave theory by means of particles only.

The structure of the chapter is as follows. In Section 2, we briefly review the wave theory of second and third-order interference. The simulation model is described in Section 3. Section 4 presents our simulation results and a discussion thereof. Our conclusions are given in Section 5.

2.2 Wave theory

Conceptually, the experiment of Fig. 2.1 can be viewed as a double-slit type experiment with three detectors, as shown in Fig. 2.2. Assume that source A emits coherent light with amplitude α and that source B emits coherent light with amplitude β. Thus, according to the superposition principle, the total amplitude falling on the n-th detector ($n = 1, 2, 3$) is

$$a_n = \alpha e^{i\phi_{An}} + \beta e^{i\phi_{Bn}}, \tag{2.1}$$

where ϕ_{An} (ϕ_{Bn}) is the accumulated phase of the photon travelling from source A (B) to the n-th detector. While the intensity is

$$I_n = |a_n|^2 = I_A + I_B + 2\mathbf{Re}\alpha\beta^* e^{i\phi_n}, \tag{2.2}$$

where $I_A = |\alpha|^2$, $I_B = |\beta|^2$, and $\phi_n = \phi_{An} - \phi_{Bn}$. If the relative phase of α and β is fixed, Eq. (2.2) predicts that interference fringes will be observed. This type of interference is referred to as first-order interference. If there is no correlation between the phases of α and β, there are no interference fringes because

$$\langle I_n \rangle = \langle I_A \rangle + \langle I_B \rangle. \tag{2.3}$$

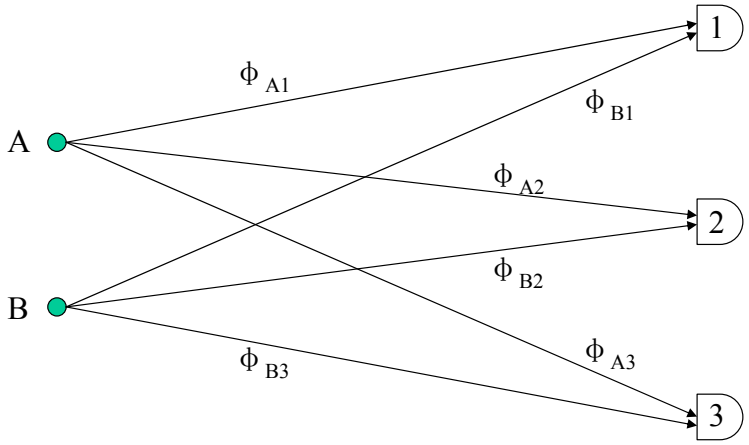

Figure 2.2: Schematic picture of third order intensity correlation. Photons emitted from sources A and B are registered by three detectors D_1, D_2 and D_3. ϕ_{An} and ϕ_{Bn} $(n = 1, 2, 3)$ are the phases accumulated during their flight from sources A or B to the n-th detector.

On the other hand, the product of the intensities is given by

$$I_n I_m = |a_n a_m|^2 = |\alpha^2 e^{i(\phi_{An}+\phi_{Am})} + \beta^2 e^{i(\phi_{Bn}+\phi_{Bm})} + \alpha\beta(e^{i(\phi_{An}+\phi_{Bm})} + e^{i(\phi_{Am}+\phi_{Bn})})|^2, \tag{2.4}$$

and after averaging over the uncorrelated phases of α and β, we find

$$\begin{aligned} G^{(2)}_{nm} &= \langle I_n I_m\rangle = \langle I_A I_A\rangle + \langle I_B I_B\rangle + \langle I_A I_B\rangle |e^{i(\phi_{An}+\phi_{Bm})} + e^{i(\phi_{Am}+\phi_{Bn})}|^2 \\ &= \langle I_A^2\rangle + \langle I_B^2\rangle + 2\langle I_A I_B\rangle(1+\cos\phi_{nm}) \end{aligned} \tag{2.5}$$

where $\phi_{nm} = \phi_n - \phi_m$ and $n, m = 1, 2, 3$. According to Eq. (2.5) the intensity-intensity correlation will exhibit interference fringes, a manifestation of the so-called Hanbury Brown-Twiss effect. This type of interference is referred to as second-order interference. It is convenient to introduce the normalized, dimensionless, correlation by

$$g^{(2)}_{nm} \equiv \frac{G^{(2)}_{nm}}{\langle I_n\rangle\langle I_m\rangle}, \tag{2.6}$$

where $\langle I_n\rangle = \langle I_m\rangle = \langle I_A\rangle + \langle I_B\rangle$. Assuming that the sources A and B have the same statistics and the same average intensities, we have $I_A = I_B$ and obtain

$$g^{(2)}_{nm} = g^{(2)}\left(1 + \frac{1}{2}\cos\phi_{nm}\right), \tag{2.7}$$

where $g^{(2)} = \langle I_A^2\rangle/\langle I_A\rangle^2$ is the second-order normalized intensity autocorrelation function. Similarly, we consider the averages of the product of three intensities given by

$$G^{(3)}_{123} = \langle I_1 I_2 I_3\rangle = \langle I_A^3\rangle + \langle I_B^3\rangle + [\langle I_A^2\rangle\langle I_B\rangle + \langle I_B^2\rangle\langle I_A\rangle][3 + 2(\cos\phi_{12} + \cos\phi_{23} + \cos\phi_{13})], \tag{2.8}$$

and, assuming $I_A = I_B$ as before, we have

$$g^{(3)}_{123} \equiv \frac{G^{(3)}_{123}}{\langle I_1\rangle\langle I_2\rangle\langle I_3\rangle} = \frac{g^{(3)}}{4} + \frac{g^{(2)}}{2}\left(\frac{3}{2} + \cos\phi_{12} + \cos\phi_{23} + \cos\phi_{13}\right), \tag{2.9}$$

where $g^{(3)} = \langle I_A^3\rangle/\langle I_A\rangle^3$ is the third-order normalized intensity autocorrelation function. This type of interference is referred to as third-order interference. In this chapter, we consider the case of coherent light only. Then we have $g^{(3)} = g^{(2)} = 1$.

2.3 Event-by-event simulation

We first discuss the general aspects of our event-by-event, particle-only simulation approach. This approach is unconventional in that it does not require knowledge of the wave amplitudes obtained by first solving the wave mechanical problem nor do we first calculate the quantum potential (which requires the solution of the Schrödinger equation) and then compute the Bohm trajectories of the particles. Instead, the detector clicks are generated event-by-event by locally causal, adaptive, classical dynamical systems. Our approach employs algorithms, that is we define processes, that contain a detailed specification of each individual event which cannot be derived from a wave theory.

The simulation algorithms define processes that are most easily viewed in terms of events, messages, and units that process these events and messages. In a pictorial description, the photon is regarded as a messenger, carrying a message that represents its time-of-flight. In this pictorial description, we may speak of "photons" generating the detection events. However, these so-called photons, as we will call them in the following, are elements of a model or theory for the real laboratory experiment only. The only experimental facts are the settings of the various apparatuses and the detection events.

The processing units mimic the role of the optical components in the experiment. A network of processing units represents the complete experimental setup. The standard processing units consist of an input stage, a transformation stage and an output stage. The input (output) stage may have several channels at (through) which messengers arrive (leave). Other processing units are simpler in the sense that the input stage is not necessary for the proper functioning of the device. A message is represented by a set of numbers, conventionally represented by a vector. As a messenger arrives at an input channel of a processing unit, the input stage updates its internal state, represented by a vector, and sends the message together with its internal state to the transformation stage that implements the operation of the particular device. Then, a new message is sent to the output stage which selects the output channel through which the messenger will leave the unit. At any given time, there is only one messenger being routed through the whole network. There is no direct communication between the messengers nor is there any communication between the processing units other

than through the messengers. We view the simulation as a message-processing and message-passing process: It routes messengers, representing the photons, through a network of message-processing units, representing the optical components in the laboratory experiment. From this general description, it should already be clear that the process that is generated by the collective of classical dynamical systems is locally causal in Einstein's sense.

2.3.1 Simulation model

The network of processing units represents the whole experimental setup. For the present purpose, that is the demonstration that the HBT effect can be explained by a particle-only model, it is sufficient to simulate the bottom part of Fig. 2.1. All the components, photons, beam splitters and photon detectors, have corresponding parts in our event-based simulation. As all the components are already presented in our previous work [29–32, 34, 55–61, 81], for completeness, we only give a brief description of each of the components of the simulation setup.

2.3.1.1 Messenger

We view each photon as a messenger. Each messenger has its own internal clock, the hand of which rotates with frequency f. When the messenger is created, the time of the clock is set to zero. As the messenger travels from one position in space to another, the clock encodes the time of flight t modulo the period $1/f$. The message, the position of the clock's hand, is most conveniently represented by a two-dimensional unit vector $\mathbf{e}_j = (e_{0,j}, e_{1,j}) = (\cos\psi_j, \sin\psi_j)$, where $\psi_j = 2\pi f t_j$ and the subscript $j > 0$ labels the successive messages. The messenger travels with the speed of light c. In this chapter, we do not need to specify the fixed frequency f and to specify a message, we use the angle ψ_j instead of the time-of-flight t_j.

2.3.1.2 Beam splitter

The structure of the processing unit for a beam splitter (BS) is shown in Fig. 2.3. The unit has two input and two output channels labeled by $k = 0, 1$ and consists of an input stage (DLM), a transformation stage (T), and an output stage (O). The input stage receives a message on either input channel 0 or 1, never on both channels simultaneously. The input events are represented by the vectors $\mathbf{v}_j = (1, 0)$ or $\mathbf{v}_j = (0, 1)$ if the jth event occurred on channel 0 or 1, respectively and are processed by a simple deterministic learning machine (DLM) [55–58, 60]. The DLM has two internal registers $\mathbf{Y}_{k,j} = (C_{k,j}, S_{k,j})$ and one internal vector $\mathbf{x}_j = (x_{0,j}, x_{1,j})$, where $x_{0,j} + x_{1,j} = 1$ and $x_{k,j} \geq 0$ for $k = 0, 1$ and all $j > 0$. Upon receiving the jth input event, the DLM performs the following steps: It stores the input message $\mathbf{e}_{k,j} = (\cos\psi_{k,j}, \sin\psi_{k,j})$ in its internal register $\mathbf{Y}_{k,j} = (C_{k,j}, S_{k,j})$. Then, it updates

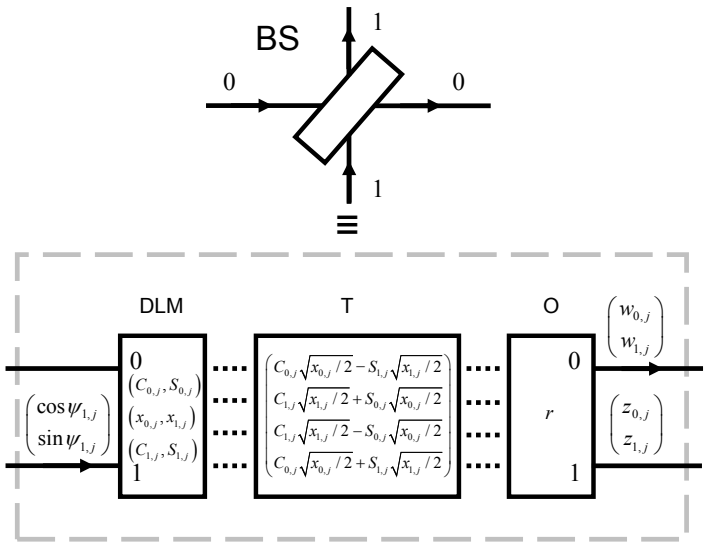

Figure 2.3: Diagram of a DLM-based processing unit that performs an event-based simulation of a beam splitter (BS). The processing unit consists of three stages: An input stage (DLM), a transformation stage (T) and an output stage (O). The solid lines represent the input and output channels of the BS. The dotted lines indicate the data flow within the BS.

its internal vector according to the rule

$$\mathbf{x}_j = \gamma \mathbf{x}_{j-1} + (1-\gamma)\mathbf{v}_j \ , \tag{2.10}$$

where $0 < \gamma < 1$. A detailed analysis of the update rule Eq. (2.10) can be found in Ref. [81].

The transformation stage accepts the messages from the input stage, and transforms them into a new four-dimensional vector

$$\mathbf{T} = \frac{1}{\sqrt{2}} \begin{pmatrix} C_{0,j}\sqrt{x_{0,j}} - S_{1,j}\sqrt{x_{1,j}} \\ C_{1,j}\sqrt{x_{1,j}} + S_{0,j}\sqrt{x_{0,j}} \\ C_{1,j}\sqrt{x_{1,j}} - S_{0,j}\sqrt{x_{0,j}} \\ C_{0,j}\sqrt{x_{0,j}} + S_{1,j}\sqrt{x_{1,j}} \end{pmatrix} . \tag{2.11}$$

The output stage sends out a messenger (representing a photon) carrying the message

$$\mathbf{w} = \begin{pmatrix} w_{0,j} \\ w_{1,j} \end{pmatrix} , \tag{2.12}$$

where

$$w_{0,j} \quad = \quad \left(C_{0,j}\sqrt{x_{0,j}/2} - S_{1,j}\sqrt{x_{1,j}/2} \right) \Big/ \, s_j \ ,$$

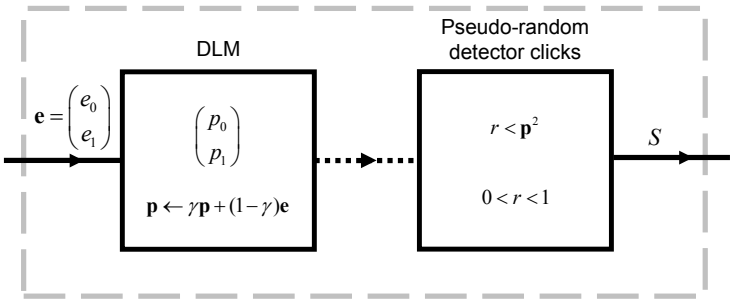

Figure 2.4: Diagram of the event-based detector model defined by Eqs. (2.16) and (2.17). The dotted line indicates the data flow within the processing unit.

$$\begin{aligned} w_{1,j} &= \left(C_{1,j}\sqrt{x_{1,j}/2} + S_{0,j}\sqrt{x_{0,j}/2}\right) \Big/ s_j \ , \\ s_j &= \sqrt{w_{0,j}^2 + w_{1,j}^2}. \end{aligned} \tag{2.13}$$

through output channel 0 if $s_j^2 > r$ where $0 < r < 1$ is a uniform pseudo-random number. Otherwise, if $s_j^2 \leq r$, the output stage sends through output channel 1 the message

$$\mathbf{z} = \begin{pmatrix} z_{0,j} \\ z_{1,j} \end{pmatrix}, \tag{2.14}$$

where

$$\begin{aligned} z_{0,j} &= \left(C_{1,j}\sqrt{x_{1,j}/2} - S_{0,j}\sqrt{x_{0,j}/2}\right) \Big/ t_j \ , \\ z_{1,j} &= \left(C_{0,j}\sqrt{x_{0,j}/2} + S_{1,j}\sqrt{x_{1,j}/2}\right) \Big/ t_j \ , \\ t_j &= \sqrt{z_{0,j}^2 + z_{1,j}^2}. \end{aligned} \tag{2.15}$$

We use pseudo-random numbers to mimic the apparent unpredictability of the experimental data only: The use of pseudo-random numbers to select the output channel is not essential [56]. Note that in our simulation model there is no need to introduce the (quantum theoretical) concept of a vacuum field, a requirement in the quantum optical description of a BS.

2.3.1.3 Photon detector

A schematic diagram of the unit that functions as a single-photon detector is shown in Fig. 2.4 [81]. The first stage consists of a DLM that receives on its input channel the jth message represented by the two-dimensional vector $\mathbf{e}_j = (\cos\psi_j, \sin\psi_j)$. In this chapter, we use the simplest DLM containing a single two-dimensional internal vector with Euclidean norm less or equal than one.

We write $\mathbf{p}_j = (p_{0,j}, p_{1,j})$ to denote the value of this vector after the jth message has been received. Upon receipt of the jth message the internal vector is updated according to the rule

$$\mathbf{p}_j = \gamma \mathbf{p}_{j-1} + (1-\gamma)\mathbf{e}_j \ , \tag{2.16}$$

where $0 < \gamma < 1$ and $j > 0$. A machine that operates according to the update rule Eq. (2.16) has memory to store an amount of information that is equivalent to the information carried by a single message only. Obviously, the rule Eq. (2.16) is the same as that used for the BS (see Eq. (2.10)) but the input data is different.

The second stage of the detector (see Fig. 2.4) uses the information stored in the internal vector to decide whether or not to generate a click. As a highly simplified model for the bistable character of the real photodetector or photographic plate, we let the machine generate a binary output signal S_j using the threshold function

$$S_j = \Theta(\mathbf{p}_j^2 - r_j), \tag{2.17}$$

where $\Theta(.)$ is the unit step function and $0 \leq r_j < 1$ is a uniform pseudo-random number. Note that in contrast to experiment, in a simulation, we could register both the $S_j = 0$ and $S_j = 1$ events such that the number of input messages equals the sum of the $S_j = 0$ and $S_j = 1$ detection events. Since in experiment it cannot be known whether a photon has gone undetected, we discard the information about the $S_j = 0$ detection events in our future analysis. The total detector count is defined as

$$N = \sum_{j=1}^{N_R} S_j \ , \tag{2.18}$$

where N_R is the number of messages received. Thus, N counts the number of one's generated by the machine.

2.3.1.4 Experiment

The processing units that simulate the optical components are connected in such a way that the network corresponds to the experimental setup in the laboratory. As explained earlier, it is sufficient to consider the bottom part of Fig. 2.1.

2.4 Simulation results

Our aim is to show that the event-based simulation model is capable of reproducing the wave mechanical results of the laboratory experiment [36] schematically shown in Fig. 2.1. As these laboratory experiments are carried out with continuous light and do not probe the individual photon regime, we cannot expect to see effects that relate to individual light quanta. Hence we expect that the results agree with those derived from classical electrodynamics. Accordingly, in this chapter we take the time

window that defines the coincidences large enough such that there are no quantum correlations. For a more extensive discussion of this important point, see Section 2.4.4.

Following Ref. [36], the phase of the coherent photons emitted by the source is "randomized" by letting the light pass through an EOM, the voltage of which is switched with a frequency of 50 Hz. To mimic this in the simulation, we send $N_{interval}$ messengers with some fixed but randomly chosen phase, then another $N_{interval}$ messengers with another fixed but randomly chosen phase, and so on. In practice, we use $N_{interval} = 2500$. The messengers (photons) are sent through either channel A or B, one at a time and are either transmitted or reflected by the beam splitters. Before hitting a detector, the messenger experiences a time delay corresponding to ϕ_{An} or ϕ_{Bn} $(n = 1, 2, 3)$. The detector processes the message carried by the messenger and decides whether or not to produce a click.

We consider three different experiments. In case 1, we remove both BSs in Fig. 2.1 (bottom) and study the signal produced by detector D_1. Then, in case 2, we remove BS2, that is we consider the HBT experiment with two detectors, as indicated by the dashed-dotted line in Fig. 2.1 (bottom). Finally, in case 3, we study the full three-photon correlation experiment, see Fig. 2.1 (bottom). In cases 2 (3), the intensity-intensity correlations are calculated by counting coincidences of two (three) messengers, meaning that the arrival times of the two (three) messengers are within a time window W, to be discussed in Section 4.4. All simulations have been carried out with $\gamma = 0.99$.

2.4.1 Case 1: One detector

Let us first demonstrate how the event-based model of the detector works [81]. To this end, we remove BS1 and BS2 in Fig. 2.1 (bottom). The messengers, randomly entering through channels A or B, are sent directly to the time-delay units that change the angle of the hand of the clock representing the time-of-flight by ϕ_{A1} or ϕ_{B1}, respectively. The messengers are then processed by detector D_1. We perform two different sets of simulations. First, we keep the differences between the time-of-flights of the messengers entering channel A and the time-of-flights of the messengers entering channel B constant. In this case, according to wave theory, we expect to see clear interference fringes. Second, the differences between the time-of-flights of the messengers entering channel A and the time-of-flights of the messengers entering channel B are taken to be random. Then, according to wave theory, there should be no sign of interference effects. Hence, as shown in Fig. 2.5, our particle-only simulation approach reproduces both features and the results are in very good agreement with the wave theoretical results (see Eq. (2.2)).

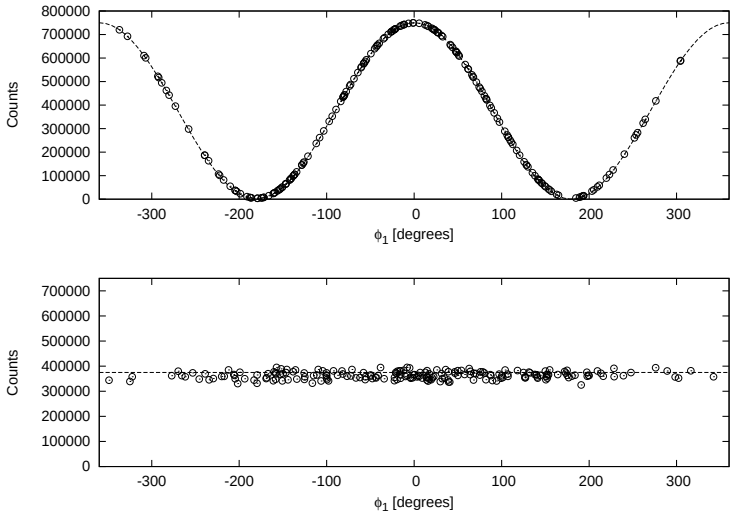

Figure 2.5: Case 1: All BSs in Fig. 2.1 (bottom) removed. Simulation results for the detector counts as a function of $\phi_1 = \phi_{A1} - \phi_{B1}$. The differences between the time-of-flights of the messengers entering channel A and the time-of-flights of the messengers entering channel B are constant (top) or random (bottom, see text). Circles: Simulation data; Dashed line: Wave theoretical solution Eq. (2.2) (top) and Eq. (2.2) averaged over ϕ_1 (bottom).

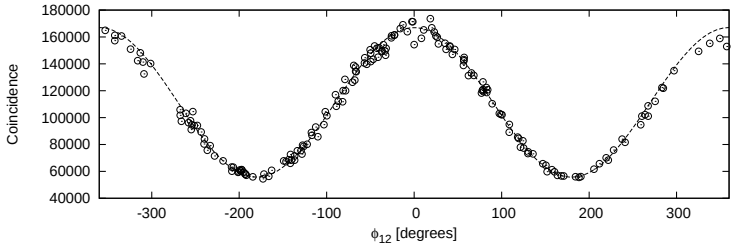

Figure 2.6: Case 2: BS2 in Fig. 2.1 (bottom) removed. Simulation results of the two-particle coincidence counts as a function of ϕ_{12} where $\phi_{12} = \phi_1 - \phi_2$, and $\phi_n = \phi_{An} - \phi_{Bn}$ $(n = 1, 2)$. The time-of-flights of the messengers entering channel A and the time-of-flights of the messengers entering channel B are taken to be random (see text). Circles: Simulation data; Dashed line: Wave theoretical solution Eq. (2.7).

2.4.2 Case 2: Hanbury Brown-Twiss experiment

We consider the HBT experiment with two detectors, that is we remove BS2 from the diagram in Fig. 2.1 (bottom). Messengers enter the apparatus through channel A or B, one by one. The time-of-flights of the messengers entering channel A and the time-of-flights of the messengers entering channel B are taken to be random. Hence, as shown in Fig. 2.5 (bottom) there is no first-order interference. When passing a BS,

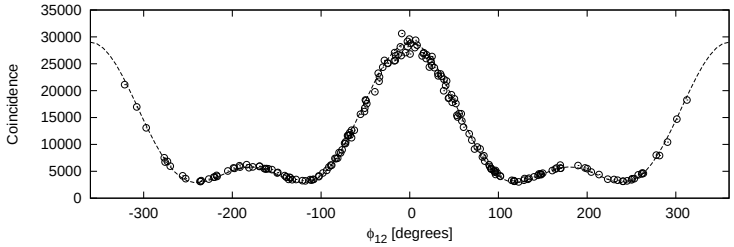

Figure 2.7: Case 3: Three particle correlation experiment (see Fig. 2.1 (bottom)). Simulation results of the three-particle coincidence counts as a function of ϕ_{12} where $\phi_{12} = \phi_1 - \phi_2$, and $\phi_n = \phi_{An} - \phi_{Bn}$ $(n = 1, 2, 3)$. We only show data for the case $\phi_{A2} = \phi_{B2} = 0$, $\phi_{A1} = \phi_{B3}$, $\phi_{B1} = \phi_{A3}$ where ϕ_{A1} and ϕ_{B1} are chosen randomly. The time-of-flights of the messengers entering channel A and the time-of-flights of the messengers entering channel B are taken to be random (see text). Circles: Simulation data; Dashed line: Wave theoretical solution Eq. (2.9).

the message changes according to the rules explained in Section 2.3.1.2. Then, before entering the detector, the message is changed once more by ϕ_{An} or ϕ_{Bn} $(n = 1, 2)$, depending on which path the messenger took. If the two detectors fire with the time window W (see Section 4.4), we increase the number of coincidences. The simulation data shown in Fig. 2.6 confirm that this procedure reproduces the results of wave theory, see Eq. (2.7).

2.4.3 Case 3: Three-particle intensity-intensity correlation

Finally, we consider the laboratory experiment [36] that measures the correlations between three detectors (see Fig. 2.1). The simulation procedure is the same as in case 2, except that we count coincidences of clicks of three different detectors. Also in this case, the simulation data shown in Fig. 2.7 confirm that this procedure reproduces the results of wave theory, see Eq. (2.9).

2.4.4 Discussion

Our simulation model is based on a particle picture and makes no reference to concepts or results from wave theory. In contrast to the conventional quantum theoretical explanation in terms of the wave-particle nature of photons, our simulation approach requires a particle picture of photons only. During the event-by-event simulation we always have full which-way information of the photons (messengers) since we can always track them. Nevertheless, depending on the settings of the optical apparatuses, intensity-intensity interference is observed. Although the appearance of an interference pattern is commonly considered to be characteristic of a wave, we have demonstrated that, as in experiment, it can also appear as a result of a collection of

particles that interact with the various optically active devices such as beam splitters and detectors.

It is of interest to ask what aspects of the model are essential for producing the correct interference patterns. There are three different aspects that need to mentioned, namely (1) the discrete-event nature of the simulation, (2) the memory in both the beam splitter and detector model and (3) the threshold feature of the detector model.

Obviously, as our model is event-based, the simulation proceeds in discrete "time steps". It has been shown [90] that Newton's equation in a discretized form with a finite time-step can also produce interference patterns (although it is not clear yet whether this approach can reproduce the results that derive from Maxwell's theory). However, in our approach the discrete time label j plays a very different role from that of the discrete time step in discretized classical equations of motion. The label j merely serves to label successive events and does not have the dimension of time. In our idealized model, it does not matter how far, in real time, successive events are separated from each other. To make our model more realistic, we could introduce a "real time" by specifying how many events per unit of time are being processed. As it is the aim of this chapter to demonstrate that the same processing units as those used for very different purposes can, without making any modification, be combined to reproduce the results of HBT experiments (as described by Maxwell's theory), the simulations are performed such that the event-based system operates in its stationary regime, corresponding to the regime in which the number of events per time unit is large.

In our approach, interference appears as a result of processing individual events. Clearly, under these circumstances it is impossible to explain in a logical, rational manner the appearance of interference without some form of indirect communication between individual events. In our models, the local memory in the DLMs together with the update rules (see Sec. 2.3.1.2 and 2.3.1.3) provide the mechanism for this indirect communication to take place. In the HBT experiments that we simulate in the present chapter, only the memory in the detector is essential. For other types of experiments [55–57, 60, 61], also the memory in the beam splitter is essential. The detector model (which does not rely on concepts of probability theory) that we employ is very different from models that are based on the hypothesis that memory effects in the equipment, operating as a random dynamical system over the field of p-adic numbers, can lead to interference phenomena [91, 92].

Regarding the threshold mechanism, it is intuitively clear that single-photon detectors must necessarily operate as a threshold device because they have to discriminate between no and one photon. The presence of a threshold may have far reaching implications. For instance, it has been shown that it may lead to apparent violations of the Bell inequalities observed in EPRB experiments with photons [93]. The detector model employed in this chapter differs from models discussed in Ref. [93] in that there is a simple, one-to-one relation between the equations describing the event-based model and the material equations in Maxwell's theory [81].

Finally, we address the question of simulating quantum correlations (changing the factor of 1/2 in Eq. (2.7) into one) in HBT experiments. In real experiments, and also in our simulation approach, it is necessary to specify the procedure by which we count coincidences of detection events. For the experiments at hand, one introduces a time window W and one defines as a two (three) particle coincidence, two (three) detection events with the time difference(s) are smaller than W. As discussed extensively in our work on the simulation of Einstein-Podolsky-Rosen-Bohm (EPRB) experiments [29], the choice of the time window W is of crucial importance, both in the simulation and in real experiments [38], to obtain the correlation of a quantum system in the singlet state. In general, only when $W \to 0$, experiment and simulation can reproduce the correlation of a quantum system in the singlet state [29]. For large enough W, the relation to a quantum system in the singlet state is lost. In this chapter, we have chosen W sufficiently large and generated groups of two (three) messengers such that if the two (three) detectors fire, this constitutes a coincidence of two (three) particles. In other words, the time delays are only used by the detector but are ignored in determining coincidences. In this sense, the simulation results presented in this chapter pertain to classical light and are therefore in excellent agreement with classical wave theory. To study the quantum aspects of two- and three-particle correlations the time delays should be used to also determine the coincidences, as in our EPRB simulations [29]. For completeness we mention that in this chapter, we considered light sources that produces photons in a coherent state only. We leave the study of quantum and thermal features in these correlation experiments for future research.

2.5 Conclusion

We have demonstrated that our classical, locally causal, particle-like simulation approach reproduces the results of the Hanbury Brown-Twiss effect. Our event-based simulation model, a classical, locally causal, adaptive dynamical system, reproduces the results of wave theory without making reference to the solution of a wave equation and provides a simple, particle-based mental picture for what each individual photon experiences as it travels from the source to the detector. Our simulation algorithm demonstrates that the wave-particle duality is not the only way to describe the nature of a photon but that there is another way that only needs the particle nature, satisfies Einstein's local causality and does not defy the common sense. Finally, we would like to emphasize that the algorithms used to simulate the optical components in this chapter have not been designed to simulate the HBT-type experiments. The algorithms have been taken, without modification, from our earlier work on very different quantum optics experiments [29–32, 34, 55–61, 81, 81]. In this sense, it seems that our approach has predictive power: The algorithms can be reused to simulate very different experiments than those for which they were originally developed.

Finally, we would like to draw attention to the fact that our event-based simulation

models make specific predictions that can be tested in properly designed experiments. First, we recall that the distribution that the simulation model produces when it has reached the stationary regime agrees with wave theory and will therefore be in concert with any experiment that reproduces the results of wave theory. However, we can also simulate the system in the transient regime in which the convergence to the correct, stationary distribution can be monitored. Our simulation models make specific predictions for the transient behavior of the distribution of events because they depend on the details of the model [81]. Thus, a meaningful confrontation of our model with experiment requires that the latter has recorded all the events, starting with the very first photon that is detected (and not after alignment, calibration etc. has been performed). We hope that our work creates a stimulus to carry out such experiments.

Chapter 3

Quantum Eraser Experiment

This chapter was previously published as
F.Jin, S.Zhao, S. Yuan, H. De Raedt, and K. Michielsen, J. Comput. Theor. Nanosci. **7**, 1771 (2010).

3.1 Introduction

According to wave-particle duality, a concept of quantum theory (QT), photons exhibit both wave and particle behavior depending upon the circumstances of the experiment [1]. The wave and particle behavior of photons is believed to be complementary. When we know (observe) the which-way (WW) information (particle behavior), there is no interference pattern (wave behavior) [54]. Parameters quantifying the interference and the WW information are the visibility $\mathcal{V}$ and the path distinguishability $\mathcal{D}$, respectively. According to the complementarity relation of QT, $\mathcal{V}^2 + \mathcal{D}^2 \leq 1$ [94, 95].

In 1982, Scully and Drühl proposed a photon interference experiment, called "quantum eraser" [96], in which the photons are labelled by WW markers (three-level atoms). In this experiment, we know (but not observe) the WW information of the photons and then we expect that there is no interference. However by erasing the WW information afterwards by a "quantum eraser", the interference pattern can be

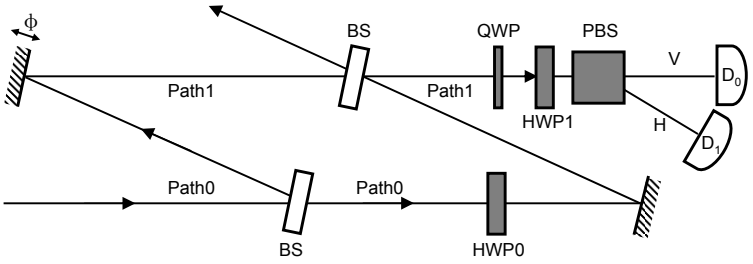

Figure 3.1: Schematic diagram of the experimental setup for the quantum eraser experiment with photons studied in Ref. [37]. BS: beam splitter; PBS: polarizing beam splitter; HWP0 and HWP1: half-wave plates; QWP: quarter-wave plate; D_0, D_1: detectors; ϕ: phase shift introduced in Path1.

recovered [96]. The interference pattern can even be recovered after the data have already been recorded and saved in a file [97].

Quantum eraser experiments have been described "as one of the most intriguing effects in quantum mechanics", but have also been regarded as "the fallacy of delayed choice and quantum eraser" [98]. Clearly, they challenge the point of view that the wave and particle behavior of photons are complementary: The observation of interference, commonly associated with wave behavior, depends on the way the data is analyzed after the photons have passed through the interferometer.

The question that we answer in the affirmative in this chapter is: "Can we simulate a quantum eraser experiment without invoking concepts of quantum theory and without first solving the wave mechanical problem?"

3.1.1 Quantum eraser with photons

3.1.1.1 Experimental realization

The quantum eraser has been implemented in several different experiments with photons, atoms, etc. [37, 97, 99–103]. Although much more difficult to realize experimentally, quantum erasers may also be realized with quantum dots [104, 105] and mesoscopic electromechanical devices [106].

In Ref. [37], Schwindt *et al.* reported an experimental realization of a quantum eraser in which the polarization of the photons has been used to encode the WW information. In this chapter, we focus on this particular experiment. The experimental setup (see Fig. 3.1) consists of a linearly polarized single-photon source (not shown), a Mach-Zehnder interferometer (MZI) of which the length of Path1 (see Fig. 3.1) can be varied, inducing a relative phase shift ϕ between Path0 and Path1, an adjustable analysis system which is a combination of a quarter-wave plate (QWP), a half-wave plate (HWP) HWP1, and a calcite prism operating as a polarizing beam splitter (PBS). Another adjustable HWP, HWP0, is inserted in Path0 of the MZI to entangle

the photon's path with its polarization.

According to Ref. [37] the pictorial description of the experimental observations is as follows. If a photon, described by a pure, vertically polarized state V is injected into the interferometer with the HWP0 set to 45°, then the photon that arrives at the second beam splitter (BS) of the MZI carries a WW marker: The photon is in the horizontally polarized state H if it followed Path0 and it is in the V state if it followed Path1. If the optical angle of HWP1 is zero, there will be no interference ($\mathcal{V} = 0$) and the detectors give us the full WW information of each detected photon ($\mathcal{D} = 1$). If the optical angle of HWP1 is nonzero, the H and V states interfere ($0 < \mathcal{V} \leq 1$) and the WW information of each photon will be partially or completely "erased" ($0 \leq \mathcal{D} < 1$). Thus, by varying the optical angle θ_{HWP1} of HWP1, the illusion is created that the character of the photon in the MZI "changes" from particle to wave and vice versa. If photons described by a completely mixed, that is an unpolarized, state are emitted, then no WW information can be obtained and also no interference can be observed ($\mathcal{D} = \mathcal{V} = 0$), independent of the orientation of HWP0. However, varying θ_{HWP1} can still lead to a recovery of interference ($0 < \mathcal{V} \leq 1$). For photons described by a partially mixed state, a state that can we expressed as containing a completely mixed component and a pure component, partial WW information can be obtained. Since the completely mixed component contains no WW information and displays no interference, the maxima of $\mathcal{D}$ and $\mathcal{V}$ are smaller than one and numerical equal to the state purity. Also in this case complete visibility can be recovered by varying θ_{HWP1}.

3.1.1.2 Event-by-event simulation model

It is important to realize that the counter-intuitive features of quantum eraser experiments result from attempts to apply the concepts and the formalism of QT to a description of the experimental results in terms of individual events [1]. Logically speaking, there are two possibilities:

1. We accept the postulate that it is fundamentally impossible to give a logically consistent description of the experimental results in terms of individual events, that is we accept that there is no explanation that goes beyond the quantum theoretical description in terms of averages over many events.

2. We search for an explanation of the experimental facts that goes beyond a description in terms of averages.

In this chapter, we demonstrate that the second option is a viable one. Thus, we adopt the point of view that although QT correctly predicts averages of many detection events, it has nothing to say about individual events [1].

We propose an event-by-event simulation model that is a one-to-one copy of the quantum eraser experiment reported in Ref. [37]. The simulation model describes a

particle-like, classical, local and causal dynamical system. Each component of the laboratory experiment such as the single-photon source, the BS, HWP, QWP, and PBS are simulated by corresponding algorithms. By connecting the output(s) of one component to the input(s) of another one, we construct the simulation equivalent of the experimental setup depicted in Fig. 3.1. By construction this network of dynamical systems satisfies Einstein's criterion of local causality. The data is analyzed by counting the detection events, just as in the real experiment.

We demonstrate that our model reproduces the results of QT, that is the averages predicted by QT and confirmed by experiment [37], without first solving a wave equation. In fact, we show that it is possible to give an entirely classical, particle-only description for the single-photon quantum eraser experiment reported in Ref. [37]. We show that the interference patterns, commonly associated with wave behavior, can be built up by many particles having full WW information (we can always track the photons during the simulation) that arrive one-by-one at a detector.

The work of this chapter builds on earlier work [29–32, 34, 55–60, 81] that demonstrates that quantum phenomena can be simulated on the level of individual events without first solving a wave equation and even without invoking concepts of QT, wave theory or probability theory. Specifically, in our earlier work we have demonstrated that it is possible to simulate event-by-event, a single-photon beam splitter and Mach-Zehnder interferometer experiments, Einstein-Podolsky-Rosen-Bohm experiments with photons, Wheeler's delayed choice experiment with single photons, the double-slit and two-beam interference, quantum cryptography protocols, and universal quantum computation. The latter proves that in principle we can perform an event-by-event (particle-like) simulation of any quantum system [85]. Some interactive demonstration programs are available for download [62, 107, 108].

3.1.2 Irrelevance of Bell's theorem

It is not uncommon to find in the recent literature, statements that it is impossible to simulate quantum phenomena by classical processes. Such statements are thought to be a direct consequence of Bell's theorem [5] but are in conflict with other work that has pointed out the irrelevance of Bell's theorem [6–28]. A survey of the literature suggests that, roughly speaking, physicists can be classified as those who believe in the reasonableness of Bell's arguments, those who advance logical and mathematical arguments to show that a violation of Bell's (and related) inequalities does not support the far-reaching conclusions of the former group of physicists and those who do not care about Bell's theorem at all. The authors of this article belong to the second group.

Although we expect discussions of philosophical or metaphysical aspects of Bell's theorem to continue forever, as explained in a review article that has appeared in this journal [29], from the viewpoint of simulating quantum phenomena on a digital computer, Bell's no-go theorem is of no relevance whatsoever.

This conclusion is supported by several explicit examples that prove that it is possible to construct algorithms that satisfy Einstein's criteria for locality and causality, yet reproduce *exactly* the two-particle correlations of a quantum system in the singlet state, without invoking any concept of quantum theory [29–34]. It is therefore an established fact that purely classical processes can produce the correlations that are characteristic for a quantum system in an entangled state, thereby disposing of the mysticism that is created by Bell's no-go theorem.

The key point is to realize that QT or the probabilistic models proposed by Bell cannot, on a fundamental level, address the (non)existence of algorithms, that is of well-defined processes, that give rise to the distributions of the events, described by these theories/models.

The philosophy behind our simulation approach is very simple: If we can construct an algorithm that

1. does not rely on the solution of a wave equation,
2. satisfies the elementary criteria of locality and causality as formulated by Einstein,
3. produces data of the same type as the data collected in the laboratory experiment,
4. by analyzing the simulated data according to the procedure used to analyze the experimental data leads to the same conclusion, namely that certain averages of the raw data agree with the quantum theoretical description of the whole experiment,
5. contains algorithms that simulate the various components (beam splitter, etc.) of the experiment and can, with no change, be re-used to simulate other experiments,

then we may conclude that we have built a simulation model for the laboratory experiment.

Loosely speaking, if the experimenter would be unable to distinguish between data recorded in a genuine experiment and data provided by the simulation algorithm, then the experiment has been "de-mystified" in the sense that we have found a process that offers a description of the observed phenomena on the level of individual events and without invoking (concepts of) wave theory.

To avoid possible misunderstandings, the work presented in this chapter is not concerned with an interpretation or an extension of QT nor does it affect the validity of QT as such. QT describes the collective result of many events, that is averages of many events, extremely well but does not provide a description on the level of individual clicks of a detector [1].

Structure of the chapter

Section 3.2 reviews the standard concepts of QT that are needed to give a quantum theoretical treatment of the quantum eraser experiment [37]. Section 3.3 discusses the general ideas that underpin our event-by-event simulation approach. We address the fundamental problem of reconciling the observation of "clicks" with a wave mechanical theory from the viewpoint of algorithms, processes and computation. We show that in general, it is impossible to attribute "clicks" to individual wave amplitudes and explain how our simulation approach circumvents this fundamental problem. Section 3.4 explains how the pure and mixed states of a quantum systems can be represented in our simulation approach. In Section 3.5, we specify the simulation model in full detail. Data of event-by-event simulations of the quantum eraser experiment are presented in Section 3.6. We show that our classical, particle-like simulation model reproduces all the results of QT for this experiment. Our conclusions can be found in Section 3.7.

3.2 Quantum theory

In QT, a system is described by the state $|\alpha\rangle$, a vector in a Hilbert space [65]. This vector can be written as a linear combination of a complete set of orthonormal basis states $|i\rangle$ for $i = 1, \ldots, d$ where d denotes the dimension of the Hilbert space. These basis states are chosen such that they facilitate the formulation of the model. The amplitude for a quantum system to go from a state $|\alpha\rangle$ to another state $|\beta\rangle$ is given by $\langle\beta|\alpha\rangle = \sum_{i=1}^{d} \langle\beta|i\rangle \langle i|\alpha\rangle$. With respect to the basis states $\{|i\rangle\}$, the optical apparatus T is defined through its transition matrix elements $\langle i|T|j\rangle$. If the optical apparatus T induces a transition from the state $|\alpha\rangle$ to the state $|\beta\rangle$, the amplitude for this transition is given by $\langle\beta|T|\alpha\rangle = \sum_{i,j=1}^{d} \langle\beta|i\rangle \langle i|T|j\rangle \langle i|\alpha\rangle$. Finally, the probability $\mathrm{Prob}(\beta, \alpha)$ for this transition to occur is related to the amplitude through the Born rule

$$\mathrm{Prob}(\beta, \alpha) = |\langle\beta|T|\alpha\rangle|^2. \tag{3.1}$$

According to the above scheme, we can easily calculate the predictions of QT for the experiment shown in Fig. 3.1. The basis states correspond to H or V polarized photons that travel along Path0 or Path1. The transition matrices of the optical components such as the BS, PBS, HWP and QWP can be found in Ref. [109] and in the appendix. In the appendix, we also give the quantum theoretical expressions for the visibility for the experiment depicted in Fig. 3.1 that will be used for the comparison with our simulation results.

The above formulation assumes that the quantum system is in the pure state [65]. Some of the experiments reported in Ref. [37] require a description in terms of a mixed state [65]. A system is in a mixed state if it is in one of its m pure states $|\alpha_1\rangle, |\alpha_2\rangle, \cdots, |\alpha_m\rangle$ with probability $p_1, p_2, \cdots, p_m$, respectively [65]. A quantum

system in a mixed state is conveniently described through the density matrix [65]

$$\rho = \sum_{j=1}^{m} p_j |\alpha_j\rangle\langle\alpha_j|, \tag{3.2}$$

where it is assumed that $\sum_{j=1}^{m} p_j = 1$, $p_j \geq 0$ for $j = 1, \ldots, m$, and that the states $|\alpha_j\rangle$ are normalized such that $\mathbf{Tr}\rho = 1$. According to QT, for a system in a mixed state ρ, the expectation value of the operator Ω is given by [65]

$$\langle\Omega\rangle = \mathbf{Tr}\rho\Omega = \sum_{j=1}^{m} p_j \langle\alpha_j|\Omega|\alpha_j\rangle. \tag{3.3}$$

3.3 Event-by-event simulation

Our event-based simulation approach is unconventional in that it does not require knowledge of the wave amplitudes obtained by first solving the quantum theoretical problem nor do we first calculate the quantum potential (which requires the solution of the Schrödinger equation) and then compute the Bohm trajectories of the particles. Instead, the detector clicks are generated event-by-event by locally causal, adaptive, classical dynamical systems. Our approach employs algorithms, that is we define processes, that contain a detailed specification of each individual event which, as we now show, cannot be derived from a wave theory such as QT.

To understand the subtleties that are involved, it is helpful to consider a simple example. Let us consider the MZI unit of the quantum eraser and omit the polarization label of the photons. According to QT, the amplitudes b_0 and b_1 to observe a photon in Path0 or Path1 after the second BS are related to the input amplitudes a_0 and a_1 by [110]

$$\begin{aligned} \begin{pmatrix} b_0 \\ b_1 \end{pmatrix} &= \frac{1}{2}\begin{pmatrix} 1 & i \\ i & 1 \end{pmatrix}\begin{pmatrix} e^{i\phi_0} & 0 \\ 0 & e^{i\phi_1} \end{pmatrix}\begin{pmatrix} 1 & i \\ i & 1 \end{pmatrix}\begin{pmatrix} a_0 \\ a_1 \end{pmatrix}, \\ &\equiv ABA\begin{pmatrix} a_0 \\ a_1 \end{pmatrix}. \end{aligned} \tag{3.4}$$

Let us assume that $a_0 = 1$ and $a_1 = 0$, meaning that the photons enter the MZI through Path0 only. The probabilities P_0 (P_1) for a click in detector D_0 (D_1) are given by

$$P_k = \left| \sum_{j=0,1} \sum_{i=0,1} A_{k,j} B_{j,i} A_{i,0} \right|^2 \quad , \quad k = 0, 1. \tag{3.5}$$

Using Eqs. (3.4) and (3.5) a simple calculation yields a closed form expression for P_k. Once we know P_k, it is trivial to use it as input for a process that generates clicks of the detectors D_0 and D_1. This approach relies on what we call the "solution"

of the quantum theoretical problem. It is irrelevant whether we have a closed form expression for P_k or only know P_k in tabulated form. The point is that we analytically worked out the sums over the indices i and j in Eq. (3.5). Let us now assume that we do not know how to perform the sums over the indices i and j in Eq. (3.5) by ourselves and that there is some "magical process" that carries out the sum for us. In other words, we assume that we do not know P_0 and P_1.

In practice, any process that performs the sums in Eq. (3.5) by selecting (one-by-one) the pairs (i, j) from the set $\mathcal{S} = (0, 0), (1, 0), (0, 1), (1, 1)$ defines a sequence of "events" (i, j). The key question now is: Can we identify the selection of the pairs with "clicks", events registered by a detector? We now prove that this is impossible.

A characteristic feature of all wave phenomena is that not all contributions to the sums in Eq. (3.5) have the same sign: In wave theory, this feature is essential to account for destructive interference. But, at the same time this feature forbids the existence of a process of which the "events" can be identified with the clicks of the detector.

This is easily seen by considering a situation for which, for instance, $P_0 = 0$. In this case, the detector D_0 should never click. However, according to Eq. (3.5), the process that samples from the set $\mathcal{S}$ produces "events" such that the sums over all these "events" vanishes. Therefore, if we want to identify these "events" with the clicks that we observe, we run into a logical contradiction: To perform the sums in Eq. (3.5), we have to generate events that in the end cannot be interpreted as clicks since in this particular case no detector clicks are observed.

Thus, the conclusion is that the individual terms in expression Eq. (3.5) do not contain the ingredients to define a process that generates the clicks of the detectors that we observe.

The crux of our event-by-event simulation approach is that we do not start from expression Eq. (3.5) but construct a process that converges to Eq. (3.5) while generating events that correspond to the observed events. To grasp this idea, consider the well-known Metropolis Monte Carlo (MMC) method for solving statistical mechanical problems [4, 78]. The MMC method generates states S, events in our terminology, with a probability density [4, 78]

$$P(S) = \frac{e^{-E(S)/k_BT}}{\sum_S e^{-E(S)/k_BT}}, \tag{3.6}$$

where $E(S)$ denotes the energy of the state S, k_B is Boltzmann's constant and T is the temperature. At first sight, sampling from Eq. (3.6) is impossible because in all but a few nontrivial cases for which the partition function $\sum_S e^{-E(S)/k_BT}$ is known, we do not know the denominator. MMC solves this problem by constructing a Markov chain that generates a sequence of events S such that asymptotically these events are distributed according to the (unknown) probability density Eq. (3.6) [4, 78].

The analogy with our event-by-event simulation approach is the following. Although very different in all technical details, our event-based method uses a deterministic

process of which the sampling distribution converges to the unknown (by assumption) probability distribution P_k for $k = 0, 1$. Initially, the system does not know about this limiting probability distribution and hence, during a short transient period, the frequencies with which events are generated may not correspond to this distribution. However, for many events, which is the situation described by QT, these first few "wrong" events disappear in the statistical fluctuations and are therefore irrelevant for the comparison of our event-based simulation results with QT. It should be clear that the foregoing does not depend on the specific example that we used for the purpose of illustration.

Let us now discuss the general aspects of our simulation approach. The simulation algorithms that we construct are most easily formulated in terms of events, messages, and units that process these events and messages. Taking the quantum eraser experiment as an example, in a pictorial description, the photon is regarded as a messenger, carrying a message that represents its time-of-flight (phase) and polarization. In this pictorial description, we may speak of "photons" generating the detection events. However, these so-called photons, as we will call them in the following, are elements of a model or theory for the real laboratory experiment only. The only experimental facts are the settings of the various apparatuses and the detection events. What happens in between activating the source and the registration of the detection events belongs to the domain of imagination.

The processing units mimic the role of the optical components in the experiment and the network by connecting the processing units represents the complete experimental setup. The standard processing units consist of an input stage, a transformation stage and an output stage. The input (output) stage may have several channels at (through) which messengers arrive (leave). Other processing units are simpler in the sense that the input stage is not necessary for the proper functioning of the device. A message is represented by a set of numbers, conventionally represented by a vector. As a messenger arrives at an input channel of a processing unit, the input stage updates its internal state, represented by a vector, and sends the message together with its internal state to the transformation stage that implements the operation of the particular device. Then, a new message is sent to the output stage which selects the output channel through which the messenger will leave the unit. At any given time, there is only one messenger being routed through the whole network. There is no direct communication between the messengers. From this general description, it should already be clear that the process that is generated by the collective of classical dynamical systems is locally causal in Einstein's sense. Our simulation approach does not rely on concepts of probability theory but instead, it generates events by way of classical, dynamical processes, the frequencies of events of which converge to the quantum theoretical results as the dynamical system relaxes to its stationary state.

3.4 Simulation of pure and mixed states

In QT, the pure state is a description of the whole experiment, not of the individual events that are recorded by the detectors [1, 65]. In our simulation approach, the messages carried by the messengers represent the pure state, corresponding to a density matrix of the form $\rho = |\alpha_k\rangle \langle\alpha_k|$, that is $p_j = 0$ for all $j \neq k$ and $p_k = 1$. In our simulation approach, the messages are constructed such that a large collection of them yields the same averages as those we obtain from quantum theory. Loosely speaking, we may say that a set of N (N sufficiently large) messages of a certain type correspond to a pure state.

In the more general case, QT describes the whole experiment through the mixed state Eq. (3.2). We simulate the mixed state by the following procedure. Given $p_1, \ldots, p_m$, we pick an index $k \in \{1, \ldots, m\}$ using a pseudo-random number and then send N_k messages of type k (corresponding to the pure state $|\alpha_k\rangle$) through the network of processing units that represent the quantum system. The precise value of N_k is unimportant, as long as it is large enough to let the classical dynamical system mimic the pure state $|\alpha_k\rangle$.

For the case at hand, the quantum eraser, the source can emit a pure state, a linear combination of V and H polarized photons, or it can produce a mixed state of the two [37]. Thus, we have $m = 2$ and it what follows we will label the N's by the subscripts V and H to facilitate the comparison with the terminology used in the experiment [37]. Although not essential, in our simulation we simply choose $N_V = N_H$ and denote the probabilities for the V- and H-polarized photons in a mixed state by p_V and p_H, respectively.

3.5 Simulation model

As explained earlier, our simulation algorithm can be viewed as a message-processing and message-passing process: It routes messengers, representing the photons, through a network of message-processing units, playing the role of the optical components in the laboratory experiment. In what follows we give a detailed description of each of the components of the network representing the complete experimental setup of the quantum eraser experiment, schematically depicted in Fig. 3.1.

3.5.1 Messenger

A messenger has its own internal clock, the hand of which rotates with frequency f. When the messenger is created, the hand of the clock is set to time zero. As the messenger travels from one position in space to another, the clock encodes the time-of-flight modulo the period $1/f$. The message, the position of the clock's hand, is most conveniently represented by a two-dimensional unit vector $\mathbf{e}_l = (e_{0,l}, e_{1,l}) =$

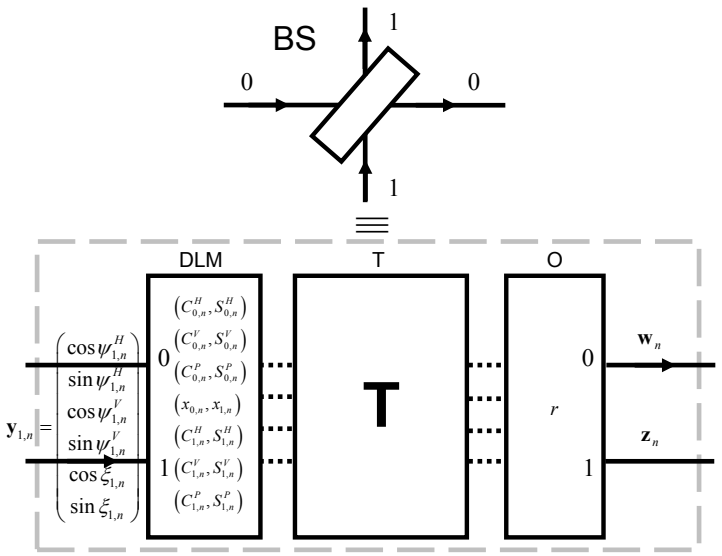

Figure 3.2: Diagram of a DLM-based processing unit that performs an event-based simulation of a beam splitter (BS). The processing unit consists of three stages: An input stage (DLM), a transformation stage (T) and an output stage (O). The solid lines represent the input and output channels of the BS. The presence of a message is indicated by an arrow on the corresponding channel line. The dashed lines indicate the data flow within the BS. The transformation matrix $\mathbf{T}$ is given in Eq. (3.15).

$(\cos\psi_l, \sin\psi_l)$, where $\psi_l = 2\pi f t$, the subscript $l \geq 0$ labeling the successive messages. The messenger travels with a speed c/n where n is the refractive index of the medium in which the messenger moves and c is the light velocity. Clearly, this messenger is the event-based equivalent of a classical, linearly polarized electromagnetic wave with frequency f: The messenger corresponds to the light ray with wave vector $\mathbf{k}(k = 2\pi f/c)$ and the clock mimics one of the electric field components in the plane orthogonal to $\mathbf{k}$ [63]. Adding another clock to the messenger suffices to model the second electric field component orthogonal to the first one, and hence the fully polarized wave [60].

Thus, each messenger carries a message represented by a six-dimensional unit vector

$$\mathbf{y}_{k,l} = \begin{pmatrix} \cos\psi^H_{k,l} \\ \sin\psi^H_{k,l} \\ \cos\psi^V_{k,l} \\ \sin\psi^V_{k,l} \\ \cos\xi_{k,l} \\ \sin\xi_{k,l} \end{pmatrix} . \tag{3.7}$$

where the superscript H (V) refers to the horizontal (vertical) component of the polarization and $\psi^H_{k,l}$, $\psi^V_{k,l}$, and $\xi_{k,l}$ represent the time of flight and polarization of the

photon, respectively. It is evident that the representation used here maps one-to-one to the plane-wave description of a classical electromagnetic field [63], except that we assign these properties to each individual messenger, not to a wave. The subscript $l \geq 0$ numbers the consecutive messages and $k = 0, 1$ labels the channel of the BS at which the message arrives (see below).

3.5.2 Beam splitter

Here we construct a processing unit that acts as a BS, not by calculating the amplitudes according to QT, but by processing individual events (see Fig. 3.2). It consists of an input stage, a simple deterministic learning machine (DLM) [55–58, 60], a transformation stage (T), an output stage (O) and has two input and two output channels labeled by $k = 0, 1$. We now define the operation of each stage explicitly.

- Input stage: The DLM receives a message on either input channel 0 or 1, never on both channels simultaneously. The arrival of a message on channel 0 (1) is named a 0 (1) event. The input events are represented by the vectors $\mathbf{v}_l = (1, 0)$ or $\mathbf{v}_l = (0, 1)$ if the lth event occurred on channel 0 or 1, respectively. The DLM has six internal registers $\mathbf{Y}^H_{k,l} = (C^H_{k,l}, S^H_{k,l})$, $\mathbf{Y}^V_{k,l} = (C^V_{k,l}, S^V_{k,l})$, $\mathbf{Y}^P_{k,l} = (C^P_{k,l}, S^P_{k,l})$ and one internal vector $\mathbf{x}_l = (x_{0,l}, x_{1,l})$, where $x_{0,l} + x_{1,l} = 1$ and $x_{k,l} \geq 0$ for $k = 0, 1$ and all $l \geq 0$. These seven two-dimensional vectors are labeled by the message number l to indicate that their values may change every time the DLM receives a message. The DLM has storage for no more than fourteen numbers.

  Upon receiving the lth input event, the DLM performs the following steps: It stores the first two elements of message $\mathbf{y}_{k,l}$ in its internal register $\mathbf{Y}^H_{k,l} = (C^H_{k,l}, S^H_{k,l})$, the middle two elements of $\mathbf{y}_{k,l}$ in $\mathbf{Y}^V_{k,l} = (C^V_{k,l}, S^V_{k,l})$, and the last two elements of $\mathbf{y}_{k,l}$ in $\mathbf{Y}^P_{k,l} = (C^P_{k,l}, S^P_{k,l})$. Then, it updates its internal vector according to the rule

  $$\mathbf{x}_l = \gamma \mathbf{x}_{l-1} + (1 - \gamma)\mathbf{v}_l, \tag{3.8}$$

  where $0 < \gamma < 1$. Note that by construction $x_{0,l} + x_{1,l} = 1$, $x_{0,l} \geq 0$ and $x_{1,l} \geq 0$, and the DLM stores information about the last message only. The information carried by earlier messages is overwritten by updating the internal registers. From the solution of Eq. (3.8),

  $$\mathbf{x}_l = \gamma^l \mathbf{x}_{l-1} + (1 - \gamma) \sum_{j=0}^{l-1} \gamma^{l-j-1} \mathbf{v}_{j+1}, \tag{3.9}$$

  the fact that in practice the sequence $\{\mathbf{v}_1, \mathbf{v}_2, \cdots, \mathbf{v}_K\}$ is finite, and the usual

trick to assume a periodic continuation of the sequence, we have

$$\begin{aligned}\mathbf{x}_{mK} &= \gamma^K \mathbf{x}_{(m-1)K} + (1-\gamma)\sum_{j=(m-1)K}^{mK-1} \gamma^{mK-j-1}\mathbf{v}_{j+1} \\ &= \gamma^K \mathbf{x}_{(m-1)K} + (1-\gamma)\sum_{j=0}^{K-1} \gamma^{K-j-1}\mathbf{v}_{j+1+(m-1)K} \\ &= \gamma^K \mathbf{x}_{(m-1)K} + (1-\gamma)\mathbf{f}_K \end{aligned} \tag{3.10}$$

where

$$\mathbf{f}_K = \sum_{j=0}^{K-1} \gamma^{K-j-1}\mathbf{v}_{j+1}, \tag{3.11}$$

and $m \geq 0$. From Eq. (3.10) we find

$$\mathbf{x}_{mK} = \gamma^{mK}\mathbf{x}_0 + (1-\gamma)\frac{1-\gamma^{mK}}{1-\gamma^K}\mathbf{f}_K, \tag{3.12}$$

and hence

$$\lim_{m\to\infty} \mathbf{x}_{mK} = \frac{1-\gamma}{1-\gamma^K}\sum_{j=0}^{K-1} \gamma^{K-j-1}\mathbf{v}_{j+1}, \tag{3.13}$$

such that

$$\lim_{\gamma\to 1^-}\lim_{m\to\infty} \mathbf{x}_{mK} = \frac{1}{K}\sum_{j=0}^{K-1} \mathbf{v}_{j+1}. \tag{3.14}$$

From Eq. (3.14), we conclude that as $\gamma \to 1^-$ the internal vector converges to the average of the vectors $\mathbf{v}_1, \mathbf{v}_2, \cdots, \mathbf{v}_K$ which represents the relative frequency of input events at the two channels of the BS ($k = 0, 1$). The parameter γ controls the speed of learning and also limits the precision with which the internal vector can represent a sequence of constant input messages [55]. Disregarding the fact that according to Eq. (3.14), we should let $\gamma \to 1^-$ to obtain the limiting value of the average of the $\mathbf{v}$'s, it is the only free parameter in the model. In practice, in the simulation we fix it once and for all.

- Transformation stage: The second stage (T) accepts the messages from the input stage, and transforms them into a new eight-dimensional vector

$$\mathbf{T} = \frac{1}{\sqrt{2}}\begin{pmatrix} C^H_{0,l}C^P_{0,l}\sqrt{x_{0,l}} - S^H_{1,l}C^P_{1,l}\sqrt{x_{1,l}} \\ C^H_{1,l}C^P_{1,l}\sqrt{x_{1,l}} + S^H_{0,l}C^P_{0,l}\sqrt{x_{0,l}} \\ C^V_{0,l}S^P_{0,l}\sqrt{x_{0,l}} - S^V_{1,l}S^P_{1,l}\sqrt{x_{1,l}} \\ C^V_{1,l}S^P_{1,l}\sqrt{x_{1,l}} + S^V_{0,l}S^P_{0,l}\sqrt{x_{0,l}} \\ C^H_{1,l}C^P_{1,l}\sqrt{x_{1,l}} - S^H_{0,l}C^P_{0,l}\sqrt{x_{0,l}} \\ C^H_{0,l}C^P_{0,l}\sqrt{x_{0,l}} + S^H_{1,l}C^P_{1,l}\sqrt{x_{1,l}} \\ C^V_{1,l}S^P_{1,l}\sqrt{x_{1,l}} - S^V_{0,l}S^P_{0,l}\sqrt{x_{0,l}} \\ C^V_{0,l}S^P_{0,l}\sqrt{x_{0,l}} + S^V_{1,l}S^P_{1,l}\sqrt{x_{1,l}} \end{pmatrix}. \tag{3.15}$$

If we rewrite the transformation T using complex numbers, we find that

$$\begin{pmatrix} b_0^H \\ b_0^V \\ b_1^H \\ b_1^V \end{pmatrix} = \frac{1}{\sqrt{2}} \begin{pmatrix} 1 & 0 & i & 0 \\ 0 & 1 & 0 & i \\ i & 0 & 1 & 0 \\ 0 & i & 0 & 1 \end{pmatrix} \begin{pmatrix} a_0^H \\ a_0^V \\ a_1^H \\ a_1^V \end{pmatrix}, \tag{3.16}$$

which is the unitary transformation in the quantum theoretical description of a BS, if $(a_0^H, a_0^V, a_1^H, a_1^V)$ and $(b_0^H, b_0^V, b_1^H, b_1^V)$ denote the input and output amplitudes of the photons with polarization H and V in the 0 and 1 channels of a BS, respectively. Note that in our simulation model there is no need to introduce the (quantum theoretical) concept of a vacuum field, a requirement in the quantum optical description of a BS.

- Output stage: The final stage (O) sends out a messenger (representing a photon) carrying the message

$$\mathbf{w} = \begin{pmatrix} w_{0,l}/s_{0,l} \\ w_{1,l}/s_{0,l} \\ w_{2,l}/s_{1,l} \\ w_{3,l}/s_{1,l} \\ s_{0,l}/s_{2,l} \\ s_{1,l}/s_{2,l} \end{pmatrix}, \tag{3.17}$$

where

$$\begin{aligned} w_{0,l} &= C_{0,l}^H C_{0,l}^P \sqrt{x_{0,l}} - S_{1,l}^H C_{1,l}^P \sqrt{x_{1,l}}, \\ w_{1,l} &= C_{1,l}^H C_{1,l}^P \sqrt{x_{1,l}} + S_{0,l}^H C_{0,l}^P \sqrt{x_{0,l}}, \\ w_{2,l} &= C_{0,l}^V S_{0,l}^P \sqrt{x_{0,l}} - S_{1,l}^V S_{1,l}^P \sqrt{x_{1,l}}, \\ w_{3,l} &= C_{1,l}^V S_{1,l}^P \sqrt{x_{1,l}} + S_{0,l}^V S_{0,l}^P \sqrt{x_{0,l}}, \\ s_{0,l} &= \sqrt{w_{0,l}^2 + w_{1,l}^2}, \\ s_{1,l} &= \sqrt{w_{2,l}^2 + w_{3,l}^2}, \\ s_{2,l} &= \sqrt{w_{0,l}^2 + w_{1,l}^2 + w_{2,l}^2 + w_{3,l}^2}, \end{aligned} \tag{3.18}$$

through output channel 0 if $s_{2,l}^2 > 2r$ where $0 < r < 1$ is a uniform pseudo-random number. Otherwise, if $s_{2,l}^2 \leq 2r$, the output stage sends through output

channel 1 the message

$$\mathbf{z} = \begin{pmatrix} z_{0,l}/t_{0,l} \\ z_{1,l}/t_{0,l} \\ z_{2,l}/t_{1,l} \\ z_{3,l}/t_{1,l} \\ t_{0,l}/t_{2,l} \\ t_{1,l}/t_{2,l} \end{pmatrix}, \tag{3.19}$$

where

$$\begin{aligned} z_{0,l} &= C^H_{1,l}C^P_{1,l}\sqrt{x_{1,l}} - S^H_{0,l}C^P_{0,l}\sqrt{x_{0,l}}, \\ z_{1,l} &= C^H_{0,l}C^P_{0,l}\sqrt{x_{0,l}} + S^H_{1,l}C^P_{1,l}\sqrt{x_{1,l}}, \\ z_{2,l} &= C^V_{1,l}S^P_{1,l}\sqrt{x_{1,l}} - S^V_{0,l}S^P_{0,l}\sqrt{x_{0,l}}, \\ z_{3,l} &= C^V_{0,l}S^P_{0,l}\sqrt{x_{0,l}} + S^V_{1,l}S^P_{1,l}\sqrt{x_{1,l}}, \\ t_{0,l} &= \sqrt{z^2_{0,l} + z^2_{1,l}}, \\ t_{1,l} &= \sqrt{z^2_{2,l} + z^2_{3,l}}, \\ t_{2,l} &= \sqrt{z^2_{0,l} + z^2_{1,l} + z^2_{2,l} + z^2_{3,l}}. \end{aligned} \tag{3.20}$$

The use of pseudo-random numbers to select the output channel is not essential [56]. We use pseudo-random numbers to mimic the apparent unpredictability of the experimental data only. Instead of a uniform pseudo-random number generator, any algorithm that selects the output channel in a systematic manner might be employed as well [56]. This will change the order in which messages are being processed but the content of the messages will be left intact and the resulting averages do not change significantly.

3.5.3 Polarizing Beam Splitter

A polarizing beam splitter (PBS) is used to redirect the photons on the basis of their polarization (H or V). The structure of the event-based processor that simulates a PBS is identical to the one of the BS and differs in the details of the transformation

stage only. For the PBS, the transformation $\mathbf{T}$ reads [60]

$$\mathbf{T} = \begin{pmatrix} C^H_{0,l+1} C^P_{0,l+1} \sqrt{x_{0,l+1}} \\ S^H_{0,l+1} C^P_{0,l+1} \sqrt{x_{0,l+1}} \\ -S^V_{1,l+1} S^P_{1,l+1} \sqrt{x_{1,l+1}} \\ C^V_{1,l+1} S^P_{1,l+1} \sqrt{x_{1,l+1}} \\ C^H_{1,l+1} C^P_{1,l+1} \sqrt{x_{1,l+1}} \\ S^H_{1,l+1} C^P_{1,l+1} \sqrt{x_{1,l+1}} \\ -S^V_{0,l+1} S^P_{0,l+1} \sqrt{x_{0,l+1}} \\ C^V_{0,l+1} S^P_{0,l+1} \sqrt{x_{0,l+1}} \end{pmatrix} . \tag{3.21}$$

3.5.4 Remaining optical components

In contrast to the BS and PBS, in terms of message processing the HWP and QWP are passive devices in the sense that the adaptive unit, the DLM, is not required for a proper functioning of the devices. As can be seen from the quantum theoretical description (see Appendix), a HWP does not only change the polarization of the photon but also changes its phase and a QWP additionally, introduces a phase difference between the H and V components. In our simulation model, the functionality of these optical components is implemented through plane rotations of the vectors $(\cos\xi_{k,l}, \sin\xi_{k,l})$, $(\cos\psi^H_{k,l}, \sin\psi^H_{k,l})$, and $(\cos\psi^V_{k,l}, \sin\psi^V_{k,l})$.

3.5.5 Data gathering and analysis procedure

In the simulation, the data is collected in the same manner as in the experiment. Detector D_0 (D_1) registers the output events at channel 0 (1) (see Fig. 3.1). During a run of N events, the algorithm generates the data set

$$\Gamma = \{x_l | l = 1, ..., N; \phi; \theta_{HWP0}; \theta_{HWP1}; \theta_{QWP}\}\,, \tag{3.22}$$

where $x_l = 0, 1$ indicates which detector fired (D_0 or D_1), ϕ denotes the phase shift (proportional to the difference in time-of-flight of Path0 and Path1) between the two interferometer arms and θ_{HWP0}, θ_{HWP1}, θ_{QWP} denote the angles of the optical axis of the respective waveplates with the laboratory frame. For fixed θ_{HWP0}, θ_{HWP1}, θ_{QWP} and ϕ, the number of detection events in detector 1 is given by $N_1 = \sum_{l=1}^{N} x_l$ and $N_0 = N - N_1$ is the number of detection events in detector 0. The appearance of interference fringes is conveniently characterized by the visibility [63]

$$\mathcal{V} = \frac{N_{max} - N_{min}}{N_{max} + N_{min}}, \tag{3.23}$$

where N_{max} and N_{min} denote the maximum and minimum of N_0 for all $\phi \in [0, 2\pi[$. Notice that for the experiment depicted in Fig. 3.1, the visibility is a function of θ_{HWP0}, θ_{HWP1}, and θ_{QWP}.

3.6 Simulation results

The processing units that simulate the optical components are connected in such a way that the simulation setup is an exact one-to-one copy of the real experiment (see Fig. 3.1). The simulation procedure is as follows: For each choice of ϕ in the range $[0, 2\pi[$, we fix θ_{HWP0}, θ_{HWP1} and θ_{QWP} and perform a simulation with 10^6 events, randomly distributed over groups of $N_H = 200$ or $N_V = 200$ events ($\alpha_1 = H$ and $\alpha_2 = V$ in the notation of Section 3.4). Then for each choice of θ_{HWP0}, θ_{HWP1}, θ_{QWP}, we repeat this procedure. The result of these calculations form the data set Γ (see Eq. (3.22)). From this data set, we compute the visibility according to Eq. (3.23). All simulations have been carried out with $\gamma = 0.99$.

3.6.1 Without QWP

In Fig. 3.3 we show our simulation results for the visibility as a function of $2\theta_{HWP1}$ for the quantum eraser experiment with the QWP removed (see Fig. 3.1). First we consider the case in which the source emits photons that in QT are described by a pure, vertically polarized (V) state. Each such photon, after passing through the first BS, has equal chance to end up in either of the two arms of the interferometer. In our simulation, the messenger representing this photon carries the message $\left(0, 0, \cos\psi_0^V, \sin\psi_0^V, 0, 1\right)$ (see Eq. (3.7)). If the photon follows Path0, it encounters HWP0, the optical axis of which makes an angle θ_{HWP0} with respect to the laboratory frame. HWP0 rotates the polarization of the photon by an angle $2\theta_{HWP0}$ [63]. The event-by-event simulation data and the results of QT are shown in Fig. 3.3(a). The simulation data are in quantitative agreement with the averages calculated from QT and in qualitative agreement with the experimental data (see Fig. 4(a) in Ref. [37]).

Next, we consider the case where in QT, the input to the quantum eraser is described by a (completely) mixed state. In QT, a mixed state simply means that photons emitted by the source are described by an incoherent mixture of horizontally and vertically polarized pure states. In Section 3.4, we explained how to implement mixed states in the event-based simulation approach. The simulation data for a source emitting photons described by a (completely) mixed state are shown in Fig. 3.3(b) and (c). Also in this case, our simulation data are in quantitative agreement with the averages computed from QT and in qualitative agreement with the experimental results reported in Ref. [37] (see Fig. 4(b) and (c)).

3.6.2 With QWP

In Fig. 3.4 we present some simulation data for the case that the QWP is present, see Fig. 3.1, and $\theta_{QWP} = 0$. If $\theta_{QWP} = 0$, the QWP does not change the polarization of the photons but changes their phase. We only consider the case that the single-photon source emits photons that in QT, are described by a pure state. Figure 3.4(a) shows

simulation data corresponding to incoming V-polarized photons, for $\theta_{HWP0} = 45^\circ$ (red bullets) and $\theta_{HWP0} = 10^\circ$ (black squares). In Fig. 3.4(b) we show the simulation data for the source that emits photons in a state that QT would characterize with $\xi = 45^\circ$, and $\theta_{HWP0} = 22.5^\circ$. In our simulation, this state is represented by messengers that carry the message $(\cos\psi_0^H, \sin\psi_0^H, \cos\psi_0^V, \sin\psi_0^V, 1/\sqrt{2}, 1/\sqrt{2})$. As in all other cases shown, the agreement between the event-based simulation data and QT is excellent.

3.7 Discussion

We have demonstrated that our classical, locally causal, particle-like simulation approach reproduces the results of the quantum eraser experiment [37] and the results of quantum theory describing the averages of these experimental results.

During the event-by-event simulation of the quantum eraser experiment we always have full which-way information of the photons (messengers) since we can always track them. Nevertheless, depending on the settings of the optical apparatuses, the photons build up an interference pattern at the detector. Although the appearance of an interference pattern is commonly considered to be characteristic for a wave, we have demonstrated that, as in experiment, it can also be built up by many photons. These photons have full which-way information and arrive one-by-one at a detector. Hence, even in the case that the source emits single photons, described by a pure state in quantum theory, and that $\mathcal{V} = 1$, commonly associated with full wave character, the photons in our simulation model have full which-way information. A consequence of our model is thus that the relation $\mathcal{V}^2 + \mathcal{D}^2 \leq 1$ cannot be regarded as quantifying the notion of complementarity: Our model always allows a particle-only description of the quantum eraser experiment, independent of the purity of the state describing the photons in quantum theory.

In summary, concepts of quantum theory applied to individual events fail to provide a logically consistent explanation for the experimental observation of single detector "clicks" building up an interference pattern and leave no option but to postulate that "this is the way it is". In contrast, our event-based simulation model, a classical locally causal dynamical system, reproduces the results of quantum theory without making reference to the solution of a wave equation and provides a simple, particle-based mental picture for what each individual photon experiences as it travels from the source to the detector. Just like in the experiments, our model produces data sets Eq. (3.22) which can be given to a third party for analysis long after the simulation has been finished. Because of the strong similarity between the experimental and simulation data sets the third party will have a very hard time, if possible at all, to identify the data sets as originating from a so-called "quantum experiment" or from a "classical simulation model".

Finally, we would like to emphasize that the algorithms used to simulate the optical

components of the quantum eraser have not designed to exclusively simulate this particular example but they can be used to reproduce the results of many other quantum optics experiments as well [29–32, 34, 55–60, 81].

Appendix

According to quantum theory (QT), photons in a pure state are described by the state vector

$$|\alpha\rangle = \begin{pmatrix} a_0^H \\ a_0^V \\ a_1^H \\ a_1^V \end{pmatrix}, \tag{3.24}$$

where H and V refer to the horizontal and vertical direction of polarization and the subscripts refer to the wave in Path0 and Path1, respectively. Within QT, the action of the various optical components is defined by the matrices

$$T_{BS} = \frac{1}{\sqrt{2}} \begin{pmatrix} 1 & 0 & i & 0 \\ 0 & 1 & 0 & i \\ i & 0 & 1 & 0 \\ 0 & i & 0 & 1 \end{pmatrix}, \tag{3.25}$$

$$T_{PBS} = \begin{pmatrix} 1 & 0 & 0 & 0 \\ 0 & 0 & 0 & i \\ 0 & 0 & 1 & 0 \\ 0 & i & 0 & 0 \end{pmatrix}, \tag{3.26}$$

$$T_{HWP0}(\theta) = -i \begin{pmatrix} c & s & 0 & 0 \\ s & -c & 0 & 0 \\ 0 & 0 & 1 & 0 \\ 0 & 0 & 0 & 1 \end{pmatrix}, \tag{3.27}$$

$$T_{HWP1}(\theta) = -i \begin{pmatrix} 1 & 0 & 0 & 0 \\ 0 & 1 & 0 & 0 \\ 0 & 0 & c & s \\ 0 & 0 & s & -c \end{pmatrix}, \tag{3.28}$$

$$T_{QWP}(\theta) = \frac{1}{\sqrt{2}} \begin{pmatrix} 1 & 0 & 0 & 0 \\ 0 & 1 & 0 & 0 \\ 0 & 0 & 1-ic & -is \\ 0 & 0 & -is & 1+ic \end{pmatrix}, \tag{3.29}$$

where θ denotes the angle of the optical axis with respect to the laboratory frame, $c = \cos 2\theta$ and $s = \sin 2\theta$.

Using these expressions, it is somewhat tedious but straightforward to calculate the visibility Eq. (3.23). We list the expressions for the cases for which we perform event-based simulations.

1. With the QWP removed, see Fig. 3.1, and for incoming photons that are described by a pure state of polarization ξ:

$$\mathcal{V} = \left| \frac{2\sin(\xi - 2\theta_0 + 2\theta_1)\sin(\xi - 2\theta_1)}{\sin^2(\xi - 2\theta_0 + 2\theta_1) + \sin^2(\xi - 2\theta_1)} \right|, \tag{3.30}$$

   where $\theta_0 = \theta_{HWP0}$ and $\theta_1 = \theta_{HWP1}$.

2. With the QWP removed and for incoming photons described by a mixed-state photon input with $p_V/p_H = \tan^2\beta$:

$$V = \left| \frac{2\sin(2\theta_0 - 2\theta_1)\sin(2\theta_1) + 2\tan^2\beta\cos(2\theta_0 - 2\theta_1)\cos(2\theta_1)}{\sin^2(2\theta_0 - 2\theta_1) + \sin^2(2\theta_1) + \tan^2\beta[\cos^2(2\theta_0 - 2\theta_1) + \cos^2(2\theta_1)]} \right|. \tag{3.31}$$

3. With the QWP present, $\theta_{QWP} = 0°$, and for incoming photons that are described by a pure state of polarization ξ:

$$V = \left| \frac{2\left[\tan^2 2\theta_1 \sin^2(2\xi - 2\theta_0) + [\sin(\xi - 2\theta_0)\sin\xi - \tan^2 2\theta_1 \cos(\xi - 2\theta_0)\cos\xi]^2\right]^{\frac{1}{2}}}{\sin^2(\xi - 2\theta_0) + \tan^2 2\theta_1 \cos^2(\xi - 2\theta_0) + \tan^2 2\theta_1 \cos^2\xi + \sin^2\xi} \right|. \tag{3.32}$$

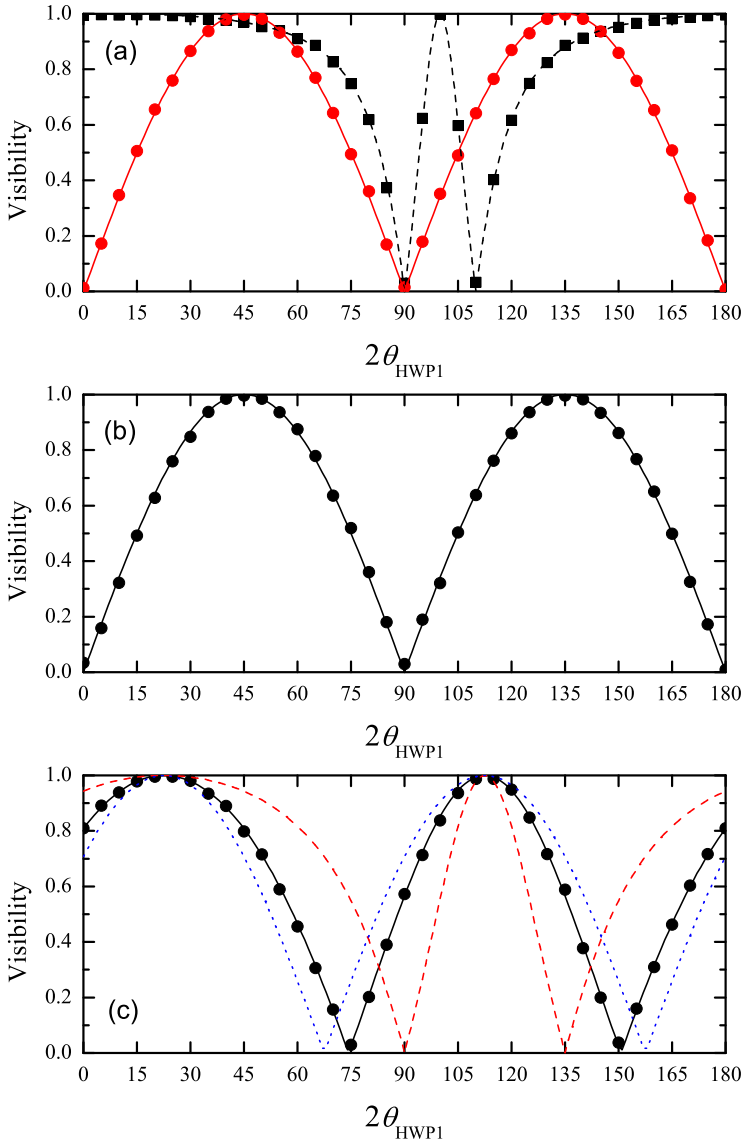

Figure 3.3: Visibility as a function of the angle $2\theta_{HWP1}$ for the quantum eraser experiment with the QWP removed (see Fig. 3.1). The markers (squares, bullets) and lines (solid, dashed) represent the event-by-event simulation data and the quantum theoretical results (see Eqs. (3.30) and (3.31)), respectively. (a) The source emits photons described by the pure vertically polarized state V and $\theta_{HWP0} = 45°$ (red bullets and solid line), $\theta_{HWP0} = 10°$ (black squares and dashed line); (b) The source emits photons described by the completely mixed state ($p_V = p_H = 1/2$) and $\theta_{HWP0} = 45°$; (c) The source emits photons described by a partially mixed state with $p_V = 2/3$, $p_H = 1/3$ and $\theta_{HWP0} = 22.5°$ (black bullets and solid line). The red dashed and blue dotted curves represent the quantum theoretical results for the pure vertically polarized state V and the completely mixed state, respectively.

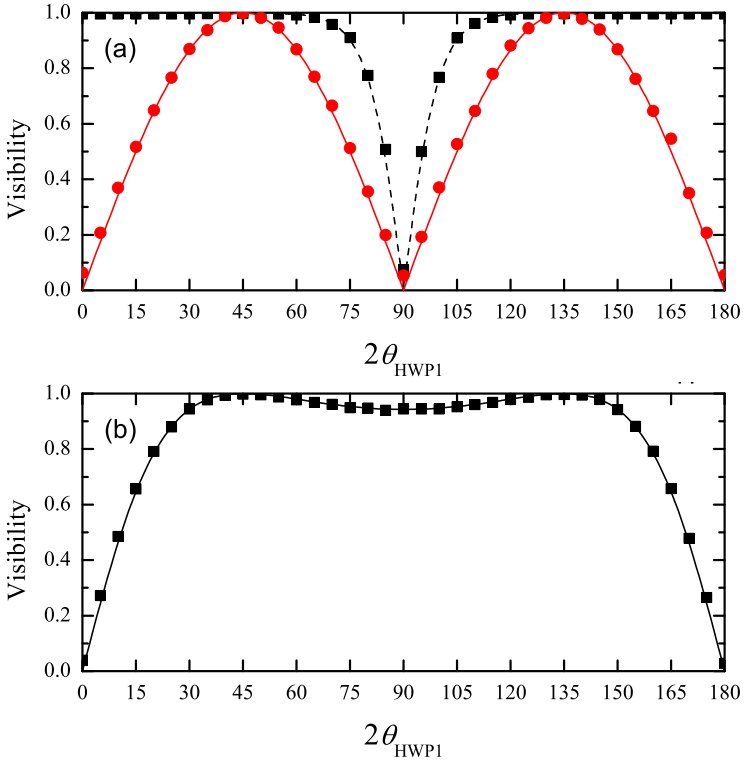

Figure 3.4: Visibility as a function of the angle $2\theta_{HWP1}$ for the quantum eraser experiment depicted in Fig. 3.1 with $\theta_{QWP} = 0$. The markers (squares, bullets) and lines (solid, dashed) represent the event-by-event simulation data and the quantum theoretical results (see Eq. (3.32)), respectively. (a) The source emits photons described by the pure vertically polarized state V and $\theta_{HWP0} = 45°$ (red bullets and solid line), $\theta_{HWP0} = 10°$ (black squares and dashed line); (b) The source emits photons described by the pure $\xi = 45°$-polarized state and $\theta_{HWP0} = 22.5°$.

Chapter 4

EPR–the Effect of Time-window W

4.1 Introduction

As stressed in the discussion section of Chapter 2, if trying to simulate the quantum correlations, we should take another factor – the coincidence time window W into account. In real experiments, it is necessary to specify the procedure by which we count coincidences of detection events. It is also important to introduce such procedure in our simulation. In this chapter we discuss a simulation model of Einstein-Podolsky-Rosen-Bohm (EPRB) experiments. The model is totally based on the experimental status and satisfies the Einstein's locality criterion. The essential part of the model is that a time tag is introduced when the particle passes through the observation station and a time window W is used to determine whether two particles are considered to be coincident. As the model shows, only when $W \to 0$, the quantum correlation can be reproduced.

In the following, we briefly review a typical EPRB experiments [38], stress the importance of time-window W by analyzing the experimental data. Then a simulation model which simulate the EPRB experiment in Ref. [40] will be introduced.

4.2 EPRB experiments

In Fig. 4.1, we show a schematic diagram of an EPRB experiment with photons (see also Fig. 2 in [38]). The source emits pairs of photons. Each photon of a pair propagates to an observation station in which it is manipulated and detected. The two stations are separated spatially and temporally [38]. This arrangement prevents the observation at station 1 (2) to have a causal effect on the data registered at station

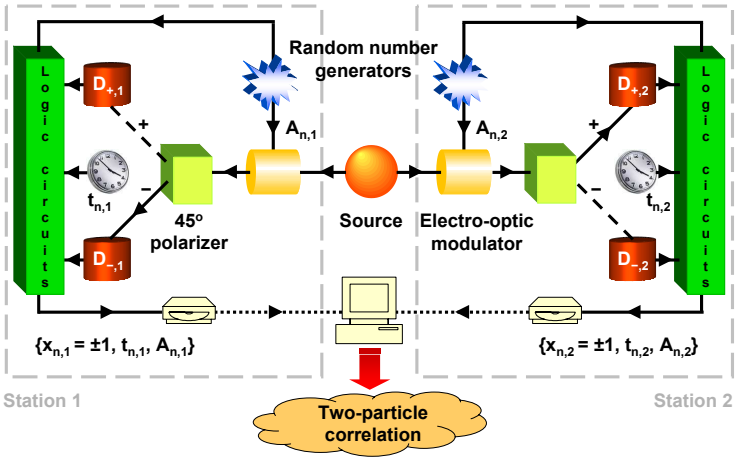

Figure 4.1: Schematic diagram of an EPRB experiment with photons.

2 (1) [38]. As the photon arrives at station $i = 1, 2$, it passes through an electro-optic modulator that rotates the polarization of the photon by an angle depending on the voltage applied to the modulator. These voltages are controlled by two independent binary random number generators. As the photon leaves the polarizer, it generates a signal in one of the two detectors. The station's clock assigns a time-tag to each generated signal. Effectively, this procedure discretizes time in intervals of a width that is determined by the time-tag resolution τ [38]. In the experiment, the firing of a detector is regarded as an event.

As we wish to demonstrate that it is possible to reproduce the results of quantum theory (which implicitly assumes idealized conditions) for the EPRB gedanken experiment by an event-based simulation algorithm, it would be logically inconsistent to "recover" the results of the former by simulating nonideal experiments. Therefore, we consider ideal experiments only, meaning that we assume that detectors operate with 100% efficiency, clocks remain synchronized forever, the "fair sampling" assumption is satisfied [25], and so on. We assume that the two stations are separated spatially and temporally such that the manipulation and observation at station 1 (2) cannot have a causal effect on the data registered at station 2 (1). Furthermore, to realize the EPRB gedanken experiment on the computer, we assume that the orientation of each electro-optic modulator can be changed at will, at any time. Although these conditions are very difficult to satisfy in real experiments, they are trivially realized in computer experiments.

In the experiment, the firing of a detector is regarded as an event. At the nth event, the data recorded on a hard disk at station $i = 1, 2$ consists of $x_{n,i} = \pm 1$, specifying which of the two detectors fired, the time tag $t_{n,i}$ indicating the time at which a detector fired, and the two-dimensional unit vector $\mathbf{a}_{n,i}$ that represents the rotation

of the polarization by the electro-optic modulator. Hence, the set of data collected at station $i = 1, 2$ during a run of N events may be written as

$$\Upsilon_i = \{x_{n,i} = \pm 1, t_{n,i}, \mathbf{a}_{n,i} | n = 1, \ldots, N\}\,. \tag{4.1}$$

In the (computer) experiment, the data $\{\Upsilon_1, \Upsilon_2\}$ may be analyzed long after the data has been collected [38]. Coincidences are identified by comparing the time differences $\{t_{n,1} - t_{m,2} | n, m = 1, \ldots, N\}$ with a time window W [38]. Introducing the symbol $\sum'$ to indicate that the sum has to be taken over all events that satisfy $\mathbf{a}_i = \mathbf{a}_{n,i}$ for $i = 1, 2$, for each pair of directions $\mathbf{a}_1$ and $\mathbf{a}_2$ of the electro-optic modulators, the number of coincidences $C_{xy} \equiv C_{xy}(\mathbf{a}_1, \mathbf{a}_2)$ between detectors $D_{x,1}$ ($x = \pm 1$) at station 1 and detectors $D_{y,2}$ ($y = \pm 1$) at station 2 is given by

$$C_{xy} \;=\; {\sum_{n,m=1}^{N}}' \delta_{x,x_{n,1}} \delta_{y,x_{m,2}} \Theta(W - |t_{n,1} - t_{m,2}|), \tag{4.2}$$

where $\Theta(t)$ is the Heaviside step function. We emphasize that we count all events that, according to the same criterion as the one employed in experiment, correspond to the detection of pairs. The average single-particle counts and the two-particle average are defined by

$$\begin{aligned} E_1(\mathbf{a}_1, \mathbf{a}_2) &= \frac{\sum_{x,y=\pm 1} x C_{xy}}{\sum_{x,y=\pm 1} C_{xy}}, \\ E_2(\mathbf{a}_1, \mathbf{a}_2) &= \frac{\sum_{x,y=\pm 1} y C_{xy}}{\sum_{x,y=\pm 1} C_{xy}}, \end{aligned} \tag{4.3}$$

and

$$\begin{aligned} E(\mathbf{a}_1, \mathbf{a}_2) &= \frac{\sum_{x,y=\pm 1} xy C_{xy}}{\sum_{x,y=\pm 1} C_{xy}} \\ &= \frac{C_{++} + C_{--} - C_{+-} - C_{-+}}{C_{++} + C_{--} + C_{+-} + C_{-+}}, \end{aligned} \tag{4.4}$$

respectively. In Eqs. (4.3) and (4.4), the denominator is the sum of all coincidences. For later use, it is expedient to introduce the function

$$S(\mathbf{a}, \mathbf{b}, \mathbf{c}, \mathbf{d}) = E(\mathbf{a}, \mathbf{c}) - E(\mathbf{a}, \mathbf{d}) + E(\mathbf{b}, \mathbf{c}) + E(\mathbf{b}, \mathbf{d}), \tag{4.5}$$

and its maximum

$$S_{max} \;\equiv\; \max_{\mathbf{a},\mathbf{b},\mathbf{c},\mathbf{d}} S(\mathbf{a}, \mathbf{b}, \mathbf{c}, \mathbf{d}). \tag{4.6}$$

4.2.1 Analysis of real experimental data

We illustrate the procedure of data analysis and the importance of the choice of the time window W by analyzing a data set (the archives Alice.zip and Bob.zip) of an EPRB experiment with photons that is publicly available [39].

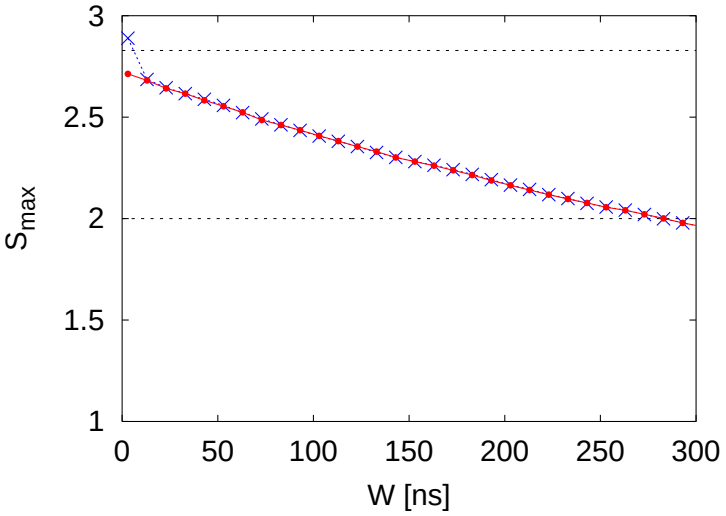

Figure 4.2: (color online) S_{max} as a function of the time window W, computed from the data sets contained in the archives Alice.zip and Bob.zip that can be downloaded from Ref. [39]. Bullets (red): Data obtained by using the relative time shift $\Delta = 4$ ns that maximizes the number of coincidences. Crosses (blue): Raw data ($\Delta = 0$). Dashed line at $2\sqrt{2}$: S_{max} if the system is described by quantum theory (see Section 4.3). Dashed line at 2: S_{max} if the system is described by the class of models introduced by Bell [5].

In the real experiment, the number of events detected at station 1 is unlikely to be the same as the number of events detected at station 2. In fact, the data sets of Ref. [39] show that station 1 (Alice.zip) recorded 388455 events while station 2 (Bob.zip) recorded 302271 events. Furthermore, in the real EPRB experiment, there may be an unknown shift Δ (assumed to be constant during the experiment) between the times $t_{n,1}$ gathered at station 1 and the times $t_{m,2}$ recorded at station 2. Therefore, there is some extra ambiguity in matching the data of station 1 to the data of station 2.

A simple data processing procedure that resolves this ambiguity consists of two steps [111]. First, we make a histogram of the time differences $t_{n,1} - t_{m,2}$ with a small but reasonable resolution (we used 0.5 ns). Then, we fix the value of the time-shift Δ by searching for the time difference for which the histogram reaches its maximum, that is we maximize the number of coincidences by a suitable choice of Δ. For the case at hand, we find $\Delta = 4$ ns. Finally, we compute the coincidences, the two-particle average, and S_{max} using the expressions given earlier. The average times between two detection events is 2.5 ms and 3.3 ms for Alice and Bob, respectively. The number of coincidences (with double counts removed) is 13975 and 2899 for ($\Delta = 4$ ns, $W = 2$ ns) and ($\Delta = 0$, $W = 3$ ns) respectively.

In Fig. 4.2 we present the results for S_{max} as a function of the time window W. First, it is clear that S_{max} decreases significantly as W increases but it is also clear that as

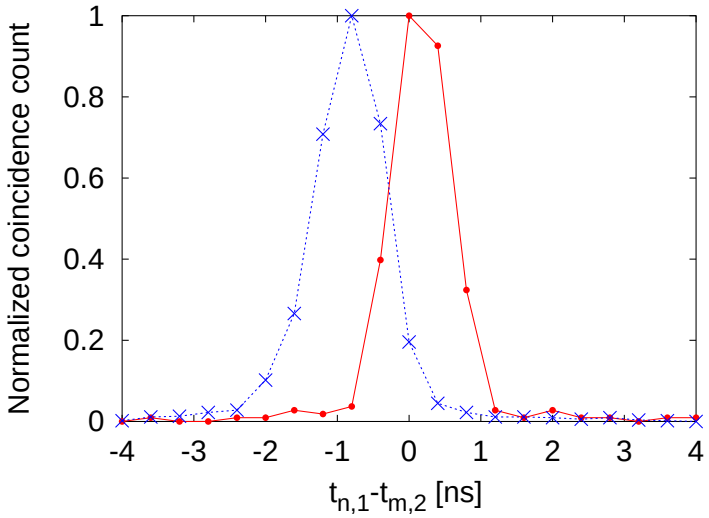

Figure 4.3: (color online) Normalized coincidence counts as a function of time tag difference $t_{n,1} - t_{m,2}$, computed from the data sets contained in the archives Alice.zip and Bob.zip [39], using the relative time shift $\Delta = 4$ ns that maximizes the number of coincidences. Bullets (red): $\theta_1 = 0$ and $\theta_2 = \pi/8$; Crosses (blue): $\theta_1 = 0$ and $\theta_2 = 3\pi/8$.

$W \to 0$, S_{max} is not very sensitive to the choice of W [111]. Second, the procedure of maximizing the coincidence count by varying Δ reduces the maximum value of S_{max} from a value 2.89 that considerably exceeds the maximum for the quantum system ($2\sqrt{2}$, see Section 4.3) to a value 2.73 that violates the Bell inequality ($S_{max} \leq 2$, see Ref. [5]) and is less than the maximum for the quantum system.

Finally, we use the experimental data to show that the time delays depend on the orientation of the polarizer. To this end, we select all coincidences between $D_{+,1}$ and $D_{+,2}$ (see Fig. 4.1) and make a histogram of the coincidence counts as a function of the time-tag difference, for fixed orientation $\theta_1 = 0$ and the two orientations $\theta_2 = \pi/8, 3\pi/8$ (other combinations give similar results). The results of this analysis are shown in Fig. 4.3. The maximum of the distribution shifts by approximately 1 ns as the polarizer at station 2 is rotated by $\pi/4$, a demonstration that the time-tag data is sensitive to the orientation of the polarizer at station 2. A similar distribution of time-delays (of about the same width) was also observed in a much older experimental realization of the EPRB experiment [112]. The time delays that result from differences in the orientations of the polarizers is much larger than the average time between detection events, which for the data that we analyzed is about 30000 ns. In other words, the loss in correlation that we observe as a function of increasing W (see Fig. 4.2) cannot be explained by assuming that we calculate correlations using photons that belong to different pairs.

Strictly speaking, we cannot derive the time delay from classical electrodynamics:

The concept of a photon has no place in Maxwell's theory. A more detailed understanding of the time delay mechanism requires dedicated, single-photon retardation measurements for these specific optical elements.

4.2.2 Role of the coincidence window W

The crucial point is that in any real EPR-type experiment, it is necessary to have an operational procedure to decide if the two detection events correspond to the observation of one two-particle system or to the observation of two single-particle systems. In standard "hidden variable" treatments of the EPR gedanken experiment [5], the operational definition of "observation of a single two-particle system" is missing. In EPRB-type experiments, this decision is taken on the basis of coincidence in time [38, 112, 113].

Our analysis of the experimental data shows beyond doubt that a model which aims to describe real EPRB experiments should include the time window W and that the interesting regime is $W \to 0$, not $W \to \infty$ as is assumed in all textbook treatments of the EPRB experiment. Indeed, in quantum mechanics textbooks it is standard to assume that an EPRB experiment measures the correlation [5]

$$C_{xy}^{(\infty)} \quad = \quad {\sum}'_{n=1}^{N} \delta_{x,x_{n,1}} \delta_{y,x_{n,2}}, \tag{4.7}$$

which we obtain from Eq. (4.2) by taking the limit $W \to \infty$. Although this limit defines a valid theoretical model, there is no reason why this model should have any bearing on the real experiments, in particular because experiments pay considerable attention to the choice of W. In experiments a lot of effort is made to reduce (not increase) W [38, 111].

4.3 Quantum theory

According to the axioms of quantum theory [65], repeated measurements on the two-spin system described by the density matrix ρ yield statistical estimates for the single-spin expectation values

$$\widetilde{E}_1(\mathbf{a}) \quad = \quad \langle \sigma_1 \cdot \mathbf{a} \rangle \quad , \quad \widetilde{E}_2(\mathbf{b}) = \langle \sigma_2 \cdot \mathbf{b} \rangle, \tag{4.8}$$

and the two-spin expectation value

$$\widetilde{E}(\mathbf{a}, \mathbf{b}) \quad = \quad \langle \sigma_1 \cdot \mathbf{a}\, \sigma_2 \cdot \mathbf{b} \rangle, \tag{4.9}$$

where $\sigma_i = (\sigma_i^x, \sigma_i^y, \sigma_i^z)$ are the Pauli spin-1/2 matrices describing the spin of particle $i = 1, 2$ [65], and $\mathbf{a}$ and $\mathbf{b}$ are unit vectors. We have introduced the tilde to distinguish the quantum theoretical results from the results obtained from the data sets $\{\Upsilon_1, \Upsilon_2\}$.

The quantum theoretical description of the EPRB experiment assumes that the system is represented by the singlet state $|\Psi\rangle = (|H\rangle_1|V\rangle_2 - |V\rangle_1|H\rangle_2)/\sqrt{2}$ of two spin-1/2 particles, where H and V denote the horizontal and vertical polarization and the subscripts refer to photon 1 and 2, respectively. For the singlet state $\rho = |\Psi\rangle\langle\Psi|$, $\widetilde{E}_1(\mathbf{a}) = \widetilde{\mathbf{E}}_\mathbf{2}(\mathbf{b}) = \mathbf{0}$ and

$$\widetilde{E}(\mathbf{a},\mathbf{b}) \quad = \quad -\mathbf{a}\cdot\mathbf{b}. \tag{4.10}$$

4.4 Simulation model

A concrete simulation model of the EPRB experiment sketched in Fig. 4.1 requires a specification of the information carried by the particles, of the algorithm that simulates the source and the observation stations, and of the procedure to analyze the data. As simulation model corresponding to the EPRB experiment in Ref. [38] has been presented in [34]. In the following, we briefly describe a simulation model corresponding to the real experiment in Ref. [40] (see Fig. 4.4). For the usually EPRB experiment setup sketched in Fig. 4.1, the observation station only can be placed in the xz plane on the Poincaré sphere. In the experimental setup of Fig. 4.4, a quarter-wave plate with the fast axis aligned along the horizontal direction at Bob side is introduced, which effectively rotates the polarization state by 90° around the z-axis on the Poincaré sphere. So the observation station in the yz plane is realized.

For later use, it is expedient to introduce another function

$$S^{'}(\phi) = |E_{11}(\phi) + E_{23}(0)| + |E_{22}(\phi) + E_{23}(0)|\,, \tag{4.11}$$

where $E_{ij}(\phi)$ is the correlation function defined in the plane of $\mathbf{a_i}$ and $\mathbf{b_j}$ with the same relative angle ϕ on the Poincaré sphere (see the bottom diagram in Fig. 4.4). Eq. (4.10) gives the quantum theory expression for $E_{ij}(\phi)$, but in the representation of Poincaré sphere, it is expressed as

$$\widetilde{E}_{ij}(\phi) \quad = \quad -\cos\phi. \tag{4.12}$$

This function has upper bound according to the theory of Ref. [40]:

$$S^{'}(\phi) \leq 4 - \frac{4}{\pi}\left|\sin\frac{\phi}{2}\right|. \tag{4.13}$$

Source and particles: The source emits particles that carry a unit vector $\mathbf{S}_{n,i} = (-1)^{i+1}(\cos\varphi_n \sin\theta_n, \sin\varphi_n \sin\theta_n, \cos\theta_n)$ (in the representation of Poincaré sphere), representing the polarization of the photons that travel to station $i = 1$ (Alice) and station $i = 2$ (Bob), respectively. Note that the two particles have opposite directions in the Poincaré sphere. The "state" of a particle is completely characterized by θ_n and

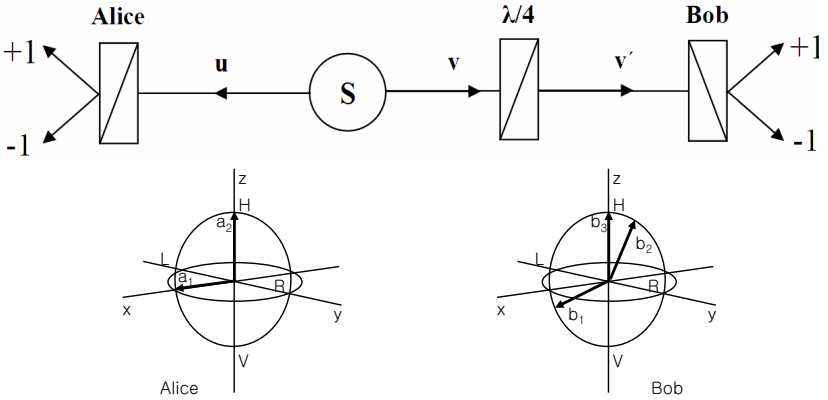

Figure 4.4: Schematic diagram of an EPRB experiment [40]. Top: The experimental setup. Bottom: The observation stations in Alice and Bob sides. The quarter-wave plate is introduced, so the observation of b_2 in yz plane on the Poincaré sphere is realized.

φ_n, which are distributed uniformly over the whole interval $[0, 2\pi]$. For the purpose of mimicking the apparent unpredictability of the experimental data, we use uniform random numbers. However, from the description of the algorithm, it will be clear that the use of random numbers is not essential. Simple counters that sample the intervals $[0, 2\pi]$ in a systematic, but uniform, manner might be employed as well.

Observation station: As in the experiment [40], there are two options $\mathbf{a}_i$ $(i = 1, 2)$ in Alice's side and three options $\mathbf{b}_j$ $(j = 1, 2, 3)$ in Bob's side (see Fig. 4.4). We use random numbers to select the poralizer in Alice's and Bob's side. We have two models for the output events:

1. **Deterministic model,**

$$\begin{aligned} x_{n,1} &= sign(\mathbf{S_{n,1}} \cdot \mathbf{a_i}), \\ x_{n,2} &= sign(\mathbf{S_{n,2}} \cdot \mathbf{b_j}). \end{aligned} \tag{4.14}$$

2. **Pseudo-random model,**

$$\begin{aligned} x_{n,1} &= \begin{cases} +1 & if \quad r_{n,1} \le \mathbf{S_{n,1}} \cdot \mathbf{a_i} \\ -1 & if \quad r_{n,1} > \mathbf{S_{n,1}} \cdot \mathbf{a_i} \end{cases}, \\ x_{n,2} &= \begin{cases} +1 & if \quad r_{n,2} \le \mathbf{S_{n,2}} \cdot \mathbf{b_j} \\ -1 & if \quad r_{n,2} > \mathbf{S_{n,2}} \cdot \mathbf{b_j} \end{cases}, \end{aligned} \tag{4.15}$$

where $0 \le r_n < 1$ are uniform pseudo-random numbers.

For conciseness, in this chapter, we show results for the first one only.

Time-tag model: To assign a time-tag to each event, we assume that as a particle passes through the detection system, it may experience a time delay. In our model,

the time delay $t_{n,i}$ for a particle is assumed to be distributed uniformly over the interval $[t_0, t_0 + T]$, an assumption that is not in conflict with available data [111]. In practice, we use uniform random numbers to generate $t_{n,i}$. The random choice of $t_{n,i}$ is merely convenient, not essential. From Eq. (4.2), it follows that only differences of time delays matter. Hence, we may put $t_0 = 0$. The time-tag for the event n is then $t_{n,i} \in [0, T]$.

There are not many options to make a reasonable choice for T. Assuming that the particle "knows" its own direction and that of the polarizer only, we can construct one number that depends on the relative angle: $\mathbf{S}_{n,i} \cdot \mathbf{a}_i$. Thus, $T = T(\xi_n)$ depends only on the relative angle ξ_n between $\mathbf{S}_{n,i}$ and $\mathbf{a}_i$. Furthermore, consistency with classical electrodynamics requires that functions that depend on the polarization have period π [63]. Thus, we must have $T(\xi_n) = F((\mathbf{S}_{n,i} \cdot \mathbf{a}_i)^2)$. We already used $\mathbf{S}_{n,i} \cdot \mathbf{a}_i$ to determine whether the particle generates a $+1$ or -1 signal. By trial and error, we found that $T(\xi_n) = T_0|1 - (\mathbf{S}_{n,i} \cdot \mathbf{a}_i)^2|^{d/2} = T_0|\sin\xi_n|^d$ yields useful results [29–33]. Here, $T_0 = \max_\xi T(\xi)$ is the maximum time delay and defines the unit of time, used in the simulation and d is a free parameter of the model which $d = 3$ for deterministic model and $d = 7$ for pseudo-random model give the quantum correlation. In our numerical work, we set $T_0 = 1$.

Data analysis: The algorithm generates the data sets Υ_i just as experiment does [38, 40]. In order to count the coincidences, we choose a time-tag resolution $0 < \tau < T_0$ and a coincidence window $\tau \leq W$. We set the correlation counts $C_{xy}(\mathbf{a_i}, \mathbf{b_j})$ to zero initially. We compute the discretized time tags $k_{n,i} = \lceil t_{n,i}/\tau \rceil$ for all events in both data sets. Here $\lceil x \rceil$ denotes the smallest integer that is larger or equal to x, that is $\lceil x \rceil - 1 < x \leq \lceil x \rceil$. According to the procedure adopted in the experiment [38, 40], an entangled photon pair is observed if and only if $|k_{n,1} - k_{n,2}| < k = \lceil W/\tau \rceil$. Thus, if $|k_{n,1} - k_{n,2}| < k$, we increment the count $C_{x_{n,1},x_{n,2}}(\mathbf{a_i}, \mathbf{b_j})$.

4.5 Simulation results

The simulation proceeds in the same way as the experiment, that is we first collect the data sets $\{\Upsilon_1, \Upsilon_2\}$, and then compute the coincidences Eq. (4.2) and the correlation Eq. (4.4). The simulation results for the coincidences $C_{xy}(\alpha, \beta)$ depend on the time-tag resolution τ, the time window W and the number of events N, just as in real experiments [38, 40].

Figure 4.5 shows simulation data for $E(\phi)$ as obtained for d=3, $N \approx 10^6$, $\tau = 0.001$ and $k = W/\tau = 1, 10, 100$. In the simulation, for each event, we use random numbers to select one pair observation station (a_i, b_j) $(i = 1, 2, j = 1, 2, 3)$. (a_i, b_j) is set as in real experiment (see Fig. 4.4) [40]. In Fig. 4.6 we present the simulation data according to the function $S'(\phi)$ (see Eq. (4.11)).

From Fig. 4.5 and 4.6, it is clear that the simulation data for $k = 1$ are in excellent agreement with quantum theory. Within the statistical noise, the simulation data (not

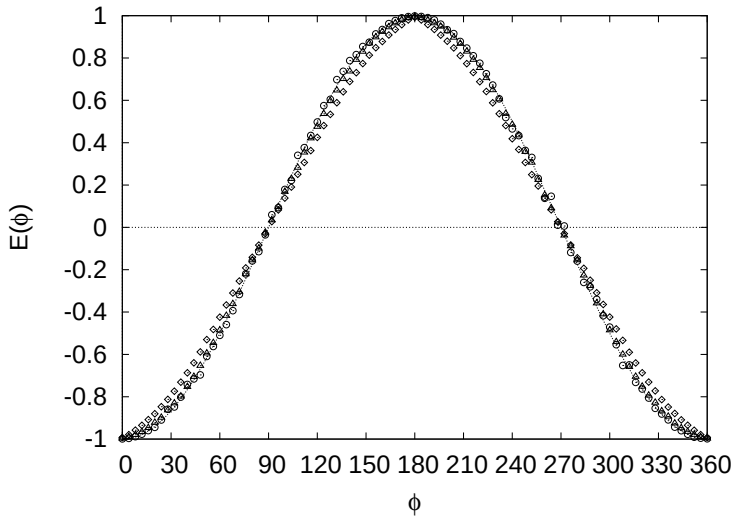

Figure 4.5: The simulation data of $E_{11}(\phi)$ (see Eq. (4.11)). Circles, triangles and diamonds correspond to the data with $k = W/\tau = 1, 10$ and 100, respectively. Dotted line: Quantum theory (Eq. (4.12)).

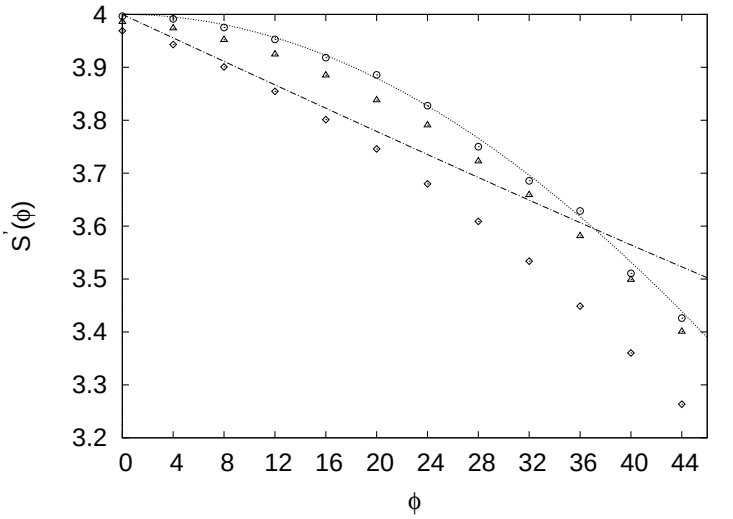

Figure 4.6: The simulation data of the function $S^{'}(\phi)$ (see Eq. (4.11)). Circles, triangles and diamonds correspond to the data with $k = W/\tau = 1, 10$ and 100, respectively. Dotted line: Quantum theory (Eq. (4.12)); Dotted-dashed line: Theory by Gröblacher *et al.* [40].

shown) for the single-spin expectation values also reproduce the results of quantum theory. As $W = \tau k \to \infty$, the simulation data deviate from the quantum theory.

For $k = 100$, the simulation data do not violate the upper bond of the function $S^{'}(\phi)$ (see Eq. (4.13)). The simulation data totally agree with the analysis of the real experimental data (see section 4.2.1).

Additional simulation results (not shown) demonstrate that the kind of models described earlier are capable of reproducing all the results of quantum theory for a system of two S=1/2 particles [29–33]. Furthermore, to first order in W and in the limit that the number of events goes to infinity, one can prove rigorously that these simulation models give the same expressions for the single- and two-particle averages as those obtained from quantum theory [29–33].

4.6 Discussion

Starting from the factual observation that experimental realizations of the EPRB experiment produce the data $\{\Upsilon_1, \Upsilon_2\}$ (see Eq. (4.1)) and that coincidence in time is a key ingredient for the data analysis, we have described a computer simulation model that satisfies Einstein's criterion of local causality and, exactly reproduces the correlation $\widetilde{E}(\mathbf{a}, \mathbf{b}) = -\mathbf{a} \cdot \mathbf{b}$ that is characteristic for a quantum system in the singlet state.

We have shown that whether or not these simulation models produce quantum correlations depends on the data analysis procedure that is performed (long) after the data has been collected: In order to observe the correlations of the singlet state, the resolution τ of the devices that generate the time-tags and the time window W should be made as small as possible. Disregarding the time-tag data ($d = 0$ or $W \longrightarrow \infty$) yields results that disagree with quantum theory but agree with the models considered by Bell [5] and by Gröblacher *et al.* [40]. Our analysis of real experimental data and our simulation results show that increasing the time window changes the nature of the two-particle correlations [29–33].

According to the folklore about Bell's theorem (and followers), a procedure such as the one that we described should not exist. Bell's theorem states that any local, hidden variable model will produce results that are in conflict with the quantum theory of a system of two $S = 1/2$ particles [5]. However, it is often overlooked that this statement can be proven for a (very) restricted class of probabilistic models only. In fact, Bell's theorem does not necessarily apply to the systems that we are interested in as both simulation algorithms and actual data do not need to satisfy the (hidden) conditions under which Bell's theorem hold [16, 114, 115].

Furthermore, the apparent conflict between the fact that there exist event-based simulation models that satisfy Einstein's criterion of local causality and reproduce all the results of the quantum theory of a system of two $S = 1/2$ particles and the folklore about Bell's theorem, stating that such models are not supposed to exist dissolves immediately if one recognizes that Bell's extension of Einstein's concept of locality

to the domain of probabilistic theories relies on the hidden, fundamental assumption that the absence of a causal influence implies logical independence [7, 12].

The simulation model that is described in this chapter is an example of a purely ontological model that reproduces quantum phenomena without first solving the quantum problem. The salient features of our simulation models [30–32, 55–59] are that they

1. generate, event-by-event, the same type of data as recorded in experiment,
2. analyze data according to the procedure used in experiment,
3. satisfy Einstein's criterion of local causality,
4. do not rely on any concept of quantum theory or probability theory,
5. reproduce the averages that we compute from quantum theory.

References

Bibliography

[1] D. Home. *Conceptual Foundations of Quantum Physics*. Plenum Press, New York, 1997.

[2] P. G. Merli, G. F. Missiroli, and G. Pozzi. On the statistical aspect of electron interference phenomena. *Am. J. Phys.*, 44:306–307, 1976.

[3] A. Tonomura, J. Endo, T. Matsuda, T. Kawasaki, and H. Ezawa. Demonstration of single-electron buildup of an interference pattern. *Am. J. Phys.*, 57:117–120, 1989.

[4] D. P. Landau and K. Binder. *A Guide to Monte Carlo Simulation in Statistical Physics*. Cambridge University Press, Cambridge, 2000.

[5] J. S. Bell. *Speakable and unspeakable in quantum mechanics*. Cambridge University Press, Cambridge, 1993.

[6] L. de la Peña, A.M. Cetto, and T.A. Brody. On Hidden-Variable Theories and Bell's Inequality. *Lett. Nuovo Cim.*, 5:177 – 181, 1972.

[7] A. Fine. On the Completeness of Quantum Theory. *Synthese*, 29:257 – 289, 1974.

[8] A. Fine. Some Local Models for Correlation Experiments. *Synthese*, 50:279 – 294, 1982.

[9] A. Fine. Hidden Variables, Joint Probability, and Bell Inequalities. *Phys. Rev. Lett.*, 48:291 – 295, 1982.

[10] A. Fine. Hidden Variables, Joint Probability, and Bell Inequalities. *J. Math. Phys.*, 23:1306 – 1310, 1982.

[11] W. M. de Muynck. The Bell inequalities and their irrelevance to the problem of locality in quantum mechanics. *Phys. Lett. A*, 114:65 – 67, 1986.

[12] E. T. Jaynes. Clearing up mysteries - The original goal. In J. Skilling, editor, *Maximum Entropy and Bayesian Methods*, volume 36, page 1, Dordrecht, 1989. Kluwer Academic Publishers.

[13] T. Brody. *The Philosphy Behind Physics*. Springer, Berlin, 1993.

[14] A. Fine. *The Shaky Game: Einstein Realism and the Quantum Theory*. University of Chicago Press, Chicago, 1996.

[15] A. Y. Khrennikov. *Interpretations of Probability*. VSP Int. Sc. Publishers, Utrecht, 1999.

[16] L. Sica. An explanation for their experimental violation. *Opt. Comm.*, 170:55 – 60, 1999.

[17] W. De Baere, A. Mann, and M. Revzen. Locality and Bell's theorem. *Found. Phys.*, 29:67 – 77, 1999.

[18] K. Hess and W. Philipp. Bell's theorem and the problem of decidability between the views of Einstein and Bohr. *Proc. Natl. Acad. Sci. USA*, 98:14228 – 14233, 2001.

[19] K. Hess and W. Philipp. Bell's theorem: Critique of Proofs with and without Inequalities. In A. Khrennikov, editor, *Foundations of Probability and Physics-3*, volume 750, page 150, Melville, New York, 2005. AIP Conference Proceedings.

[20] L. Accardi. Some loopholes to save quantum nonlocality. In A. Khrennikov, editor, *Foundations of Probability and Physics-3*, volume 750, page 21, Melville, New York, 2005. AIP Conference Proceedings.

[21] A. F. Kracklauer. Bell's Inequalities and EPR-B Experiments: Are They Disjoint? In A. Khrennikov, editor, *Foundations of Probability and Physics-3*, volume 750, page 219, Melville, New York, 2005. AIP Conference Proceedings.

[22] E. Santos. Bell's theorem and the experiments: Increasing empirical support to local realism? *Phil. Mod. Phys.*, 36:544 – 565, 2005.

[23] P. Morgan. Bell inequalities for random fields. *J. Phys. A*, 39:7441 – 7445, 2006.

[24] A. Yu. Khrennikov. A Mathematicians Viewpoint to Bell's Theorem. In G. Adenier, C. A. Fuchs, and A. Y. Khrennikov, editors, *Foundations of Probability and Physics-4*, volume 889, page 7, Melville, New York, 2007. AIP Conference Proceedings.

[25] G. Adenier and A. Y. Khrennikov. Is the fair sampling assumption supported by EPR experiments. *J. Phys. B: At. Mol. Opt. Phys.*, 40:131 – 141, 2007.

[26] Th. M. Nieuwenhuizen. Where Bell Went Wrong. In L. Accardi, G. Adenier, C. Fuchs, G. Jaeger, A.Y. Khrennikov, J. A. Larsson, and Stig Stenholm, editors, *Foundations of Probability and Physics - 5*, volume 1101, page 127, Melville and New York, 2009. AIP Conference Proceedings.

[27] A. Matzkin. Is Bell's theorem relevant to quantum mechanics? On locality and non-commuting observables. In L. Accardi, G. Adenier, C. Fuchs, G. Jaeger, A.Y. Khrennikov, J. A. Larsson, and Stig Stenholm, editors, *Foundations of Probability and Physics - 5*, volume 1101, page 339, Melville and New York, 2009. AIP Conference Proceedings.

[28] H. De Raedt, K. Hess, and K. Michielsen. Extended Boole-Bell inequalities applicable to quantum theory. `http://arxiv.org/abs/0901.2546`.

[29] H. De Raedt, K. De Raedt, K. Michielsen, K. Keimpema, and S. Miyashita. Event-by-event simulation of quantum phenomena: Application to Einstein-Podolosky-Rosen-Bohm experiments. *J. Comp. Theor. Nanosci.*, 4:957 – 991, 2007.

[30] K. De Raedt, K. Keimpema, H. De Raedt, K. Michielsen, and S. Miyashita. A local realist model for correlations of the singlet state. *Euro. Phys. J. B*, 53:139 – 142, 2006.

[31] H. De Raedt, K. De Raedt, K. Michielsen, K. Keimpema, and S. Miyashita. Event-based computer simulation model of Aspect-type experiments strictly satisfying Einstein's locality conditions. *J. Phys. Soc. Jpn.*, 76:104005, 2007.

[32] K. De Raedt, H. De Raedt, and K. Michielsen. A computer program to simulate Einstein-Podolsky-Rosen-Bohm experiment with photons. *Comp. Phys. Comm.*, 176:642 – 651, 2007.

[33] H. De Raedt, K. Michielsen, S. Miyashita, and K. Keimpema. Reply to Comment on "A local realist model for correlations of the singlet state". *Euro. Phys. J. B*, 58:55 – 59, 2007.

[34] S. Zhao, H. De Raedt, and K. Michielsen. Event-by-event simulation model of Einstein-Podolosky-Rosen-Bohm experiments. *Found. of Phys.*, 38:322 – 347, 2008.

[35] R.L Pfleegor and L. Mandel. Interference of Independent Photon Beams. *Phys. Rev.*, 159:1084 – 1088, 1967.

[36] I. N. Agafonov, M. V. Chekhova, T. Sh. Iskhakov, and A. N. Penin. High-visibility multiphoton interference of Hanbury Brown-Twiss type for classical light. *Phys. Rev. A*, 77:053801, 2008.

[37] P. D. D. Schwindt, P. G. Kwiat, and B.-G. Englert. Quantitative wave-particle duality and nonerasing quantum erasure. *Phys. Rev. A*, 60:4285 – 4290, 1999.

[38] G. Weihs, T. Jennewein, C. Simon, H. Weinfurther, and A. Zeilinger. Violation of Bell's Inequality under Strict Einstein Locality Conditions. *Phys. Rev. Lett.*, 81:5039 – 5043, 1998.

[39] `http://www.quantum.at/research/photonentangle/bellexp/data.html`. The results presented here have been obtained by assuming that the data sets *_V.DAT contain IEEE-8 byte (instead of 8-bit) double-precision numbers and that the least significant bit in *_C.DAT specifies the position of the switch instead of the detector that fired.

[40] S. Gröblacher, T. Paterek, R. Kaltenbaek, Č. Brukner, M. Żukowski, M. Aspelmeyer, and A. Zeilinger. An experimental test of non-local realism. *Nature*, 446:871–875, 2007.

[41] T. Young. On the theory of light and colors. *Philos. Trans. R. Soc. London*, 92:12–48, 1802.

[42] A.A. Michelson and E.W. Morley. On the Relative Motion of the Earth and the Luminiferous Ether. *Am. J. Sc.*, 34:333 – 345, 1887.

[43] A. Einstein. Über einen die erzeugung und verwandlung des lichtes betreffenden heuristischen gesichtspunkt. *Annalen der Physik*, 17:132–148, 1905.

[44] L. de Broglie. Recherches sur la théorie des quanta. *Annales de Physique*, 3:22, 1925.

[45] C. Jönsson. Elektroneninterferenzen an mehreren künstich hergestellten feinspalten. *Zeitschrift für Physik*, 161:454–474, 1961.

[46] M. W. Noel and C. R. Stroud Jr. Young's double-slit interferometry within an atom. *Phys. Rev. Lett.*, 75:1252–1255, 1995.

[47] A. Zeilinger, R. Gähler, C. G. Shull, W. Treimer, and W. Mampe. Single and double slit diffraction of neutrons. *Rev. Mod. Phys.*, 60:1067–1073, 1988.

[48] H. Rauch and S. A. Werner. *Neutron Interferometry: Lessons in Experimental Quantum Mechanics*. Oxford Univ. Press, London, 2000.

[49] O. Carnal and J. Mlynek. Young's double-slit experiment with atoms: a simple atom interferometer. *Phys. Rev. Lett.*, 66:2689–2692, 1991.

[50] David W. Keith, Christopher R. Ekstrom, Quentin A. Turchette, and David E. Pritchard. An interferometer for atoms. *Phys. Rev. Lett.*, 66:2693–2696, 1991.

[51] M. Arndt, O. Nairz, J. Vos-Andreae, C. Keller, G. van der Zouw, and A. Zeilinger. Wave-particle duality of c60 molecules. *Nature*, 401:680–682, 1999.

[52] B. Brezger, L. Hackermüller, S. Uttenthaler, J. Petschinka, M. Arndt, and A. Zeilinger. Matter-wave interferometer for large molecules. *Phys. Rev. Lett.*, 88:100404, 2002.

[53] V. Jacques, E. Wu, T. Toury, F. Treussart, A. Aspect, P. Grangier, and J.-F. Roch. Single-photon wavefront-splitting interference – An illustration of the light quantum in action. *Eur. Phys. J. D*, 35:561–565, 2005.

[54] R. P. Feynman, R. B. Leighton, and M. Sands. *The Feynman Lectures on Physics, Vol. 3*. Addison-Wesley, Reading MA, 1965.

[55] H. De Raedt, K. De Raedt, and K. Michielsen. Event-based simulation of single-photon beam splitters and Mach-Zehnder interferometers. *Europhys. Lett.*, 69:861 – 867, 2005.

[56] K. De Raedt, H. De Raedt, and K. Michielsen. Deterministic event-based simulation of quantum interference. *Comp. Phys. Comm.*, 171:19 – 39, 2005.

[57] H. De Raedt, K. De Raedt, and K. Michielsen. New method to simulate quantum interference using deterministic processes and application to event-based simulation of quantum computation. *J. Phys. Soc. Jpn. Suppl.*, 76:16 – 25, 2005.

[58] K. Michielsen, K. De Raedt, and H. De Raedt. Simulation of Quantum Computation: A Deterministic Event-Based Approach. *J. Comput. Theor. Nanosci.*, 2:227 – 239, 2005.

[59] S. Zhao and H. De Raedt. Event-by-event Simulation of Quantum Cryptography Protocols. *J. Comp. Theor. Nanosci.*, 5:490 – 504, 2008.

[60] S. Zhao, S. Yuan, H. De Raedt, and K. Michielsen. Computer simulation of Wheeler's delayed choice experiment with photons. *Europhys. Lett.*, 82:40004, 2008.

[61] F. Jin, S. Zhao, S. Yuan, H. De Raedt, and K. Michielsen. Event-by-event simulation of a quantum eraser experiment. *J. Comp. Theor. Nanosci.*, (in press), 2010. `http://arxiv.org/abs/0908.1036`.

[62] `http://demonstrations.wolfram.com/EventByEventSimulationOfDoubleSlitExperimentsWithSinglePhoto/`.

[63] M. Born and E. Wolf. *Principles of Optics*. Pergamon, Oxford, 1964.

[64] I. G. Saveliev, M. Sanz, and N. Garcia. Time-resolved young's interference and decoherence. *J. Opt. B: Quantum Semiclass. Opt.*, 4:S477–S481, 2002.

[65] L. E. Ballentine. *Quantum Mechanics: A Modern Development*. World Scientific, Singapore, 2003.

[66] R. H. Hadfield. Single-photon detectors for optical quantum information applications. *Nature Photonics*, 3:696 – 705, 2009.

[67] A. Tonomura. *The Quantum World Unveiled by Electron Waves*. World Scientific, Singapore, 1998.

[68] D. G. Manolakis, V. K. Ingle, and S. M. Kogon. *Statistical and Adaptive Signal Processing*. Artech House, Boston, 2005.

[69] G. R. Grimmet and D. R. Stirzaker. *Probability and Random Processes*. Clarendon Press, Oxford, 1995.

[70] A. Taflove and S.C. Hagness. *Computational Electrodynamics: The Finite-Difference Time-Domain Method*. Artech House, Boston, 2005.

[71] M. Tribus. *Rational Descriptions, Decisions and Designs*. Expira Press, Stockholm, 1999.

[72] E. T. Jaynes. *Probability Theory: The Logic of Science*. Cambridge University Press, Cambridge, 2003.

[73] L. E. Ballentine. Probability-theory in quantum-mechanics. *Am. J. Phys.*, 54:883 – 889, 1986.

[74] L.E. Ballentine. Interpretations of Probability and Quantum Theory. In A. Khrennikov, editor, *Foundations of Probability and Physics*, page 71, Singapore, 2001. World Scientific.

[75] A. Khrennikov. Structure of Probabilistic Information and Quantum Laws. In A. Khrennikov, editor, *Foundations of Probability and Physics*, page 180, Singapore, 2001. World Scientific.

[76] K. Hess, W. Philipp, and M. Aschwanden. What is Quantum Information? *Int. J. Quant. Inf.*, 4:585 – 625, 2006.

[77] R. P. Feynman and A. R. Hibbs. *Quantum Mechanics and Path Integrals*. McGraw-Hill, New York, 1965.

[78] J. H. Hammersley and D. C. Handscomb. *Monte Carlo Methods*. John Wiley, New York, 1964.

[79] P. Grangier, G. Roger, and A. Aspect. Experimental evidence for a photon anticorrelation effect on a beam splitter: A new light on single-photon interferences. *Europhys. Lett.*, 1:173, 1986.

[80] K. Hess, K. Michielsen, and H. De Raedt. Possible Experience: from Boole to Bell. *Europhys. Lett.*, 87:60007, 2009.

[81] F. Jin, S. Yuan, H. De Raedt, K. Michielsen, and S. Miyashita. Copuscular model of two-beam interference and double-slit experiments with single photons. *J. Phys. Soc. Jpn.*, 79:074401, 2010.

[82] A. Aspect, P. Grangier, and G. Roger. Experimental realization of Einstein-Podolsky-Rosen-Bohm gedankenexperiment: A new violation of Bell's inequalities. *Phys. Rev. Lett.*, 49:91 – 94, 1982.

[83] A. Aspect, J. Dalibard, and G. Roger. Experimental test of Bell's inequalities using time-varying analyzers. *Phys. Rev. Lett.*, 49:1804 – 1807, 1982.

[84] V. Jacques, E. Wu, F. Grosshans, F. Treussart, P. Grangier, A. Aspect, and J.-F. Roch. Experimental Realization of Wheeler's Delayed-Choice Gedanken Experiment. *Science*, 315:966–968, 2007.

[85] M. Nielsen and I. Chuang. *Quantum Computation and Quantum Information*. Cambridge University Press, Cambridge, 2000.

[86] R. Hanbury Brown and R. Q. Twiss. A Test of a New Type of Stellar Interferometer on Sirius. *Nature*, 178:1046–1048, 1956.

[87] R. J. Glauber. Photon correlations. *Phys. Rev. Lett.*, 10:84 – 86, 1963.

[88] R. J. Glauber. The quantum theory of optical coherence. *Phys. Rev.*, 130:2529 – 2539, 1963.

[89] L. Mandel. Quantum effects in one-photon and two-photon interference. *Rev. Mod. Phys.*, 71:S274 – S282, 1999.

[90] A. Khrennikov and Y. Volovich. Discrete time dynamical models and their quantum-like context-dependent properties. *J. Mod. Opt.*, 51:1113 – 1114, 2004.

[91] D. Dubischar, V.M. Gundlach, O. Steinkamp, and A. Khrennikov. The interference phenomenon, memory effects in the equipment and random dynamical systems over the fields of p-adic numbers. *Nouvo Cimento B*, 114:373 – 382, 1999.

[92] D. Dubischar, V.M. Gundlach, O. Steinkamp, and A. Khrennikov. A hidden variables model for interference phenomena based on p-adic random dynamical systems. `http://arxiv.org/abs/0906.0514`.

[93] G. Adenier. Violation of Bell Inequalities as a Violation of Fair Sampling in Threshold Detectors. In L. Accardi, G. Adenier, C. Fuchs, G. Jaeger, A.Y. Khrennikov, J. A. Larsson, and Stig Stenholm, editors, *Foundations of Probability and Physics - 5*, volume 1101, pages 8 – 18, Melville and New York, 2009. AIP Conference Proceedings.

[94] G. Jaeger, A. Shimony, and L. Vaidman. Two interferometric complementarities. *Phys. Rev. A*, 51:54 – 67, 1995.

[95] B.-G. Englert. Fringe Visibility and Which-Way Information: An Inequality. *Phys. Rev. Lett.*, 11:2154 – 2157, 1996.

[96] M. O. Scully and K. Drühl. Quantum eraser: A proposed photon correlation experiment concerning observation and "delayed choice" in quantum mechanics. *Phys. Rev. A*, 25:2208 – 2213, 1982.

[97] Y. H. Kim, R. Yu, S. P. Kulik, Y. Shih, and M. O. Scully. Delayed choice quantum eraser. *Phys. Rev. Lett.*, 84:1, 2000.

[98] Y. Aharonov and M. S. Zubairy. Time and the quantum: Erasing the past and impacting the future. *Science*, 307:875 – 879, 2005.

[99] M. O. Scully, B.-G. Englert, and H. Walther. Quantum optical tests of complementarity. *Nature*, 351:111 – 116, 1991.

[100] P. G. Kwiat, A. M. Steinberg, and R. Y. Chiao. Observation of a quantum eraser: A revival of coherence in a two-photon interference experiment. *Phys. Rev. A*, 45:7729 – 7739, 1992.

[101] T. B. Pittman, D. V. Strekalov, A. Migdall, M. H. Rubin, A. V. Sergienko, and Y. H. Shih. Can two-photon interference be considered the interference of two photons? *Phys. Rev. Lett.*, 77:1916 – 1920, 1996.

[102] S. P. Walborn, M. O. Terra Cunha, S. Pádua1, and C. H. Monken. Double-slit quantum eraser. *Phys. Rev. A*, 65:033818–1 – 033818–6, 2002.

[103] G. Scarcelli, Y. Zhou, and Y. Shih. Random delayed-choice quantum eraser via two-photon imaging. *Eur. Phys. J. D*, 44:167 – 173, 2007.

[104] G. Hackenbroich, B. Rosenow, and H. A. Weidenmüller. A mesoscopic quantum eraser. *Europhys. Lett.*, 44:693 – 699, 1998.

[105] Kicheon Kang. Electronic mach-zehnder quantum eraser. *Phys. Rev. B*, 75:125326, 2007.

[106] A. D. Armour and M. P. Blencowe. Possibility of an electromechanical which-path interferometer. *Phys. Rev. B*, 64:035311, 2001.

[107] `http://www.compphys.net/`.

[108] `http://demonstrations.wolfram.com/EventByEventSimulationOfTheMachZehnderInterferometer/`.

[109] B.-G. Englert, C. Kurtsiefer, and H. Weinfurther. Universal unitary gate for single-photon two-qubit states. *Phys. Rev. A*, 63:032303, 2001.

[110] J. G. Rarity and P. R. Tapster. *Phil. Trans. R. Soc. Lond. A*, 355:2267, 1997.

[111] G. Weihs. *Ein Experiment zum Test der Bellschen Ungleichung unter Einsteinscher Lokalität*. PhD thesis, University of Vienna, 2000. `http://www.quantum.univie.ac.at/publications/thesis/gwdiss.pdf`.

[112] C. A. Kocher and E. D. Commins. Polarization correlation of photons emitted in an atomic cascade. *Phys. Rev. Lett.*, 18:575 – 577, 1967.

[113] J. F. Clauser and M. A. Horne. Experimental and consequences of objective local theories. *Phys. Rev. D*, 10:526 – 535, 1974.

[114] K. Hess and W. Philipp. Breakdown of Bell's theorem for certain objective local parameter spaces. *Proc. Natl. Acad. Sci. USA*, 101:1799 – 1805, 2004.

[115] K. Hess and W. Philipp. Bell's Theorem as a Special Case of a Theorem of Bass. *Found. of Phys.*, 35:1749 – 1767, 2005.

[116] S. Zhao. *Event-based simulation of Quantum phenomena*. PhD thesis, University of Groningen, 2009.

Summary

This thesis presents a collection of event-by-event models that simulate fundamental optical experiments. The simulation approach is completely based on the experimental facts. Each component in the model corresponds to one kind of optical device, such as a beam splitter, a wave plate, a detector and so on. Networks of such components build computational experiments which are one-to-one copies of real experiments. As all components share the same mechanism (leaning machine) as in the previous work (see PhD. thesis of S. Zhao, RuG, Groningen [116]), our event-by-event simulation models are systematic and consistent with each other. As the model provides a description of interference and other wave phenomena on the level of individual event, it goes beyond the description of quantum theory.

In Chapter 1 we demonstrate that a modified learning machine for the detector, which shares the same essential features as that of previous work (as it also should be), can be used to simulate the double-slit experiment with single photons. As the individual photons build up the interference pattern one-by-one and there is no direct communication between photons, the interference pattern can only be due to the internal operation of the detector. The model for the detector accounts for the memory and the threshold behavior of the detectors and builds up the interference by individual clicks which quantitively agree with the theoretical results and qualitatively agree with the experimental results. We also mathematically prove that the behavior of the model satisfies the constitutive equations in Maxwell's theory.

Chapter 2 directly uses the model of the detector described in Chapter 1 and the models of the optical components such as the beam splitter which successfully simulates the Mach-Zehnder interferometer, to build an computational experiment which is a one-to-one copy of a real Hanbury Brown-Twiss experiment in Ref. [36]. The simulation results agree with the experimental data and wave theory.

In Chapter 3 we present a computer simulation model for a type of quantum eraser experiment. The model has all the parts that correspond to the real optical components, such as a beam splitter, a polarized beam splitter, a half-wave plate and a quarter-wave plate. The simulation results agree with the experimental data and wave theory.

In Chapter 4 we describe an Einstein-Podolosky-Rosen-Bohm experiment with polar-

ized photons and, by analyzing the real experimental data, show that the time window W is essential to get a quantum correlation. Then we present an event-based simulation of EPRB experiment that satisfies Einstein's criteria of local causality, generates the same kind of data as in experiment, and is capable of reproducing exactly the single- and two-particle averages of quantum correlation of singlet state.

All the results presented in this thesis demonstrate that it is possible to simulate quantum phenomena by classical, non-Hamiltonian, local, causal and dynamical models. In many respects the model expresses itself.

Samenvatting

In deze thesis wordt een collectie van event-per-event modellen gepresenteerd die fundamentele optische experimenten kunnen simuleren. De constructie van deze modellen is volledig gebaseerd op experimentele feiten. Elke afzonderlijk component in het model komt overeen met een optisch apparaat, zoals een beam splitter, een wave plate, een detector enzovoorts. Een netwerk van dergelijke componenten definieert dan een numeriek experiment dat één-op-één overeenkomt met een realistische experiment. Omdat alle componenten dezelfde mechanismes (leermachine) als in het vorige werk bevatten, (zie Ph.D. Thesis van S. Zhao, RuG, Groningen [116]), zijn onze event-per-event simulatie modellen systematisch en consistent met elkaar. Aangezien het model een beschrijving geeft van interferentie en andere golffenomenen op het niveau van een enkel event, gaat deze verder dan de kwantummechanische beschrijving.

In hoofdstuk 1 geven wij een demonstratie hoe een aangepaste leermachine voor een detector, die dezelfde essentiële eigenschappen deelt als die in het vorige werk (zoals het zou moeten zijn), gebruikt kan worden om het twee spleten experiment met enkele fotonen te simuleren. Omdat de individuele fotonen het interferentiepatroon één voor één opbouwen en er geen directe communicatie is tussen deze fotonen, kan het interferentiepatroon enkel gegeven worden door de interne werking van de detector. Het detectormodel zorgt voor het geheugen- en grens gedrag van de detectoren en bouwt de interferentie op door individuele klikken die kwantitatief overeen komen met de theoretische- en kwalitatief overeen komen met de experimentele resultaten. Verder geven we het wiskundige bewijs dat het gedrag van het model voldoet aan de constitutieve vergelijkingen in Maxwell's theorie.

Hoofdstuk 2 maakt, in combinatie met de modellen voor de optische componenten zoals de beam splitter welke de Mach-Zehnder interferometer succesvol simuleert, direct gebruik van het detector model beschreven in hoofdstuk 1. Er wordt een computationeel experiment gebouwd dat een directe kopie is van een echt Hanbury Brown-Twiss experiment zoals beschreven in Ref. [36]. De gesimuleerde resultaten zijn in overeenstemming met de experimentele data en met golftheorie.

In Hoofdstuk 3 presenteren we een computersimulatie model voor een bestaand kwantum eraser experiment. Het model heeft alle onderdelen die overeenkomen met de daadwerkelijke optische componenten zoals een beam splitter, een gepolariseerde

beam splitter, een halve golflengte plaat en een kwart golflengte plaat. De gesimuleerde resultaten komen overeen met de experimentele data en golftheorie.

In hoofdstuk 4 beschrijven we een Einstein-Podolsky-Rosen-Bohm experiment met gepolariseerde fotonen en tonen aan, door vergelijking met experimentele data, dat het tijdsinterval W essentieel is om een kwantum correlatie te verkrijgen. Daarna presenteren we een event gebaseerde simulatie van het EPRB experiment die voldoet aan Einsteins criterium van lokale causaliteit. De simulatie genereert dezelfde data als het experiment en is in staat om de enkele en twee deeltjes gemiddeldes van een singlet-toestand te reproduceren.

Alle resultaten die in deze thesis gepresenteerd worden, demonstreren dat het mogelijk is om kwantum fenomenen te simuleren door middel van klassieke, niet-Hamiltoniaanse, lokale, causale en dynamische modellen. In veel opzichten spreekt het model voor zichzelf.

Publications

[1] K. Michielsen, F. Jin, and H. De Raedt, *Event-based Corpuscular Model for Quantum Optics Experiments* accepted for publication in J. Comp. Theor. Nanoscience;

[2] F. Jin, S. Yuan, H. De Raedt, K. Michielsen, and S. Miyashita, *Corpuscular model of two-beam interference and double-slit*, J. Phys. Soc. Jpn. **79**, 074401 (2010);

[3] F. Jin, H. De Raedt, and K. Michielsen, *Event-by-event simulation of the Hanbury Brown-Twiss experiment with coherent light*, Commun. Comput. Phys. **7**, 813-830 (2010);

[4] F. Jin, S. Zhao, S. Yuan, H. De Raedt, and K. Michielsen, *Event-by-event simulation of quantum eraser experiments with single photons*, J. Comput. Theor. Nanoscience **7**, 1771-1782 (2010);

[5] K. Michielsen, S. Yuan, S. Zhao, F. Jin, H. De Raedt, *Coexistence of full which-path information and interference in Wheelers delayed choice experiment with photons*, Physica E **42**, 348-353 (2010);

[6] H. De Raedt, S. Zhao, S. Yuan, F. Jin, K. Michielsen, and S. Miyashita, *Event-by-event simulation of quantum phenomena*, Physica E **42**, 298-302 (2010);

[7] F. Jin, H. De Raedt, and K. Michielsen, *Particle-based simulation approach for single-particle interference experiments: Application to double-slit experiments*, in Quantum Theory: Reconsiderations of Foundations - 5, edited by A. Khrennikov (AIP Conference Proceedings, Melville and New York, 2010), vol. **1232**, p. 93 - 104;

[8] F. Jin, H. De Raedt, S. Yuan, M. I. Katsnelson, S. Miyashita and K. Michielsen, *Approach to equilibrium in nano-scale systems at finite temperature*, J. Phys. Soc. Jpn. **79**, 124005 (2010).

Acknowledgements

I received a lot of help and support from all the people around me during my four-year PhD study. At the end of this PhD thesis, I would grab the opportunity to express my sincere appreciations to all people.

First and foremost, I would like to express my deep sense of appreciation to my supervisor, Prof.dr. Hans De Raedt. I am grateful for your faith in my work, and for your excellent guidance and inspiration during my study. Special thanks go to Prof.dr. Kristel Michielsen for her kindnesses and helps.

Many thanks go to my (former) colleagues in the computational physics group, Dr. Shengjun Yuan, Dr. Shuang Zhao, Dr. Aard Keimpema, Mutia Delina, O. Zinchenko, and Bodo Wilts. I would like to thank Yuan and Zhao especially as it is actually you that brought us to Nederland and helped us a lot.

I would like to thank all the Chinese friends we met in the Netherlands, Shengjun Yuan and his family (especially to your pretty daughter Zixuan), Jiwu Lu, Linjuan Yu, Daren Zhou, Yu Wu and Ji Liu, Youchun Zhang, Jia Gao and Zhe Guo, Yuan Zhang, Xiaonan Sun, Bian Wu and your family, Fei Xiang, Huanjun Yu, Xiaoming Liu, Jie Yin, Bin Mao, Mingtao Lu, Wenqiang Zou, Lifei Zheng, Liya Zhu and her family, and many other friends. Because of all of you, we have a wonderful memory in Groningen. Special thanks from my wife go to Liya and her family.

I would like to thank Krijn de Vries for your excellent translation of my summary. I would like to thank the reading committee, Prof.dr. S. Miyashita, Prof.dr. K. Michielsen and Prof.dr. J.TH.M. De Hosson for their careful reading and valuable comments.

And I would like to thank my family for your love and support. Most of all, I would especially thank my wife, Enda Meng, for your love and support all through this four years.